DEFENSE DOCUMENTATION CENTER

FOR

SCIENTIFIC AND TECHNICAL INFORMATION

CAMERON STATION, ALEXANDRIA, VIRGINIA

64-12

3-27-63-4 • DECEMBER 1963

DASA 1465

TECHNICAL REPORT

THE CALCULATIONS OF SPECTRAL ABSORPTION IN HEATED AIR

APR 3 0 1964

TECHNICAL REPORT

THE CALCULATIONS OF SPECTRAL ABSORPTION IN HEATED AIR

by
D.R. Churchill
S.A. Hagstrom
R.K.M. Landshoff

Lockheed

MISSILES & SPACE COMPANY

A GROUP DIVISION OF LOCKHEED AIRCRAFT CORPORATION

SUNNYVALE, CALIFORNIA

CONTENTS

ILLUSTRATIONS

TABLES

ix

ABSTRACT

The spectral absorption coefficient of heated air has been calculated over the frequency interval and temperature range where electronic transitions in diatomic molecules are the dominant mechanism. With the aid of experimentally determined constants, the spectra of six important band systems have been theoretically reconstructed. These spectra and the corresponding line intensities have been preserved in the form of a magnetic tape atlas. Average absorption coefficients and their role in radiative transfer are discussed. A method of calculating group absorption coefficients based on a sampling technique is described. Digital computer programs based on this procedure have been used to compute optical transmissions through heated air. Typical results of the calculation are presented.

1

I. INTRODUCTION

Electronic transitions in diatomic molecules contribute appreciably to the absorption coefficient of air at optical frequencies for air temperatures of a few thousand degrees[1, 2]. Such transitions are discrete when they occur between two bound states of a molecule. Continuum transitions occur from bound to free states or between two free states (inverse bremsstrahlung). This paper discusses line absorption arising in six prominent molecular band systems in heated air and presents the results of some recent calculations on those systems.

Basic theoretical expressions for the line absorption coefficient are presented in Section II. Section III contains a brief discussion of the molecular spectra for the six band systems: the Schumann-Runge bands of O_2, first and second positive systems of N_2, beta and gamma bands of NO, and the first negative system of N_2^+. Magnetic tape atlases for the above spectra are also described in this section.

Some average absorption coefficients and their utility in radiation transport will be discussed in Section IV, which also contains a description of an average transmission calculation and presents sample results of that calculation.

The spectroscopic notation used herein is that of Herzberg[3], to which the reader is referred for any necessary background material.

II. THE SPECTRAL ABSORPTION COEFFICIENT OF A DIATOMIC MOLECULE

A theoretical expression for the spectral absorption coefficient will be obtained which is valid for electronic transitions in diatomic molecules when the Born-Oppenheimer[4] approximation may be applied with sufficient accuracy. Consider an electronic transition between two nondegenerate levels or sub-levels, where a sub-level

is one of the components of a degenerate electronic state. The absorption coefficient for such a transition between a lower state L and an upper state U is:

$$\mu(\nu) = N_L B_{L \to u} h \nu_{L \to u} F(\nu) \tag{1}$$

where $\nu_{L \to u}$ is the line frequency, N_L is the particle density of the lower state, $B_{L \to u}$ is the Einstein coefficient for absorption, and $F(\nu)$ is a line shape factor such that $\int F(\nu)\, d\nu = 1$. By spectroscopic convention[3] the lower level is given by (n'', v'', J''), where n'' is the electronic state indicator, v'' is the vibrational quantum number, and J'' is the rotational quantum number. The upper level is then specified by (n', v', J'). Primes always refer to upper levels and double primes to lower levels. When ν is expressed in "wave numbers" (cm^{-1}), the Einstein coefficient for absorption is given by

$$B_{n'', v'', J'', n', v', J'} = \frac{8\pi^3}{3h^2 c} \frac{\sum_{M'', M'} \left| R^{M'', M'} \right|^2}{2J'' + 1} \tag{2}$$

where

$$\vec{R}^{M'', M'} = \int \bar{\psi}''_{n'', v'', J'', M''} \vec{R} \, \psi'_{n', v', J', M'} \, d\tau \tag{3}$$

is the matrix element of the electric moment operator $\vec{R} = \vec{R}_e + \vec{R}_n$ of the electrons and nuclei. Here M'' and M' are azimuthal quantum numbers numbering the spatially degenerate rotational levels of the lower and upper states, and the summation is over all possible combinations of the rotational sub-levels of the lower with those of the upper state.

3

Since the Born-Oppenheimer approximation is assumed, the molecular wave function may be written as a product

$$\psi = \psi_e \psi_{vib} \psi_{rot.} \tag{4}$$

of the electronic, vibrational, and rotational wave functions. Substituting (4) into (3) leads to an expression for the sum in (2):

$$\sum_{M'',M'} \left| R^{M'',M'} \right|^2 = \left| R_e \right|^2 q(v',v'') S_{J''} \tag{5}$$

where

$$\left| R_e \right|^2 = \left| \int \overline{\psi}_e' \vec{R}_e \psi_e'' d\tau_e \right|^2 \tag{6}$$

and

$$q(v',v'') = \left| \int \overline{\psi}_{vib}' \psi_{vib}'' d\tau_n \right|^2 \tag{7}$$

The $d\tau_n$ in (7) can be replaced with dR, since the vibrational eigenfunctions depend only on the internuclear separation. R_e is the electronic transition moment and $q(v',v'')$ is the Franck-Condon factor. $S_{J''}$ is that part of $\sum_{M'',M'} \left| R^{M'',M'} \right|^2$ that depends on the rotational quantum number J'' and the coupling in the molecule. The S_J's are often called Honl-London intensity factors; they are available in the literature for all the important types of electronic transitions. Franck-Condon factors have been calculated for many band systems of diatomic molecules by Nicholls and co-workers[5,6,7].

4

Equation (2) becomes

$$B_{n'',n',v'',v',J'',J'} = \frac{8\pi^3}{3h^2C} \left|R_e\right|^2 q(v',v'') \frac{S_{J''}}{2J''+1} \tag{8}$$

The particle density in the lower level is given by

$$N_{n'',v'',J''} = \frac{N(2J''+1)\omega_I \exp\left[\frac{-E_{n'',v'',J''}}{kT}\right]}{Q} \tag{9}$$

where N is the total particle density for all levels, $E_{n'',v'',J''}$ is the energy of the level and ω_I its nuclear spin statistical weight. Q is the total partition function and may be written as the sum of contributions from all the electronic states:

$$Q = \sum_n Q_n \tag{10}$$

Taking into account electronic (orbital + spin), vibrational, rotational, and nuclear (spin only) degrees of freedom, we may write

$$Q_n = Q_{electronic} \, Q_{vib.-rot.} \, Q_{nuclear} \tag{11}$$

where

$$Q_{electronic} = \omega_\Lambda (2S+1) \exp\left[\frac{-\nu_{oo} \, hc}{kT}\right] \tag{12}$$

$$Q_{vib.-rot.} = \sum_{v=0}^{\infty} \exp\left[\frac{-G_o(v) hc}{kT}\right] Q_{rot.}^{(v)} \tag{13}$$

5

$$Q_{rot.}^{(v)} = \int_0^\infty (2J + 1) \, \exp\left[\frac{-F_v(J)hc}{kT}\right] dJ \cong \frac{kT}{hcB_v} \qquad (14)$$

$$Q_{nuclear} = \frac{(2I_a + 1)(2I_b + 1)}{\sigma} \qquad (15)$$

In these formulas ν_{oo} is the energy of the lowest vibrational level of electronic state n above that of the ground state, $G_o(v)$ is the vibrational term referred to the lowest vibrational level, $F_v(J)$ is the rotational term for the vth vibrational level with B_v its corresponding rotational constant, and S is the total electron spin. ω_Λ is the statistical weight for orbital angular momentum Λ about the internuclear axis and takes the value 1 if $\Lambda = 0$ and value 2 if $\Lambda \neq 0$. I_a and I_b are the nuclear spins of the two nuclei and σ is a symmetry number having the value 2 for homonuclear molecules and 1 for heteronuclear systems.

An approximate formula for $Q_{vib.-rot.}$ that is more convenient for calculation and yet accurate enough for our problem was developed by Bethe[8] and later corrected by Brinkley[9]:

$$Q_{vib.-rot.} = \frac{1}{1 - \exp\left(\frac{-1.4388\omega_o}{T}\right)} \frac{T}{1.4388B_o} (1 + \gamma T) \qquad (16)$$

where γ, Bethe's correction factor for anharmonicity and non-rigidity, has the value

$$\gamma = \frac{1}{1.4388\omega_o} \left(\frac{2\omega_o x_o}{\omega_o} + \frac{\alpha_o}{B_o} + \frac{8B_o}{\omega_o}\right) \qquad (17)$$

Here ω_o and B_o are the vibrational and rotational constants of the $v = 0$ vibrational level, $\omega_o x_o$ is the first anharmonic constant and α_o is the interaction constant for coupling between rotation and vibration.

6

Returning now to Eq (9), we multiply numerator and denominator by Q_n as given by Eqs. (11), (12), and (15) and obtain after a little algebra

$$N_{n''v''J''} = N_{total} \frac{Q_{n''}}{Q_{total}} \frac{\omega_I (2J''+1) \exp\left[-\left\{G_0(v'') + F_{v''}(J'')\right\}\frac{hc}{kT}\right]}{(2S+1)\omega_\Delta Q_{nuclear} Q_{vib.-rot.}} \quad (18)$$

where use has been made of the relation

$$E_{n''v''J''} = \left[\nu_{00} + G_0(v'') + F_{v''}(J'')\right] hc \quad (19)$$

now let $P_{n''} = Q_{n''}/Q_{total}$ denote the fractional population of the n''^{th} electronic state and introduce the notation

$$H_{n''n', v''v', J''J'} = \frac{8\pi^2 L_0}{3hc} \frac{\omega_I}{(2S+1)\omega_\Lambda Q_{nuclear}} \nu_{n''n', J''J', v''v'} |R_e|^2 q(v', v'') S_{J''} \quad (20)$$

and

$$E_{v''J''} = \left[G_0(v'') + F_{v''}(J'')\right]\frac{hc}{k} \quad (21)$$

where $L_0 = 2.6875 \times 10^{19}$ particles/cm^3 is Loschmidt's number.

We now obtain the desired form of Eq. (1) by substitution, using Eqs. (18), (20), and (21):

$$\mu(\nu) = \left[\frac{N_{total}P_{n''}}{L_0 Q_{vib-rot}}\right] H_{n''n', v''v', J''J'} \exp\left(\frac{-E_{v''J''}}{T}\right) \pi F(\nu) \quad (22)$$

Here the quantities H and E are characteristic of the isolated molecule, i.e., do not depend on the temperature and density. Since the bracketed term in (22) is

7

dimensionless, H has dimensions cm^{-2}, and $F(\nu)$ has dimensions cm (discussion follows), the absorption coefficient $\mu(\nu)$ has the required dimension cm^{-1}.

Although Eq. (22) is valid for arbitrary form factor $F(\nu)$, in our calculations for for air we have assumed a Lorentz line profile, viz.,

$$F(\nu) = \frac{1}{\pi} \frac{\sigma}{\sigma^2 + \left(\nu - \nu_{n'n', v'v', J'J'}\right)^2} \qquad (23)$$

where σ is the line half-width at half-maximum. The absorption coefficient $\mu(\nu)$ at ν due to several contributing (overlapping) lines is just the sum of the separate line absorption coefficients:

$$\mu(\nu) = \sum_i \mu_i(\nu) \qquad (24)$$

where i labels the lines and the sum runs over all lines whose profiles overlap significantly* at ν.

_____

*Obviously some suitable criterion must be chosen to limit the calculation to some reasonable number of lines per frequency considered.

III. LINE FREQUENCIES AND INTENSITIES FOR AIR

The frequency, "H" function, and "E" function must now be found for each line which is to be included in the calculation. Theoretical reconstruction of the spectrum for each of the six electronic systems is accomplished by utilization of experimental constants as cited under the separate systems below.

Fine structure (composite lines) due to spin splitting and Λ-type doubling[3] has been ignored in the calculation for the following reasons: (1) the spin splitting is not well known, (2) actual line widths and profiles are not generally known, (3) Λ-type doubling increases with increasing J and lines are probably not well resolved until very high J is reached, and (4) it is felt some compensation is obtained by choosing the line half-width large enough to include partially resolved lines.

Schematic energy-level diagrams are presented in Figs. 1 through 6; these illustrate levels and transitions for the band systems included in the discussion. The conventions used in the diagrams are those of Herzberg[3]. The resolution due to spin splitting and the Λ-type doubling in Π states have both been greatly exaggerated for purposes of clarity. Vertical lines (transitions) are drawn in composite line groupings.

Intensity factors used in the calculation are in accord with the rotational sum rule with the exception of the NO gamma system, whose composite line intensity factors cannot be expressed in simple form. However, only two very weak transitions have been omitted.

A few of the levels for the N_2 second positive system are labeled with the associated nuclear spin statistical weight, which is written to the right of the level.

9

The $B\,^3\Sigma_u^-$ – $X\,^3\Sigma_g^-$ (Schumann-Runge) System of O_2

With small dispersion, $^3\Sigma$ – $^3\Sigma$ bands consist of a single R and a single P
branch. Larger dispersion shows each line to be resolved into three components of
about the same intensity. There are, thus, six main branches. Six very weak satellite
branches for which $\Delta J \neq \Delta K$ are also present. Alternate triplets in the P and R
branches are missing, since the nuclear spin of the oxygen atom is zero. Even K
rotation levels are missing in the X state, and odd K levels are missing in the B
state. In our calculation, lines will be treated as unresolved. Figure 1 shows two
groups of lines which are considered to be composite lines whose Hönl-London factors
are obtained by simply adding up the S_J's for the individual components. These fac-
tors turn out to be 3K'' for the P branch lines and 3(K'' + 1) for the R-branch lines.

Rotational terms of both Σ states are then given by

$$F_v(K) = B_v K(K + 1) - D_v K^2 (K + 1)^2 \qquad (1)$$

The rotational constants B_v and D_v for the ground state were calculated from
the molecular constants of Herzberg[3]. For the $B\,^3\Sigma_u^-$ state, the B_v's and D_v's
were obtained from experiment[10].

For the O_2 Schumann-Runge system, then, the $H_{J'',J'}$'s are given by

$$H_{J'',J'} = H_{K'',K'} = \frac{8\pi^2 L_0}{3hc}\cdot\frac{1}{3}\left(\frac{\omega_J}{Q_{nuclear}}\right) \nu_{K'',K'} |R_e|^2 q(v',v'') S_J \qquad (2a)$$

$$= \frac{16\pi^2 L_0}{3hc} \nu_{K'',K'} |R_e|^2 q(v',v'') \cdot \begin{cases} K'' + 1 & \text{if } K' = K'' + 1 \\ \\ K'' & \text{if } K' = K'' - 1 \end{cases} \qquad (2b)$$

where K'' 1, 3, 5,

The $B\,^3\Pi_g - A\,^3\Sigma_u^-$ (First Positive) System of N_2

The structure of $^3\Pi - {}^3\Sigma$ bands is very complicated (Fig. 2), particularly if, as is the case here, the coupling in the Π state is near Hund's case "a." Since there are three sub-bands, $^3\Pi_0 - {}^3\Sigma^+$, $^3\Pi_1 - {}^3\Sigma^+$, $^3\Pi_2 - {}^3\Sigma^+$, and each sub-band has nine branches (three for each triplet component of the lower state), there are, in all, 27 branches. Of these, we expect nine branches to be relatively strong, ten satellite branches to be somewhat weaker, and eight to be weak branches; the latter are represented by dashed lines in the figure. We will omit the latter eight branches entirely. The 19 remaining branches, along with their corresponding intensity factors, are included in the calculations.

Formulas for the rotational levels of a $^3\Sigma$ state have been derived by Schlapp[11].

Now in the case of the $A\,^3\Sigma_u^+$ state of N_2, the spin splitting is very small, and, furthermore, is known only very approximately for most of the vibrational levels. Therefore, we ignore the spin splitting and use instead the term formula for $^1\Sigma$ states given by Eq. (1).

The values of B_v and D_v for each of the vibrational levels considered were calculated from molecular constants given by Naude.[12]

Rotational term formulas for the $^3\Pi_g$ state are from Budo[13] and are for any degree of uncoupling:

$$F_{v1}(J) = B_v\left[J(J+1) - \sqrt{Z_1} - 2Z_2/3Z_1\right] - D_v\left(J - \tfrac{1}{2}\right)^4 \qquad (3)$$

$$F_{v2}(J) = B_v\left[J(J+1) + 4Z_2/3Z_1\right] - D_v\left(J + \tfrac{1}{2}\right)^4 \qquad (4)$$

$$F_{v3}(J) = B_v\left[J(J+1) + \sqrt{Z_1} - 2Z_2/3Z_1\right] - D_v(J + 3/2)^4 \qquad (5)$$

1.

where

$$Z_1 = Y_v (Y_v - 4) + 4/3 + 4J(J + 1) \tag{6}$$

$$Z_2 = Y_v (Y_v - 1) - 4/9 + 2J(J + 1) \tag{7}$$

and $Y_v = A_v/B_v$ is a measure of the degree of coupling of the spin to the internuclear axis. For large rotation, F_{v1}, F_{v2}, and F_{v3} go over into a case "b" term series with $J - K + 1$, K, and $K - 1$ respectively. Note that levels $F_{v2}(0)$, $F_{v3}(0)$, and $F_{v3}(1)$ do not exist because of the requirement that $J \geq \Omega = |\Lambda + \Sigma|$ for Hund's case "a." The B_v, D_v, and Y_v values for each vibrational level are taken from Budo[13]. Since Λ-type doubling is small except for very large K, it has been neglected in the above formulas.

$H_{J''}$ for the first positive system is given by

$$H_{J''} = \frac{8}{9} \frac{\pi^2 L_c}{hc} \nu |R_e|^2 q(v', v'') \times \begin{Bmatrix} 2/3 \text{ if } K'' \text{ even} \\ \\ 4/3 \text{ if } K'' \text{ odd} \end{Bmatrix} \cdot S_{K''} \tag{8}$$

$$S_{K''} = K'' \quad \text{(P-branch)}$$

$$= K'' + 1 \quad \text{(R-branch)}$$

The N_2 $C^3\Pi_u - B^3\Pi_g$ Second Positive) System

The structure of $^3\Pi - {}^3\Pi$ bands is simple if both states belong either to Hund's case "a" or to Hund's case "b." If both $^3\Pi$ states belong to case "a," the selection rule $\Delta\Sigma = 0$ allows division into three sub-bands: $^3\Pi_0 - {}^3\Pi_0$, $^3\Pi_1 - {}^3\Pi_1$, and $^3\Pi_2 - {}^3\Pi_2$. Should Λ tape doubling be disregarded, each sub-band has a strong R, a strong P, and (except for $^3\Pi_0 - {}^3\Pi_0$) a weak Q branch. If both $^3\Pi$ states belong to case "b" or if both go over from case "a" to case "b" with increasing rotation, the same six strong bands occur. For all values of K in case "a," and for

12

large values of K in case "b," the three P branches are close together and the three R branches are close together, giving rise to a characteristic triplet structure.

In the N_2 second positive system, both $^3\Pi$ states belong to case "a" for small K values. Both go over to case "b" for large values of K. Figure 3 shows the six main branches of the $C^3\Pi_u - B^3\Pi_g$ system and the corresponding energy level diagram. A rapid transition from case "a" to case "b" has been assumed. Since nitrogen nuclei follow Bose statistics ($I = 1$), the symmetrical levels (s) will have the higher statistical weight $\omega_I(s) = (2I + 1)(I + 1)$, and the antisymmetrical levels (a) will have the lower statistical weight $\omega_I(a) = (2I + 1)I$, i.e., $\omega_I(s) = 6$ and $\omega_I(a) = 3$. Therefore the total weight for the Δ doublet is $\omega_I = 9$ which is just 1/2 of the "maximum" weight $\omega_\Omega(2I + 1)^2 = 18$ that one would expect for a heteronuclear system of the same type and for which both nuclei have $I_a = I_b = 1$.

The Q_2 and Q_3 branches have line intensities that fall off as $1/J''$, and hence the total intensity residing in these branches is small. Therefore, these branches will be omitted in the present study.

Formulas for the rotational terms are given by Eqs. (3) through (7).

If $\nu_{v'',v'} = \nu_{oo} + G_o'(v') - G_o''(v'')$, then the frequencies of the lines will be given by

$$\nu_{J''}^{R_n} = \nu_{v'',v',J''(J''+1)} = \nu_{v'',v'} + F_n'(J'' + 1) - F_n''(J'') \qquad (9)$$

and

$$\nu_{J''}^{P_n} = \nu_{v'',v',J''(J''-1)} = \nu_{v'',v'} + F_n'(J'' - 1) - F_n''(J'') \qquad (10)$$

for $n = 1, 2, 3$.

13

The two lines arising from the components of a Λ-type doublet overlap in frequency and are identical except for the ω_I, one having the value 6 (symmetrical) and the other 3 (antisymmetrical). This allows us to construct the $H_{n'',n',v'',v',J'',J'}$ $= H_{J'',J'}$ for the whole doublet by simply adding the H's for the individual components, viz:

$$H_{J'',J'} = \frac{8\pi^2 L_o}{3hc} \cdot \frac{1}{2 \cdot 3} \cdot \nu_{J'',J'} \mid R_e \mid^2 q(v',v'') S_{J''}\left(\frac{3}{9/2} + \frac{6}{9/2}\right) \qquad (11a)$$

$$= \frac{8\pi^2 L_o}{9hc} \nu_{J'',J'} \mid R_e \mid^2 q(v',v'') S_{J''} \qquad (11b)$$

where $9/2$ is the value of $Q_{nuclear}$.

Hönl-London factors for $^3\Pi-^3\Pi$ systems under various coupling conditions have been given by Budó (15). For this study it will be sufficiently accurate to use the Hönl-London factors for a $^1\Pi-^1\Pi$ type transition:

$$S_{J''}^R = J'' + 1 \qquad (12)$$

$$S_{J''}^P = J'' \qquad (13)$$

The final formulas for $H_{n'',n',v'',v',J'',J'}$ then become

$$H_{J''}^{R_n} = \frac{8\pi^2 L_o}{9hc} \nu_{J''}^{R_n} \mid R_e \mid^2 q(v',v'') [J'' + 1] \qquad (14)$$

and

$$H_{J''}^{P_n} = \frac{8\pi^2 L_o}{9hc} \nu_{J''}^{P_n} \mid R_e \mid^2 q(v',v'') J'' \qquad (15)$$

for $n = 1,2,3$.

13

The values of B_v, D_v, and Y_v for the $C\,^3\Pi_u$ and $B\,^3\Pi_g$ states of N_2 which were used in this study are due to Budó[13-14].

The $B\,^2\Sigma_u^+ - X\,^2\Sigma_g^+$ (First Negative) System of N_2^+

Since $^2\Sigma$ states always belong strictly to Hund's coupling case "b," giving rise to the selection rule $\Delta K = \pm 1$ with $\Delta K = 0$ being forbidden, the structure of a $^2\Sigma - ^2\Sigma$ transition is simple. There are two principal branches, an R branch and a P branch, each of which may be resolved into three components according to the rule $\Delta J = 0$, ± 1. For one of these $(\Delta J = 0)$ $\Delta J \neq \Delta K$.

The energy level diagram and transitions which apply to first negative bands are shown in Fig. 4. Rotation terms of lower $^2\Sigma_g^+$ and upper $^2\Sigma_u^+$ states are both given by Eq. (1).

Douglas [16] lists the values of B_v, D_v, and $G_0(v)$ used in the calculation.

Ignoring the spin, the rotational levels can be labeled by K. Grouping lines arising from the same K'' level, we have

$$H_{K'',\,K'} = \frac{16\pi^2 I_0}{3hc}\,\nu_{K'',K'}\,|R_e|^2\,q(v',v'')\,S_{K''} \cdot \begin{cases} 2/3 & \text{if } K'' \text{ even} \\ \\ 1/3 & \text{if } K'' \text{ odd} \end{cases} \tag{16}$$

where

$$S''_K \quad K'' + 1 \ \text{ if } \ K' \quad K'' + 1$$

$$K'' \ \text{ if } \ K' \quad K'' - 1$$

The factors to allow for K odd or even arise because of the effect of symmetry properties on $^2\Sigma - ^2\Sigma$ transitions of homonuclear molecules. Even K'' levels are symmetric $(\omega_1(s) \quad 6)$, while odd K'' levels are antisymmetric $(\omega_1(s) \quad 3)$.

15

The $B\,^2\Pi - X\,^2\Pi$ (Beta) System of NO

The structure of a $^2\Pi - {}^2\Pi$ system is simple if both states belong to Hund's coupling case "a" or both belong to case "b" or if, as in the present case, both states are intermediate between cases "a" and "b" and go over together from case "a" to case "b" with increasing nuclear rotation. There are two sub-bands in the NO Beta system: $^2\Pi_{1/2} - {}^2\Pi_{1/2}$ and $^2\Pi_{3/2} - {}^2\Pi_{3/2}$. Each sub-band consists of a strong R, a strong P, and weak Q branch. Since the intensity of the Q branches falls off like J^{-1}, we will neglect these branches entirely. Figure 5 shows the NO beta system.

Both the $B\,^2\Pi$ and $X\,^2\Pi$ states of NO are intermediate between Hund's coupling cases "a" and "b," with the X state being nearer case "a" $(A = 124.2\text{ cm}^{-1})$ than the B state (for which $A \sim 32\text{ cm}^{-1}$). A general formula for the term values of a $^2\Pi$ state with coupling intermediate between cases "a" and "b" has been derived by Hill and Van Vleck[17].

$$T_n(v,J) = T_e + G_n(v) + B_v\left[\left(J + \frac{1}{2}\right)^2 - 1 + (-1)^n \mu(J)\right] - D_v \cdot \begin{cases} J^4 & (n = 1) \\ \\ (J + 1)^4 & (n = 2) \end{cases} \tag{17}$$

where

$$\mu(J) = \sqrt{\left(J + \frac{1}{2}\right)^2 - Y_v + Y_v^2/4} \quad \text{and} \quad Y_v = A/B_v \tag{18}$$

Here the subscript $n = 1$ stands for a $^2\Pi_{1/2}$ and $n = 2$ stands for $^2\Pi_{3/2}$. A subscript n has been affixed to the vibrational term $G(v)$ since the different sub-states of the multiplet may have slightly different vibrational levels. Formulas for the line frequencies of the two R and two P branches follow.

$$R_1(J) = \nu_e + \nu_v^{(1)} + F_1'(J'' + 1) - F_1''(J'') \tag{19}$$

$$R_2(J) = \nu_e + \nu_v^{(2)} + F_2'(J'' + 1) - F_2''(J'') \tag{20}$$

$$P_1(J) = \nu_e + \nu_v^{(1)} + F_1'(J'' - 1) - F_1''(J'') \tag{21}$$

$$P_2(J) = \nu_e + \nu_v^{(2)} + F_2'(J'' - 1) - F_2''(J'') \tag{22}$$

where

$$\nu_e = T_e' - T_e'' \tag{23}$$

$$\nu_v^{(n)} = \nu_{v'',v'}^{(n)} = G_n'(v') - G_n''(v'') , \quad n = 1, 2 \tag{24}$$

and

$$F_n(J) = F_n(v,J) = B_v \left\{ \left(J + \frac{1}{2}\right)^2 - 1 + (-1)^n \left[\left(J + \frac{1}{2}\right)^2 - Y_v + Y_v^2/4 \right]^{1/2} \right\}$$
$$- D_v \cdot \begin{cases} J^4 & n = 1 \\[2ex] (J + 1)^4 & n = 2 \end{cases} \tag{25}$$

with B_v and D_v having been calculated with the aid of molecular constants given by Gillette and Eyster[18].

As the $^2\Pi$ states approach case "b," the selection rule $\Delta K = 0, \pm 1$ holds. Also branches with $\Delta K \neq \Delta J$ are very weak. Disregarding Λ-type doubling and neglecting the weak Q branches and satellite branches, we see that the band structure is similar to that of a $^2\Sigma - ^2\Sigma$ transition, i.e., 4 strong branches. If the satellite lines are

17

considered as part of a composite line, but Q branches are still ignored, the intensity factors may be given with sufficient accuracy for our purpose by

$$S_{J''}^{R}{}^2 = S_{J''}^{R}{}^1 = J'' + 1 \tag{26}$$

$$S_{J''}^{P}{}^2 = S_{J''}^{P}{}^1 = J'' \tag{27}$$

and the H factors are then

$$H_{J'',J'} = \frac{4\pi^2 L_o}{3hc} |R_e|^2 \nu_{J'',J'} q(v',v'') S_{J''} \tag{28}$$

The $A^2\Sigma - X^2\Pi$ (Gamma) System of NO

The $X^2\Pi$ state of NO belongs neither strictly to coupling case "a" nor to case "b," but to a transition case which goes from case "a" to case "b" with increasing rotation. However, the $A^2\Sigma$ state belongs strictly to case "b," and as a result of this combination the structure of the NO gamma bands is quite complicated. The $^2\Pi$ state has been discussed previously (see NO Beta system). Figure 6 shows levels and transitions applicable to the NO gamma system.

The general term formula for the $X^2\Pi$ state is given in the preceding discussion of the NO Beta system. The quantum number K has been formally extended to levels having small rotation in the case of the $A^2\Sigma$ state. Rotational terms for this state are given by Eq. (1), where the rotational constants were chosen to agree with experiment[19-20].

Intensity factors for the twelve branches are given (apart from an arbitrary constant) by Earls[21]. These formulas were normalized to obey the sum rule.

After combining branches and satellites and omitting two weak transitions, six

composite lines serve the needs of our calculation. Intensity factors for these

lines are given in Table 1.

Table 1

INTENSITY FACTORS

| Transition and Branch | S_J |

$$P_1(J) = \frac{(2J + 1)^2 + (2J + 1) U(4J^2 + 4J + 1 - 2Y)}{8J}$$

$$R_2(J) = \frac{(2J + 1)^2 + (2J + 1) U(4J^2 + 4J + 1 - 2Y)}{8(J + 1)}$$

$$R_1(J) + {}^R Q_{21}(J) = \frac{2J + 1}{8J} \left\{ 6J - 1 - U(4J^2 + 4J + 1 - 2Y) \right\}$$

$$Q_1(J) + {}^Q P_{21}(J) = \frac{2J + 1}{8(J + 1)} \left\{ 6J + 7 + U(4J^2 + 4J + 1 - 2Y) \right\}$$

$$Q_2(J) + {}^Q R_{12}(J) = \frac{2J + 1}{8J} \left\{ 6J - 1 + U(4J^2 + 4J + 1 - 2Y) \right\}$$

$$P_2(J) + {}^P Q_{12}(J) = \frac{2J + 1}{8(J + 1)} \left\{ 6J + 7 - U(4J^2 + 4J + 1 - 2Y) \right\}$$

where

$$U = \left[Y^2 - 4Y + (2J + 1)^2 \right]^{-1/2}$$

The $H_{J'',J'}$'s for the NO Gamma system are then

$$H_{J'',J'} = \frac{2\pi^2 L_o}{3hc} \nu_{J'',J'} |R_e|^2 q(v',v'') S_{J''}^{\bullet} \qquad (29)$$

where the $S_{J''}^{\bullet}$ are the composite intensity factors described above

19

Spectral Atlases for Air

Digital computer codes (for the IBM 7090) have been constructed to write the magnetic-tape line atlases for the six molecular systems to be included in the calculation. For each system, the spectral lines and their "H" and "E" functions are generated according to vibrational and rotational quantum numbers and labeled by an identification vector. These lines are then merged and sorted according to line frequency. For each spectral line, there are three decimal numbers and one octal number (the identification vector) on tape:

$$\nu \qquad\qquad \alpha \qquad\qquad H_\alpha \qquad E_\alpha$$

$$\text{(frequency)} \qquad \text{(identification vector)}$$

where α is formed of the upper and lower vibrational and rotational quantum numbers, the branch number, and an integer from 1 to 6 which specifies the molecular system to which the line belongs.

The systems, their "key" integer η, and the total number of lines stored on tape for each system are

$\eta = 1$	O_2	Schumann-Runge	13,836
2	N_2	First Positive	58,476
3	N_2	Second Positive	16,750
4	N_2^+	First Negative	21,306
5	NO	Beta	15,760
6	NO	Gamma	25,400
		Total Lines	151,528

20

Table 2 contains basic information pertaining to the band systems. Note that the 4th vibrational level is the highest included for the $C\,^3\Pi_u$ state of N_2. Since the C state is perturbed by another electronic state above the $v' = 4$ level, v' was not extended to higher values.* A further restriction on v' and v'' (as well as on J' and J'') is that the total vibrational and rotational energy of any level was not permitted to exceed the dissociation energy for the state.

Table 2
BAND SYSTEM PARAMETERS

Molecule and Transition	v'_{max}	v''_{max}	Number of Bands Included	f-number	$\|R_e\|^2$ $(\times 10^{-36})$	Range (10^3 cm^{-1})
$O_2\ B\,^3\Sigma_u^-\ -\ X\,^3\Sigma_g^-$	20	19	217	0.048	3.29	21.5−50.0
$N_2\ B\,^3\Pi_g\ -\ A\,^3\Sigma_u^+$	10	11	66	0.02	3.34	1.97−19.5
$N_2\ C\,^3\Pi_u\ -\ B\,^3\Pi_g$	4	10	34	0.07	4.6	21.5−36.4
$N_2^+\ B\,^2\Sigma_u^+\ -\ X\,^2\Sigma_g^+$	17	18	106	0.0348	2.85	14.9−32.8
$NO\ B\,^2\Pi\ -\ X\,^2\Pi$	6	16	40	0.008	0.7	17.3−49.5
$NO\ A\,^2\Sigma\ -\ X\,^2\Pi$	7	16	55	0.0025	0.14	31.0−50.0

Equation (1) was used to fairly high J (~100). The extent to which this formula fails at high J is not known, but it is felt that accuracy is only fair at $J = 80$.

---

*Weak bands observed by Y. Tanaka and A. S. Jursa [22] have been identified as $v' = 5$ bands.

21

In addition to the individual system line atlases, a tape consisting of all the systems merged according to frequency has been written. This merged tape, containing all 151,528 lines, will serve as the spectral line atlas for air. By masking techniques, the origin of each line may be found from its identification vector, i.e., its species, lower level, etc. To compute the absorption coefficient, the atlas tapes must be used in conjunction with population numbers and partition functions corresponding to the desired air temperature and density. Population factors may be obtained by interpolating in the tables of Gilmore[23]. The vibration-rotation partition functions are given, with sufficient accuracy for our problem, in Table 3.

Table 3

PARTITION FUNCTIONS

Molecule and State	Vibration-Rotation Partition Functions
$O_2 \; X \; {}^3\Sigma_g^-$	$Q_1(T) = \dfrac{0.4834 \; T(1 + 0.0000149 \; T)}{1 - \exp(-2256/T)}$
$N_2 \; A \; {}^3\Sigma_u^+$	$Q_2(T) = \dfrac{0.48468 \; T(1 + 0.0000174 \; T)}{1 - \exp(-2081.2/T)}$
$N_2 \; B \; {}^3\Pi_g$	$Q_3(T) = \dfrac{0.42670 \; T(1 + 0.0000144 \; T)}{1 - \exp(-2474/T)}$
$N_2^+ \; X \; {}^2\Sigma_g^+$	$Q_4(T) = \dfrac{0.3617 \; T(1 + 0.0000102 \; T)}{1 - \exp(-3152.5/T)}$
$NO \; X \; {}^2\Pi$	$Q_5(T) = \dfrac{0.4098 \; T(1 + 0.0000119 \; T)}{1 - \exp(-2719/T)}$

All of the Franck-Condon factors used in the atlas construction are from R. W. Nicholls[5-7]. The electronic f-values were taken from Treanor and Wurster (O_2 Schumann-Runge), Bennett and Dalby[25] (N_2^+ First Negative), and the compilation of Meyerott et al.[2] (remaining band systems).

IV. RADIATION TRANSPORT AND MEAN ABSORPTION COEFFICIENTS

One manner in which the spectral atlas for air has been utilized is in the numerical determination of some mean absorption coefficients for application in radiation transport problems. These coefficients and the method of their determination will now be discussed.

Radiation Transport

The radiative transfer of energy in a medium can be calculated if one knows the intensity of radiation I_ν as a function of position and time, direction of ray and frequency. Along a given ray, I_ν changes in a manner which is determined by emission and absorption of the radiation by the material through which it passes. Such changes are calculated from the equation of transfer. If the material is in local thermodynamic equilibrium, the equation of transfer is

$$\frac{dI_\nu}{ds} = \mu'_\nu (B_\nu - I_\nu) \tag{1}$$

where s denotes the length measured along the ray,

$$\mu'_\nu = \rho \kappa'_\nu = \rho \kappa_\nu (1 - e^{-h\nu/kT}) \tag{2}$$

is defined in terms of the absorption coefficient $\kappa_\nu(\rho, T)$ and

$$B_\nu(T) = \frac{2h\nu^3}{c^2} (e^{h\nu/kT} - 1)^{-1} \tag{3}$$

23

is Planck's blackbody distribution function. The primed coefficients differ from the unprimed ones by a factor $(1 - e^{-h\nu/kT})$. This distinction arises because of the presence of the so-called induced emission. Since that term is proportional to I_ν, it is convenient to subtract it from the absorption $\mu_\nu I_\nu$ and denote the difference, which appears on the right-hand side of Eq. (1) as $\mu_\nu' I_\nu$.

The integration of Eq. (1) is formally straightforward and leads to

$$I_\nu(s_1) = e^{-\tau_\nu(s_1)} \left(I_\nu(s_0) + \int_{s_0}^{s_1} B_\nu(s) \, e^{-\tau_\nu} \, d\tau_\nu \right) \tag{4}$$

where

$$\tau_\nu = \int_{s_0}^{s} \mu_\nu'(s^*) \, ds^* \tag{5}$$

If I_ν has been calculated for all rays going through a given point, the integral over all directions and frequencies

$$\dot{Q} = \iint \left(-\frac{dI_\nu}{ds} \right) d\Omega \, d\nu = \int \mu_\nu' \int (I_\nu - B_\nu) \, d\Omega \, d\nu \tag{6}$$

is the difference between absorbed and emitted power per unit volume and it determines the net rate of heating of the material.

The formal simplicity of the above program of calculation is unfortunately misleading because the numerical work is generally prohibitive. The difficulty lies in the fact that the optical properties of air in the temperature range covered by this

article result mainly from transitions between molecular levels. The spectrum associated with the major band systems consists of an enormous number of lines and the absorption coefficient fluctuates from large values at the line centers to small ones between the lines. Because of these "windows" the radiation at some point generally comes from points along the ray which are an appreciable distance further back. The frequency dependence of the distance and with it I_ν fluctuates just as strongly as μ'_ν. One can define an absorption coefficient which varies smoothly with ν by forming the average

$$\overline{\mu'_\nu} = \frac{1}{\Delta\nu} \int_\nu^{\nu+\Delta\nu} \mu'_\nu \, d\nu \tag{7}$$

where $\Delta\nu$ is chosen to be large compared to the width of individual lines but narrow enough to contain only a few strong lines. Similarly one can define a smoothly varying average $\overline{I_\nu}$. When one uses these averages one must, however, be very careful because the quantities μ'_ν and I_ν fluctuate so strongly that it is obviously a poor approximation to replace the average product $\overline{\mu'_\nu I_\nu}$ by the product $\overline{\mu'_\nu}\ \overline{I_\nu}$. It is for example, not correct to determine $\overline{I_\nu}$ by direct integration of Eq. (1) with $\overline{\mu'_\nu}$ in place of μ'_ν. Instead, it is in principle necessary to integrate Eq. (1) at all frequencies to obtain a detailed spectral distribution before one can calculate averages.

There are two limiting situations where this enormous amount of computation can be avoided. The one situation arises when I_ν is very much smaller than B_ν which can only happen for a transparent medium, i.e., if $\mu'_\nu L$ (L being the size of the radiating region) is uniformly small compared to unity. In that case one can

neglect the absorption and one obtains

$$\dot{Q} = -4\pi \int_0^\infty \mu_\nu' B_\nu \, d\nu \qquad (8)$$

By introducing the so-called Planck mean absorption coefficient

$$\overline{\mu_p} = \frac{\int \mu_\nu' B_\nu \, d\nu}{B(t)} \qquad (9)$$

where

$$B(T) = \int_0^\infty B_\nu(T) \, d\nu = \frac{\sigma T^4}{\pi} \qquad (10)$$

this can be written as

$$\dot{Q} = 4\overline{\mu_p}\sigma T^4 \qquad (11)$$

In the opposite extreme of an opaque region for which $\mu_\nu' l \gg 1$ one can also simplify Eq. (6). The length l in this relation is the size of the region where the optical properties change by less than say 5 percent and the inequality is supposed to be valid at those frequencies where B_ν contributes significantly to B. For an opaque region the transfer of radiation is most conveniently treated in the diffusion approximation. This approximation follows from the observation that I_ν is almost equal to B_ν which leads to an approximation where one replaces I_ν on the left-hand side

of Eq. (1) by B_ν so that

$$I_\nu = B_\nu - \frac{1}{\mu_\nu'} \frac{dB_\nu}{ds} \tag{12}$$

The derivative $\dfrac{dB_\nu}{ds} = \dfrac{dB_\nu}{dT} \dfrac{dT}{ds}$ adds a small anisotropic contribution to the isotropic B_ν so that the energy flow in different directions does not completely cancel out. There is therefore a flux

$$\vec{F} = - \frac{4\pi}{3} \frac{1}{\overline{\mu}_R} \vec{\nabla} B \tag{13}$$

where

$$\frac{1}{\overline{\mu}_R} = \frac{\displaystyle\int_0^\infty \frac{1}{\mu_\nu'} \frac{dB_\nu}{dT} d\nu}{\displaystyle\int_0^\infty \frac{dB_\nu}{dT} d\nu} \tag{14}$$

defines the so-called Rosseland mean absorption coefficient $\overline{\mu}_R$. The rate of radiative heating now becomes

$$\dot{Q} = - \vec{\nabla} \cdot \vec{F} = \frac{4\sigma}{3} \vec{\nabla} \cdot \left(\frac{1}{\overline{\mu}_R} \vec{\nabla} T^4 \right) \tag{15}$$

With an absorption coefficient which varies between very large and very small values neither the averaging procedure of Eq. (9) nor that of Eq. (14) is justified. It is therefore necessary to find other methods for reducing the labor to a reasonable level.

27

The Sampling Method

The average intensity of radiation in high temperature air appears to change quite slowly with wave length. This suggests that it may be sufficient to solve the transport equation in a few sample intervals of the spectrum whose widths are large compared to the width of individual lines but small enough to contain only a few strong lines. After performing the transport calculations to find I_{ν_i} at a large number n (say 100) of evenly spaced frequencies ν_i in that interval one can use these to obtain a meaningful average $\overline{I_\nu} = \frac{1}{n}\sum I_{\nu_i}$ for the sample interval. Calculations of this type form an important part of this paper and are discussed in a later subsection.

Grouping of Intensities (Part 1)

One can imagine that the frequencies ν_i in a small interval from ν to $\nu + \Delta\nu$ have been arranged into groups a, b, c, etc. where the absorption coefficients of group a are all larger than those of group b, which are in turn larger than in group c, etc. There will now be less of a spread between the absorption coefficients within each group than between all of them.

The intensities within each group are also showing much less spread. This follows because the intensity at some point along a ray reflects the conditions existing approximately one mean free path $(\mu'_\nu)^{-1}$ behind so that a small spread in μ'_ν implies that the points of origin lie closely together.

If one defines averages within each group, i.e., $\overline{\mu'_a}$, $\overline{\mu'_b}$, ... and $\overline{I_a}$, $\overline{I_b}$, ... it is now quite reasonable to approximate the average products by products of the averages like

$$\overline{\mu'_a I_a} \approx \overline{\mu'_a}\, \overline{I_a} \tag{16}$$

25

etc. It is therefore reasonable to assume that the average intensities obey separate transport equations like

$$\frac{d\overline{I_a}}{ds} = \overline{\mu_a'}(B_\nu - \overline{I_a}) \tag{17}$$

If there are k groups, the heating term $\mu_\nu' I_\nu$ in Eq. (6) can be replaced by

$$\frac{1}{k}(\overline{\mu_a'}\,\overline{I_a} + \overline{u_b'}\,\overline{I_b} + \overline{\mu_c'}\,\overline{I_c} + \dots) \tag{18}$$

It is actually a fairly good approximation to use only two groups.

An Average Transmission Calculation

Consider a frequency interval $\Delta \nu$ which is small enough that gross radiation transport features do not change appreciably over the interval, yet is large enough to contain-many lines (say ~ 200). Let ν_j denote a fixed frequency point within the interval and let α label a line whose maximum lies within that same interval. A transmission point function may then be defined for an isothermal, homogeneous slab of thickness x :

$$Tr(\nu_j) = \exp\left\{-\left[\sum_\alpha \mu_\alpha'(\nu_j) + \mu_c'(\nu_j)\right] x\right\} \tag{19}$$

where the summation is taken over all lines which contriubte significantly at ν_j . In the above expression, μ_c is an absorption coefficient containing continuum contributions as well as other effects not included in the spectral calculation (i.e., contributions from polyatomic molecules).

The average transmission through the slab for a frequency interval $\Delta \nu$ centered at frequency ν may then be written

$$\overline{Tr}^{\Delta\nu}(\nu) = \frac{1}{\Delta\nu} \int_{\Delta\nu} \exp\left\{-\left[\sum_\alpha \mu_\alpha'(\nu) + \mu_c(\nu)\right] x\right\} d\nu \tag{20}$$

29

Thus far, results have been obtained only for the case where $\mu_c = 0$, and so we now omit it from the equations. An approximation to the integral is made by evaluating the argument at many points in $\Delta\nu$ and utilizing the trapezoidal integration scheme.

An average absorption coefficient may now be defined through the relation

$$e^{-\overline{\mu}(\nu)x} = \overline{Tr}^{\Delta\nu}(\nu) \tag{21}$$

Deleting superscripts we obtain

$$\overline{\mu}(\nu) = -\frac{\log_e \overline{Tr}(\nu)}{x} \tag{22}$$

The sum over α may include line contributions from several molecular species. Only in the optically thin case can an average absorption coefficient for air be obtained by summing average absorption coefficient contributions from the individual species. The present calculation is not restricted to any particular opacity region. Based on the preceding equations, a digital computer code was written to calculate the average transmission of optical radiation through an isothermal, homogeneous slab of heated air. Variable parameters in the calculation are the air composition and electronic population, slab temperature T, line half width σ, basic frequency intervals, and the number of frequency points on the line wings.

Results have been obtained for temperatures from $1,000°$ K to $12,000°$ K and densities from atmospheric normal to 10^{-4} that of normal. Thus far a value of 1 cm^{-1} for σ has been used consistently for all calculations with the exception of a parameter study for oxygen.

Intervals of 100 cm^{-1} size were picked at 2,000 cm^{-1} spacing except for the density case $\frac{\rho}{\rho_0} = 10^{-1}$, where double the usual number of intervals was calculated.

Sample curves from the results are presented in Figs. 7-91. Smooth curves have been drawn through the computed points, which fall at 2,000 cm^{-1} intervals from 49,500 cm^{-1} on down. (Except the case where $\frac{\rho}{\rho_0} = 10^{-1}$, as was previously mentioned.)

Grouping of Intensities (Part 2)

One way of calculating two group absorption coefficients utilizes the results on transmission which are obtained by means of the sampling method. After obtaining the transmission through a plane slab, one can fit its dependence on the slab thickness x by the expression

$$Tr(x) = \frac{1}{2}\left(e^{-\mu'_a x} + e^{-\mu'_b x}\right) \tag{23}$$

To show the accuracy of this fit, we compare the x-dependence of the effective absorption coefficient

$$\bar{\mu} = -\frac{\log_e \overline{Tr}}{x} \tag{24}$$

as calculated from the slab calculation and from the formula of Eq. (23).

31

Table 4. Comparison of calculated and fitted values of the effective absorption coefficient for a typical case $T = 5,000°K$, $\nu = 25,500$ cm^{-1}, $\rho/\rho_0 = 1.0$

x (cm)	4	8	16	32	64	128	256	512	1024
$10^5 \mu_{calc}$	685	683	678	670	653	622	568	488	395
$10^5 \mu_{fit}$	681	680	676	670	653	622	569	495	434

The differences at large values of x are not important because the transmission is negligible in that case.

Some tables of μ_a and μ_b for various cases follow the sample curves from the average transmission calculation.

Continuum Contributions

Inclusion of the continuum in the calculations awaits a more accurate analysis of the various effects that are involved. For the readers convenience, however, a means of including any desired contribution will be indicated.

Returning to Eq. (20) and assuming μ_c to be a slowly varying function of frequency over the interval $\Delta\nu$, we obtain as an approximation

$$\overline{Tr}^{\Delta\nu}(\nu) = \frac{e^{-\mu_c(\nu)x}}{\Delta\nu} \int\limits_{\Delta\nu} \exp\left\{-\left[\sum_\alpha \mu'_\alpha(\nu)\right]x\right\} d\nu \tag{25}$$

By applying Eq. (22) the total average absorption coefficient is given by

$$\overline{\mu}(\nu) = \overline{\mu}_c(\nu) + \overline{\mu}_l(\nu) \tag{26}$$

32

where ℓ labels that part of the absorption coefficient arising from the lines. The same procedure can be followed when one is using the two group absorption coefficients. The corresponding equations are

$$\mu_a' = \overline{\mu_c} + \mu_{a\ell}' \tag{27}$$

and

$$\mu_b' = \overline{\mu_c} + \mu_{b\ell}' \tag{28}$$

where the label ℓ has been affixed to those coefficients that were calculated when continuum processes were omitted.

Photodetachment of O^-, inverse bremsstrahlung, and the O_2 Schumann-Runge continuum are among the contributors to the continuous absorption coefficient. In addition, important polyatomic line transitions might be best handled by empirical means as a part of the continuum. One known important polyatomic contributor which is receiving special attention is NO_2. All these will eventually be integrated into the calculations.

Discussion of Sample Results

Sample curves of T vs. X in Figs. $7-38$ exhibit the smooth behavior that allows the two-group approximation to be a fairly good one. As the temperature is raised and density lowered, however, some of the complicated frequency dependence shows up in the crossing of these curves, for which frequency is a parameter. Figures $39-70$ present the same sort of results in a different fashion, i.e., in the form of an average absorption coefficient.

33

Influenced by the sensitivity of the fractional species concentrations and electronic level populations to changes in temperature (and density),the frequency dependence of the transmission becomes very complicated above 3,000°K at densities 10^{-1} normal atmospheric and below. The predominant absorption system at temperatures from 1,000 to 3,000°K is the O_2 Schumann-Runge system which is strongest in the higher frequency regions, i.e., about 30,000 cm^{-1} on up. At 3,000°K, NO starts to contribute appreciably and increases in importance as the temperature increases. A very important constituent at the higher temperatures (6,000 to 8,000°K) is N_2^+, whose first negative system exhibits a strong peak and valley behavior which is apparent in the lower density plots.

More points were computed for the density case $\rho/\rho_0 = 10^{-1}$, leading to lower energy information not on the other graphs. In particular, the point at 18,500 cm^{-1} shows a relatively more opaque region. This is apparently the high-energy end of the N_2 first-positive contribution and is to be expected, according to the work of Meyerott, Sokoloff, and Nicholls[2].

Where gross energy transfer is being considered, it must be remembered that the vibration-rotation spectrum of NO, which is especially important at lower frequencies for temperatures up to 3,000°K, has not yet been included in the calculations, and therefore is not contained in these results.

Table 5

TWO-GROUP ABSORPTION COEFFICIENTS

$T = 5000°$ K

$\rho/\rho_o =$

Frequency (cm⁻¹)	1.0		10^{-1}		10^{-2}		10^{-4}	
	μ_a	μ_b	μ_a	μ_b	μ_a	μ_b	μ_a	μ_b
19500	1.92^{-4}	3.54^{-5}	4.05^{-6}	7.95^{-7}	2.84^{-8}	5.74^{-8}		
21500	1.22^{-3}	4.34^{-4}	2.56^{-5}	9.37^{-6}	1.75^{-6}	$6.28{-7}$		
23500	3.93^{-3}	1.38^{-3}	7.06^{-5}	2.73^{-5}	4.61^{-6}	1.64^{-6}		
25500	1.00^{-2}	3.66^{-3}	1.61^{-4}	6.07^{-5}	9.61^{-6}	3.32^{-6}	1.82^{-8}	1.45^{-9}
27500	1.76^{-2}	5.84^{-3}	2.83^{-4}	1.06^{-4}	1.68^{-5}	6.07^{-6}	1.40^{-8}	5.03^{-9}
29500	4.06^{-2}	1.52^{-2}	6.54^{-4}	2.68^{-4}	3.90^{-5}	1.51^{-5}	3.21^{-8}	1.19^{-8}
31500	4.49^{-2}	1.53^{-2}	6.95^{-4}	2.55^{-4}	4.04^{-5}	1.35^{-5}	3.17^{-8}	1.01^{-8}
33500	8.31^{-2}	3.27^{-2}	1.30^{-3}	5.62^{-4}	7.54^{-5}	3.12^{-5}	5.94^{-8}	2.35^{-8}
35500	1.43^{-1}	6.42^{-2}	2.44^{-3}	1.05^{-3}	1.51^{-4}	5.65^{-5}	1.23^{-7}	4.34^{-8}
37500	2.24^{-1}	7.94^{-2}	3.40^{-3}	1.25^{-3}	1.94^{-4}	6.47^{-5}	1.52^{-7}	4.60^{-8}
39500	3.34^{-1}	1.02^{-1}	5.32^{-3}	1.57^{-3}	$3.2?^{-4}$	7.58^{-5}	2.49^{-7}	5.71^{-8}
41500	5.39^{-1}	2.15^{-1}	8.91^{-3}	3.44^{-3}	5.42^{-4}	1.82^{-4}	4.31^{-7}	1.37^{-7}
43500	6.87^{-1}	2.57^{-1}	1.13^{-2}	4.34^{-3}	6.70^{-4}	2.47^{-4}	5.37^{-7}	1.87^{-7}
45500	9.95^{-1}	4.63^{-1}	1.71^{-2}	8.07^{-3}	1.06^{-3}	4.65^{-5}	8.61^{-7}	3.62^{-7}
47500	1.09	3.90^{-1}	1.75^{-2}	6.45^{-3}	1.03^{-3}	3.59^{-4}	8.30^{-7}	2.63^{-7}
49500	1.38	6.70^{-1}	2.37^{-2}	1.19^{-2}	1.45^{-3}	6.97^{-4}	1.18^{-6}	5.42^{-7}

Table 5 (Cont.)

$$T = 6000° \text{ K}$$

$$\rho/\rho_0 =$$

Frequency (cm^{-1})	1.0		10^{-1}		10^{-2}		10^{-4}	
	μ_a	μ_b	μ_a	μ_b	μ_a	μ_b	μ_a	μ_b
19500	5.07^{-4}	1.08^{-4}	9.63^{-6}	2.33^{-6}	3.50^{-25}	2.12^{-26}		
21500	2.44^{-3}	8.93^{-4}	4.27^{-5}	1.61^{-5}	7.58^{-22}	7.92^{-23}	2.47^{-8}	5.37^{-9}
23500	5.68^{-3}	2.26^{-3}	9.48^{-5}	3.88^{-5}	1.01^{-17}	5.08^{-19}	9.23^{-8}	1.22^{-8}
25500	1.13^{-2}	4.36^{-3}	1.81^{-4}	6.86^{-5}	1.10^{-15}	1.33^{-16}	2.13^{-8}	1.72^{-9}
27500	1.81^{-2}	7.01^{-3}	2.85^{-4}	1.08^{-4}	2.66^{-15}	1.08^{-17}	1.29^{-8}	4.22^{-9}
29500	3.61^{-2}	1.50^{-2}	5.59^{-4}	2.27^{-4}	$3.44^{-1?}$	1.64^{-15}	2.99^{-8}	1.40^{-8}
31500	3.76^{-2}	1.34^{-2}	5.71^{-4}	1.94^{-4}	2.49^{-12}	1.49^{-13}	1.79^{-8}	6.30^{-9}
33500	6.32^{-2}	2.77^{-2}	9.63^{-4}	4.12^{-4}	1.21^{-10}	4.97^{-12}	1.99^{-8}	8.01^{-9}
35500	1.05^{-1}	4.57^{-2}	1.71^{-3}	6.50^{-4}	1.12^{-9}	9.92^{-11}	3.99^{-8}	1.50^{-8}
37500	1.42^{-1}	5.08^{-2}	2.11^{-3}	7.11^{-4}	1.51^{-8}	3.50^{-9}	4.32^{-8}	1.33^{-8}
39500	2.04^{-1}	6.12^{-2}	3.12^{-3}	8.62^{-4}	1.15^{-7}	1.79^{-8}	6.52^{-8}	1.58^{-8}
41500	3.15^{-1}	1.24^{-1}	4.92^{-3}	1.80^{-3}	8.73^{-7}	5.24^{-8}	1.03^{-7}	3.47^{-8}
43500	3.79^{-1}	1.47^{-1}	5.87^{-3}	2.25^{-3}	4.12^{-6}	5.88^{-7}	1.22^{-7}	5.40^{-8}
45500	5.33^{-1}	2.47^{-1}	8.56^{-3}	3.78^{-3}	2.69^{-5}	3.81^{-6}	1.82^{-7}	7.61^{-8}
47500	5.23^{-1}	1.88^{-1}	8.08^{-3}	2.79^{-3}	1.46^{-4}	1.30^{-5}	1.69^{-7}	5.38^{-8}
49500	6.45^{-1}	3.20^{-1}	1.04^{-2}	4.97^{-3}	8.41^{-4}	1.10^{-4}	2.20^{-7}	1.01^{-7}

Table 5 (Cont.)

$$T = 7000° K$$

$$\rho/\rho_o =$$

Frequency (cm^{-1})	1.0		10^{-1}		10^{-2}		10^{-4}	
	μ_a	μ_b	μ_a	μ_b	μ_a	μ_b	μ_a	μ_b
19500	1.02^{-3}	2.74^{-4}	2.18^{-5}	7.14^{-6}	2.30^{-6}	9.34^{-7}		
21500	3.55^{-3}	1.33^{-3}	6.32^{-5}	2.69^{-5}	1.02^{-5}	3.19^{-6}	2.39^{-8}	5.26^{-9}
23500	7.35^{-3}	2.90^{-3}	1.49^{-4}	6.44^{-5}	3.12^{-5}	7.44^{-6}	7.48^{-8}	1.30^{-8}
25500	1.30^{-2}	5.06^{-3}	3.11^{-4}	6.94^{-5}	3.51^{-5}	1.78^{-6}	2.10^{-8}	1.27^{-9}
27500	1.88^{-2}	7.63^{-3}	2.95^{-4}	1.26^{-4}	1.91^{-5}	8.16^{-6}	1.19^{-8}	2.61^{-9}
29500	3.29^{-2}	1.37^{-2}	4.92^{-4}	2.10^{-4}	3.27^{-5}	1.57^{-5}	3.24^{-8}	1.34^{-8}
31500	3.33^{-2}	1.12^{-2}	4.76^{-4}	1.61^{-4}	2.57^{-5}	9.25^{-6}	1.20^{-8}	3.54^{-9}
33500	5.12^{-2}	2.23^{-2}	7.03^{-4}	3.00^{-4}	3.29^{-5}	1.35^{-5}	4.97^{-9}	2.04^{-9}
35500	8.30^{-2}	3.33^{-2}	1.22^{-3}	4.82^{-4}	6.36^{-5}	2.43^{-5}	1.05^{-8}	4.10^{-9}
37500	1.00^{-1}	3.48^{-2}	1.37^{-3}	4.53^{-4}	6.33^{-5}	2.03^{-5}	9.68^{-9}	3.00^{-9}
39500	1.44^{-1}	3.85^{-2}	1.92^{-3}	5.31^{-4}	9.23^{-5}	2.25^{-5}	1.38^{-8}	3.44^{-9}
41500	2.06^{-1}	7.97^{-2}	2.87^{-3}	1.06^{-3}	1.36^{-4}	4.70^{-5}	2.06^{-8}	7.14^{-9}
43500	2.41^{-1}	9.13^{-2}	3.31^{-3}	1.27^{-3}	1.56^{-4}	5.71^{-5}	2.36^{-8}	8.69^{-9}
45500	3.25^{-1}	1.45^{-1}	4.58^{-3}	1.98^{-3}	2.14^{-4}	9.07^{-5}	3.27^{-8}	1.36^{-8}
47500	2.99^{-1}	1.06^{-1}	4.15^{-3}	1.42^{-3}	1.94^{-4}	6.46^{-5}	2.91^{-8}	9.87^{-9}
49500	3.58^{-1}	1.73^{-1}	5.06^{-3}	2.39^{-3}	2.37^{-4}	1.10^{-4}	3.60^{-8}	1.66^{-8}

Table 5 (Cont.)

$$T = 8000° K$$

$$\rho/\rho_o =$$

Frequency (cm^{-1})	1.0		10^{-1}		10^{-2}		10^{-4}	
	μ_a	μ_b	μ_a	μ_b	μ_a	μ_b	μ_a	μ_b
19500	1.95^{-3}	6.00^{-4}	4.78^{-5}	1.72^{-5}	3.42^{-6}	1.49^{-6}		
21500	4.26^{-3}	1.79^{-3}	1.29^{-4}	4.85^{-5}	1.60^{-5}	4.52^{-6}	1.79^{-8}	4.44^{-9}
23500	9.01^{-3}	4.18^{-3}	3.55^{-4}	1.12^{-4}	4.98^{-5}	8.87^{-6}	5.56^{-8}	8.58^{-9}
25500	1.82^{-2}	5.76^{-3}	4.45^{-4}	9.14^{-5}	3.68^{-5}	2.01^{-6}	2.04^{-8}	1.10^{-9}
27500	2.01^{-2}	8.92^{-3}	3.61^{-4}	1.54^{-4}	2.02^{-5}	6.65^{-6}	1.11^{-8}	1.88^{-9}
29500	3.01^{-2}	1.31^{-2}	5.42^{-4}	2.57^{-4}	3.81^{-5}	1.80^{-5}	3.21^{-8}	1.30^{-8}
31500	2.85^{-2}	9.90^{-3}	4.12^{-4}	1.49^{-4}	1.93^{-5}	6.60^{-6}		
33500	3.79^{-2}	1.64^{-2}	4.46^{-4}	1.89^{-4}	1.35^{-5}	5.68^{-6}		
35500	6.47^{-2}	2.61^{-2}	9.02^{-4}	3.58^{-4}	3.10^{-5}	1.22^{-5}		
37500	6.86^{-2}	2.29^{-2}	7.92^{-4}	2.63^{-4}	2.42^{-5}	7.73^{-6}		
39500	9.30^{-2}	2.56^{-2}	1.10^{-3}	2.88^{-4}	3.30^{-5}	8.74^{-6}		
41500	1.31^{-1}	4.92^{-2}	1.53^{-3}	5.77^{-4}	4.70^{-5}	1.70^{-5}		
43500	1.47^{-1}	5.61^{-2}	1.74^{-3}	6.52^{-4}	5.26^{-5}	1.98^{-5}		
45500	1.91^{-1}	8.34^{-2}	2.27^{-3}	9.71^{-4}	6.93^{-5}	2.91^{-5}		
47500	1.69^{-1}	6.07^{-2}	2.01^{-3}	6.95^{-4}	6.04^{-5}	2.12^{-5}		
49500	1.97^{-1}	9.41^{-2}	2.34^{-3}	1.11^{-3}	7.13^{-5}	3.33^{-5}		

38
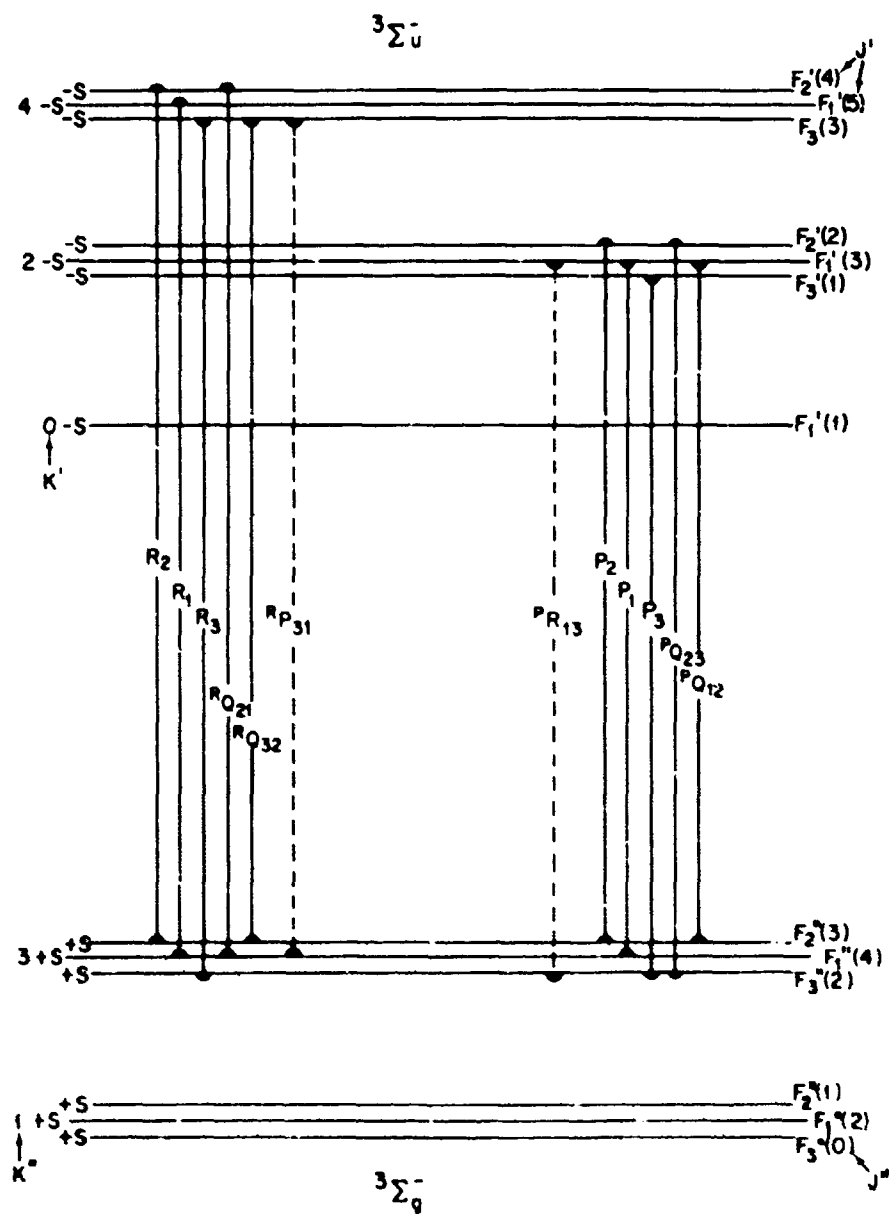
Fig. 1 B $^3\Sigma_u^-$ – X $^3\Sigma_g^-$ Band of O_2 (Schumann-Runge system)

39
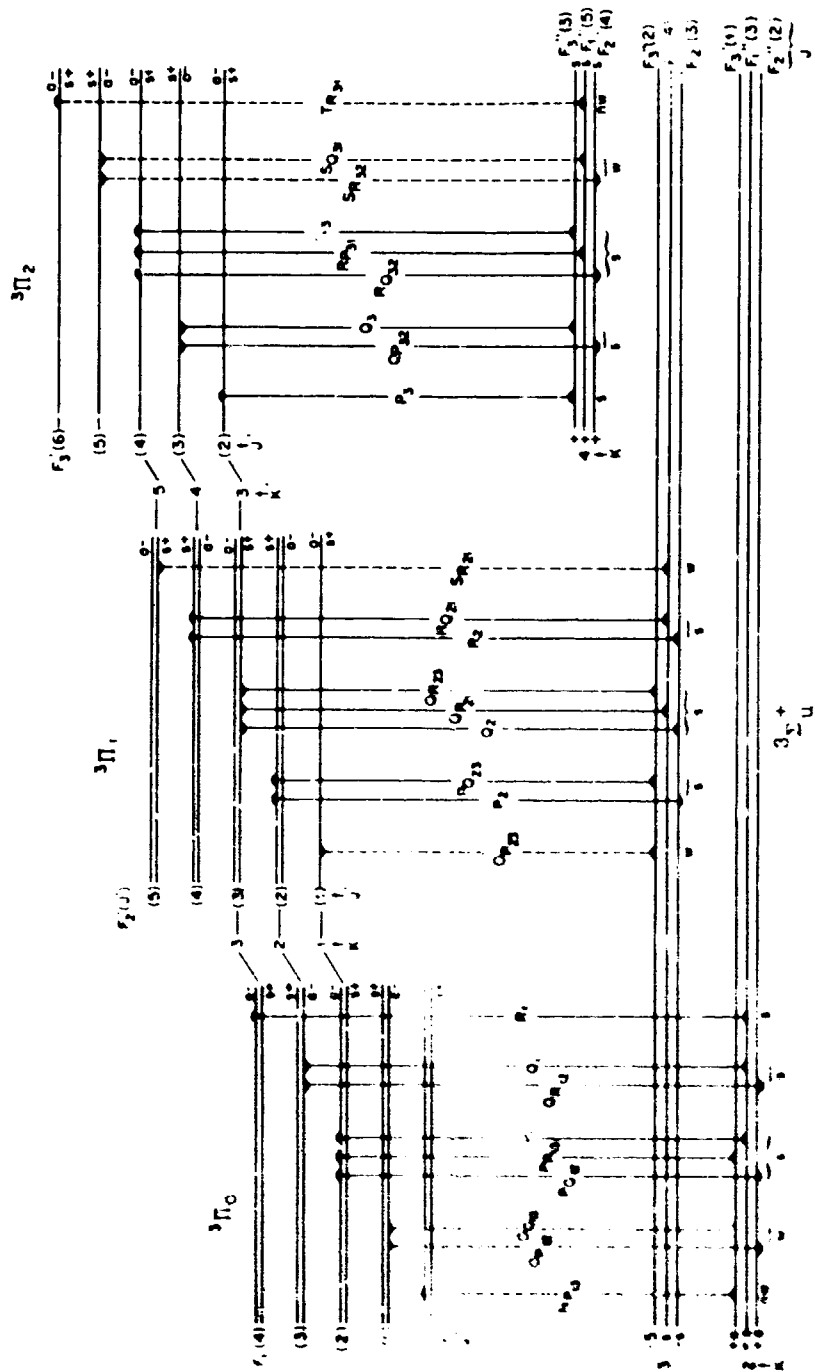
Fig. 2 B $^3\Pi_g$ — A $^3\Sigma_u^+$ Band of N_2 (First positive system)
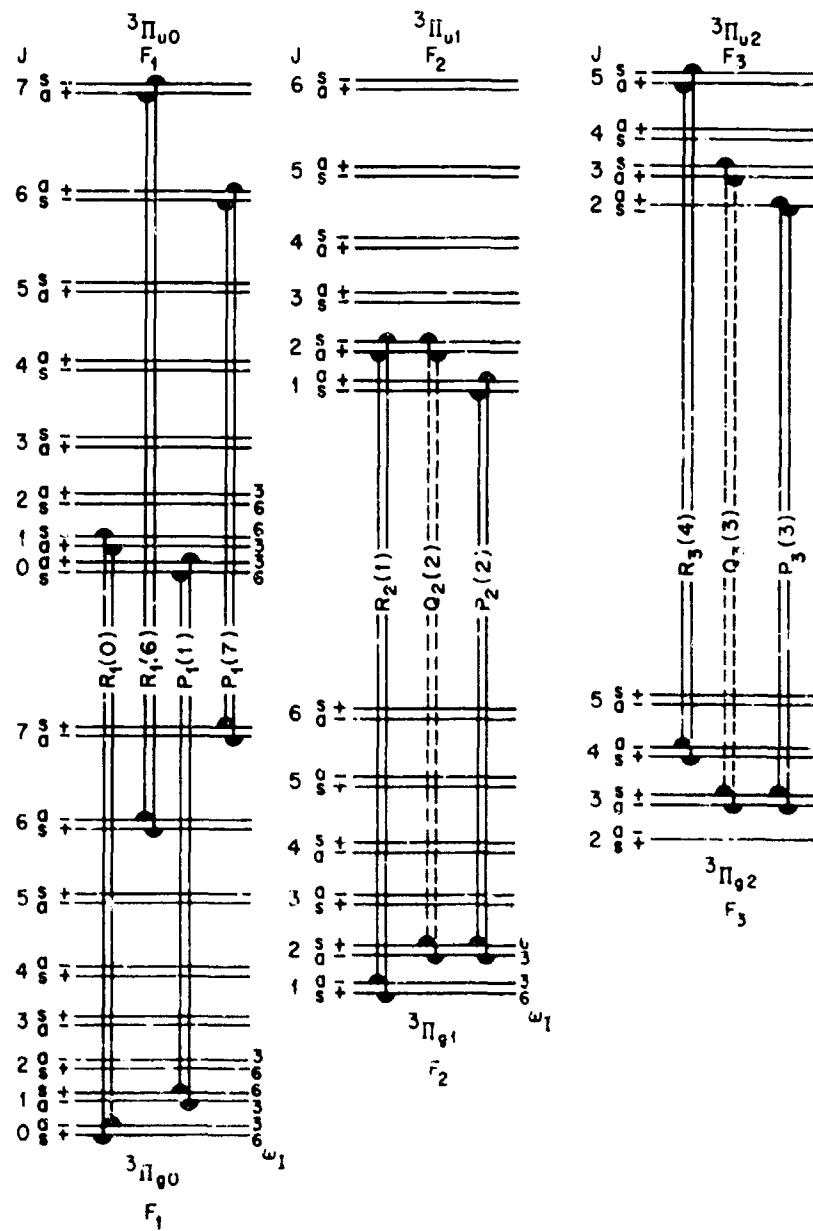
Fig. 3   C $^3\Pi_u$ – B $^3\Pi_g$ Band of N_2 (Second positive system)

41
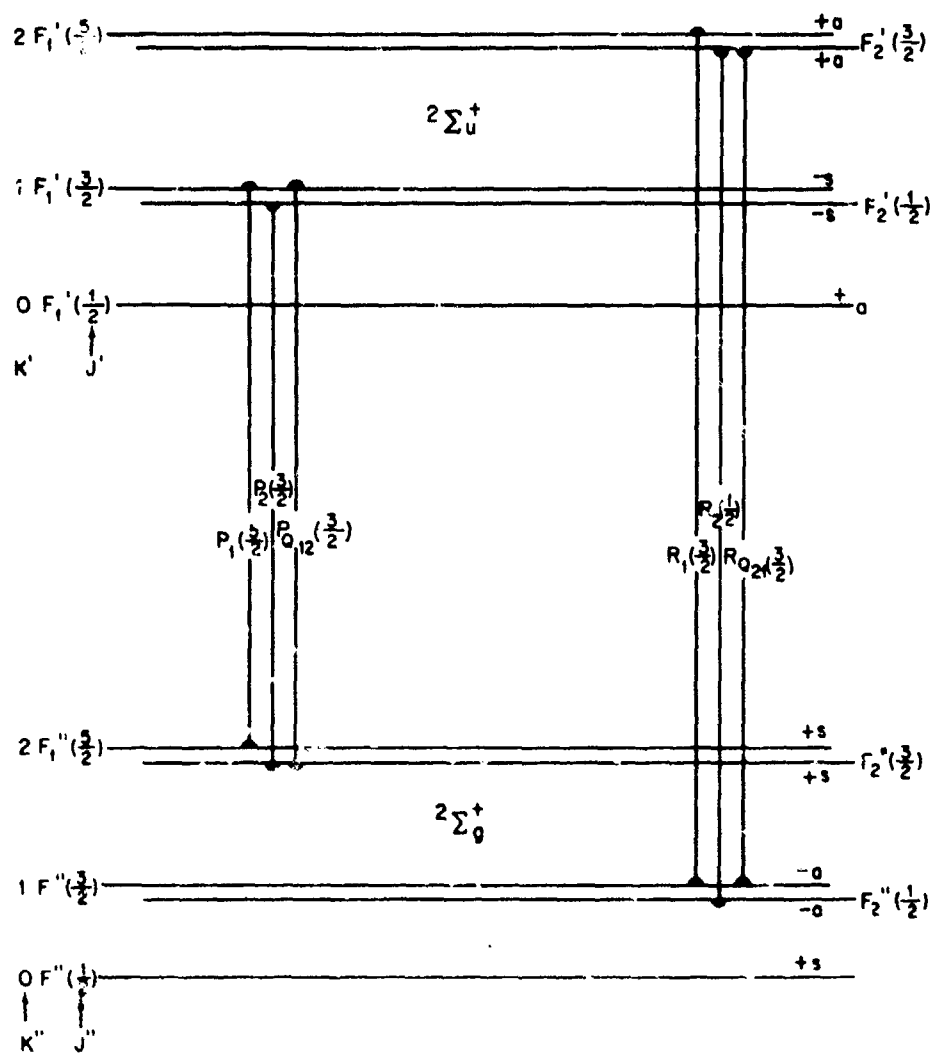
Fig. 4 B $^2\Sigma_u^+$ – X $^2\Sigma_g^+$ Band of N_2^+ (First negative system)

Fig. 5   B $^2\Pi$ – X $^2\Pi$ Band of NO (Beta system)

43
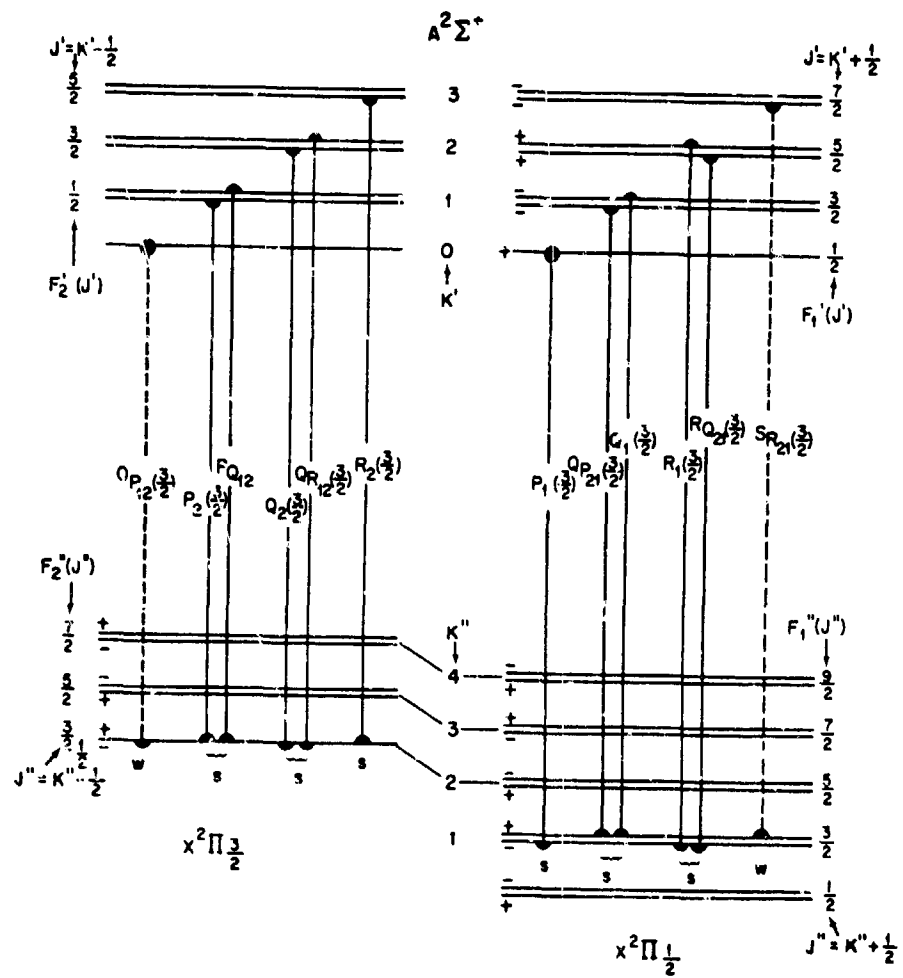
Fig. 6 A $^2\Sigma$ – X $^2\Pi$ Band of NO (Gamma system)

44
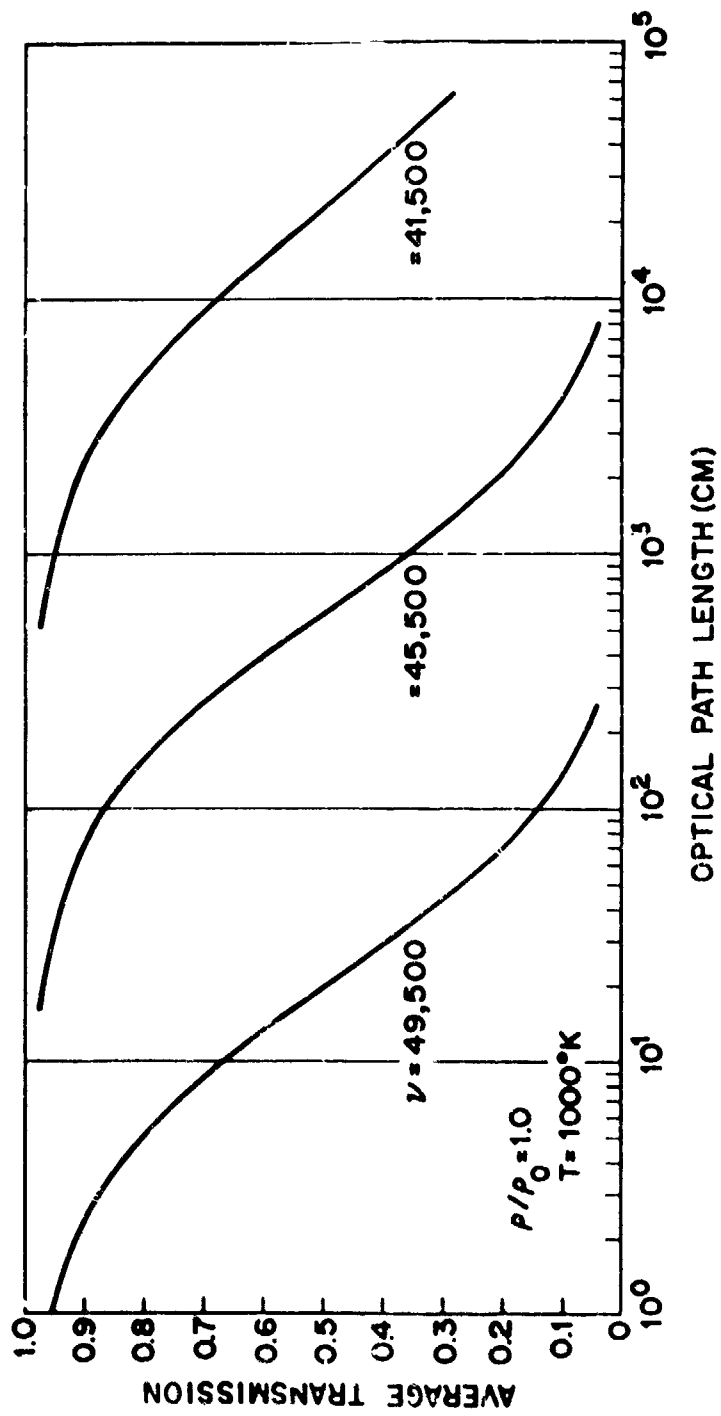
Fig. 7   Average transmission of optical radiation through a slab of heated air as a function of optical path length.

45
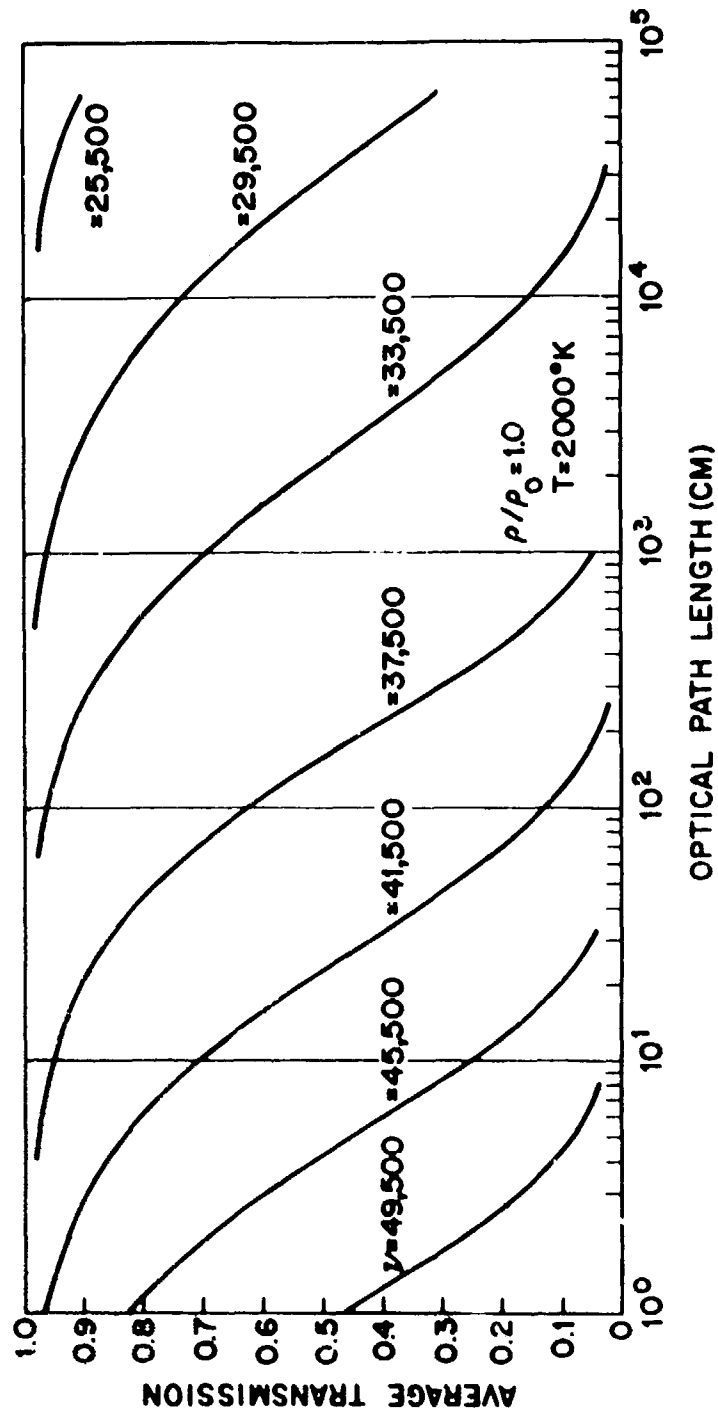
Fig. 8 Average transmission of optical radiation through a slab of heated air as a function of optical path length.

46
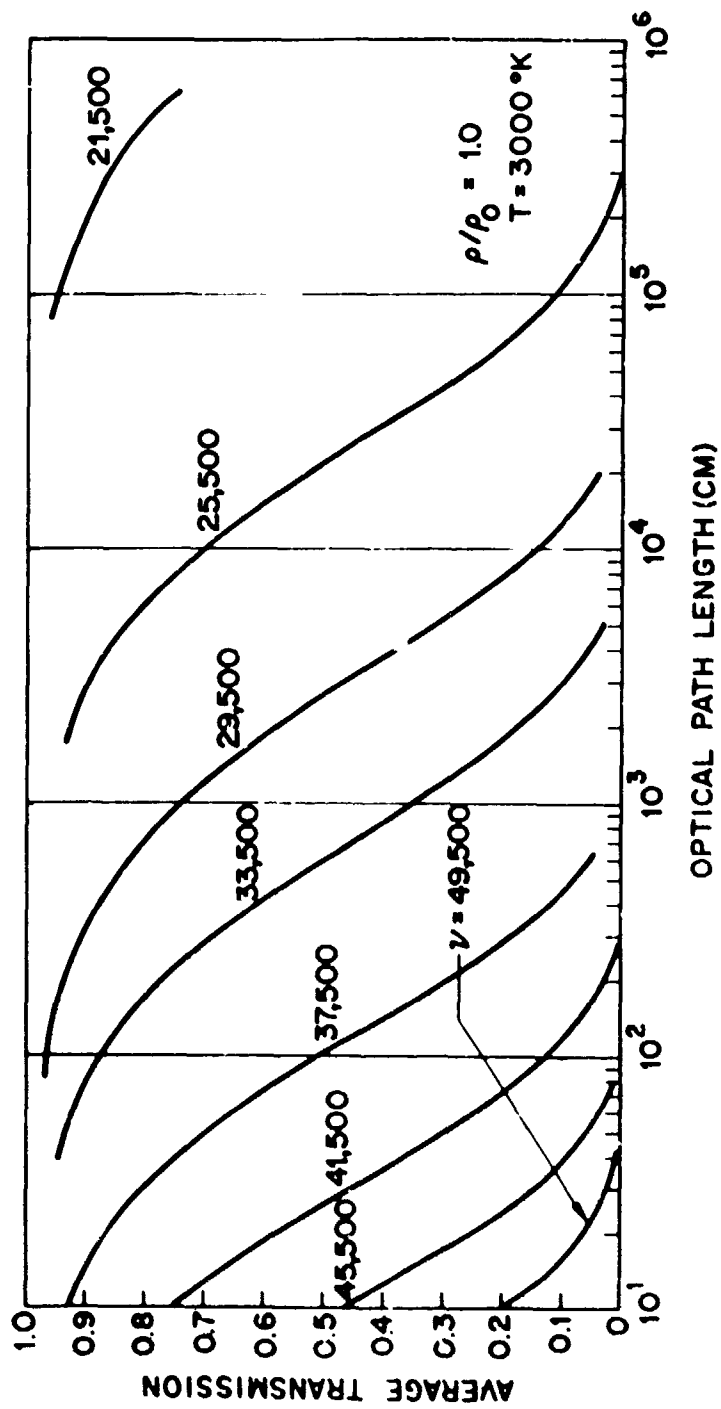
Fig. 9 Average transmission of optical radiation through a slab of heated air as a function of optical path length.
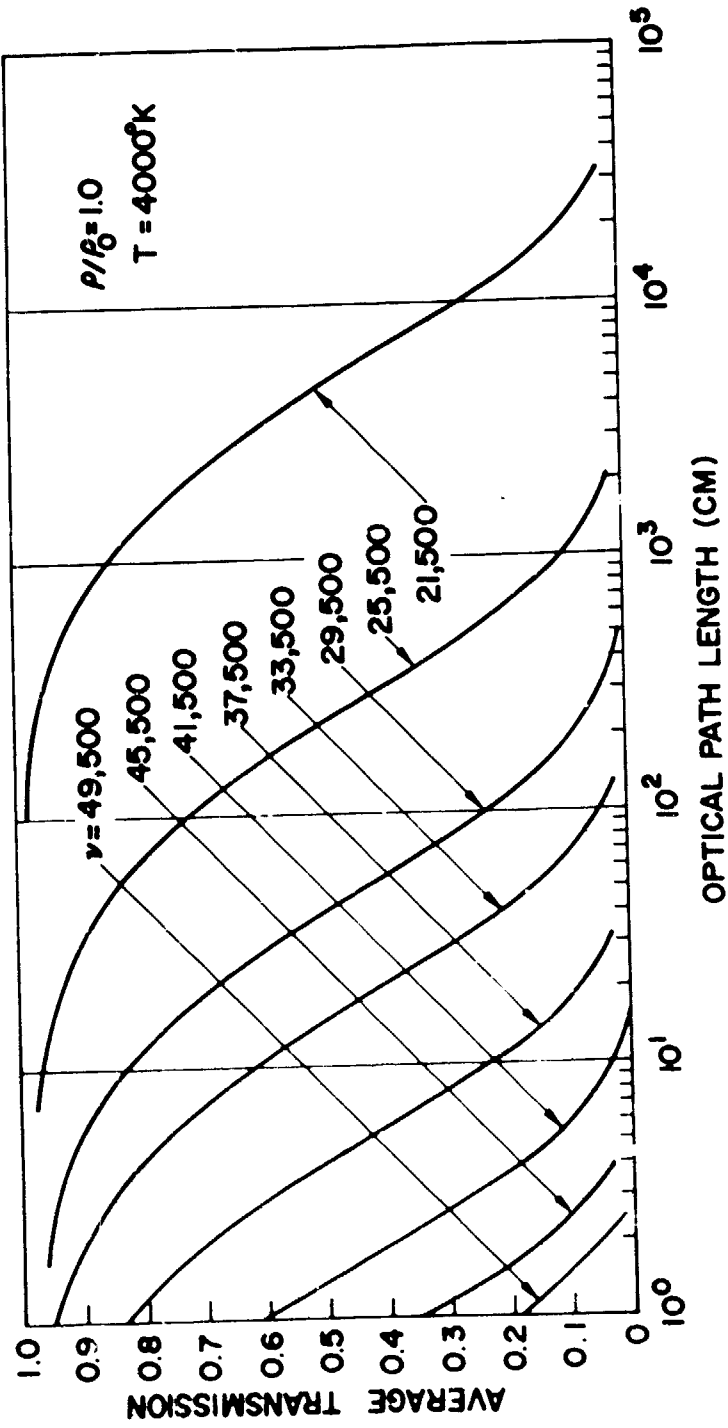
Fig. 10 Average transmission of optical radiation through a slab of heated air as a function of optical path length.

48
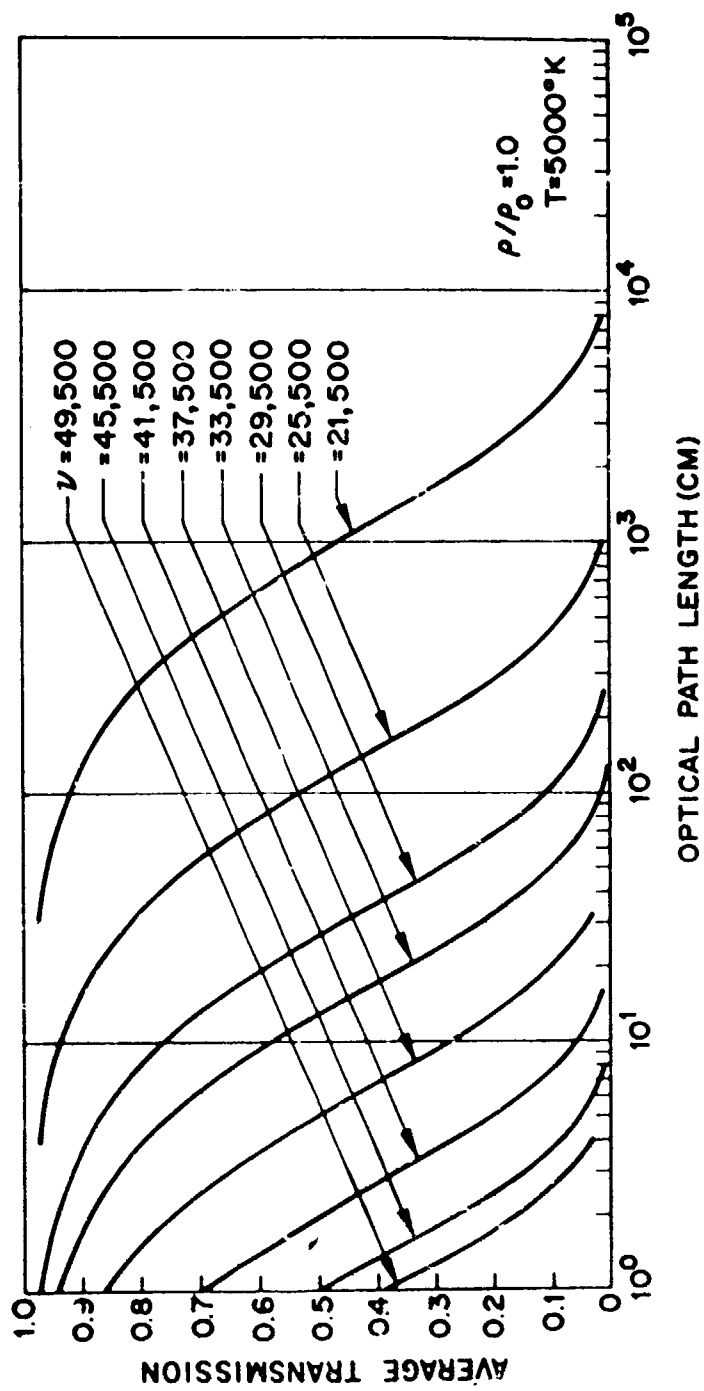
Fig. 11   Average transmission of optical radiation through a slab of heated
air as a function of optical path length.

49
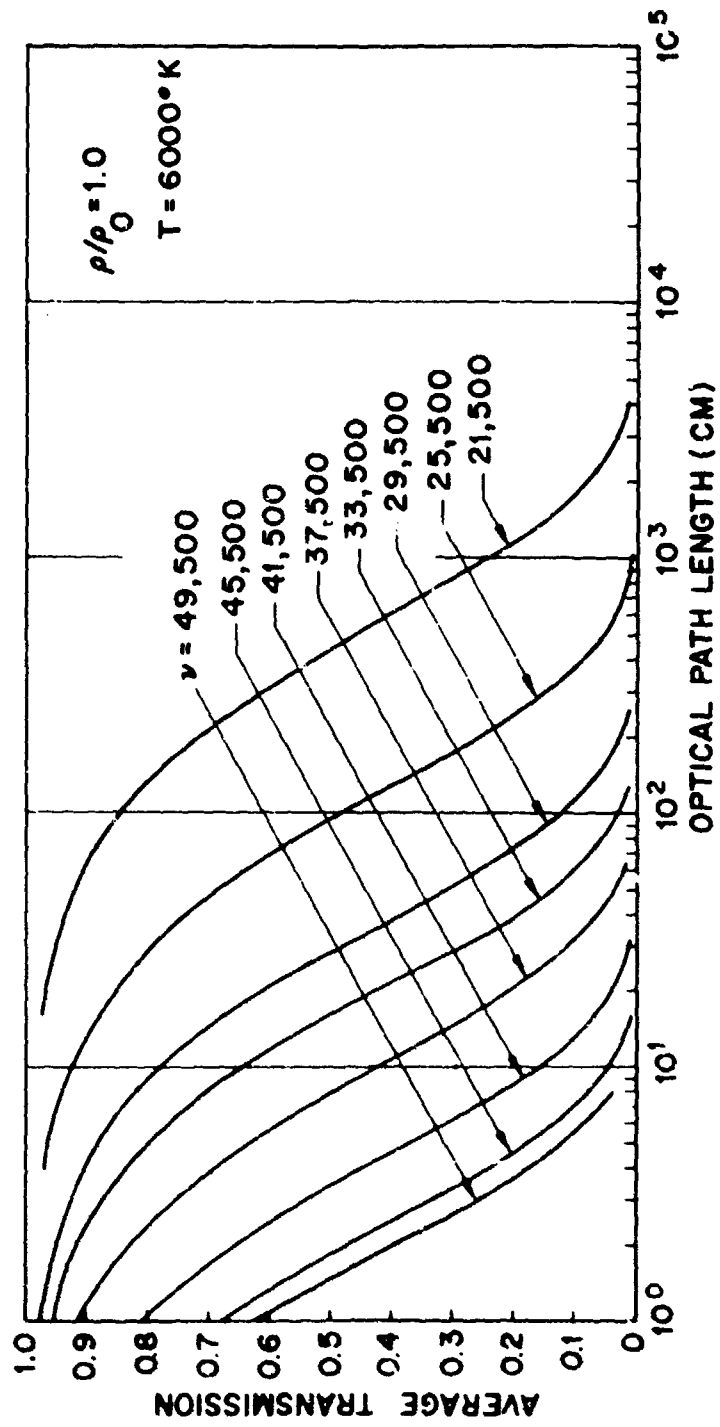
Fig. 12. Average transmission of optical radiation through a slab of heated air as a function of optical path length.
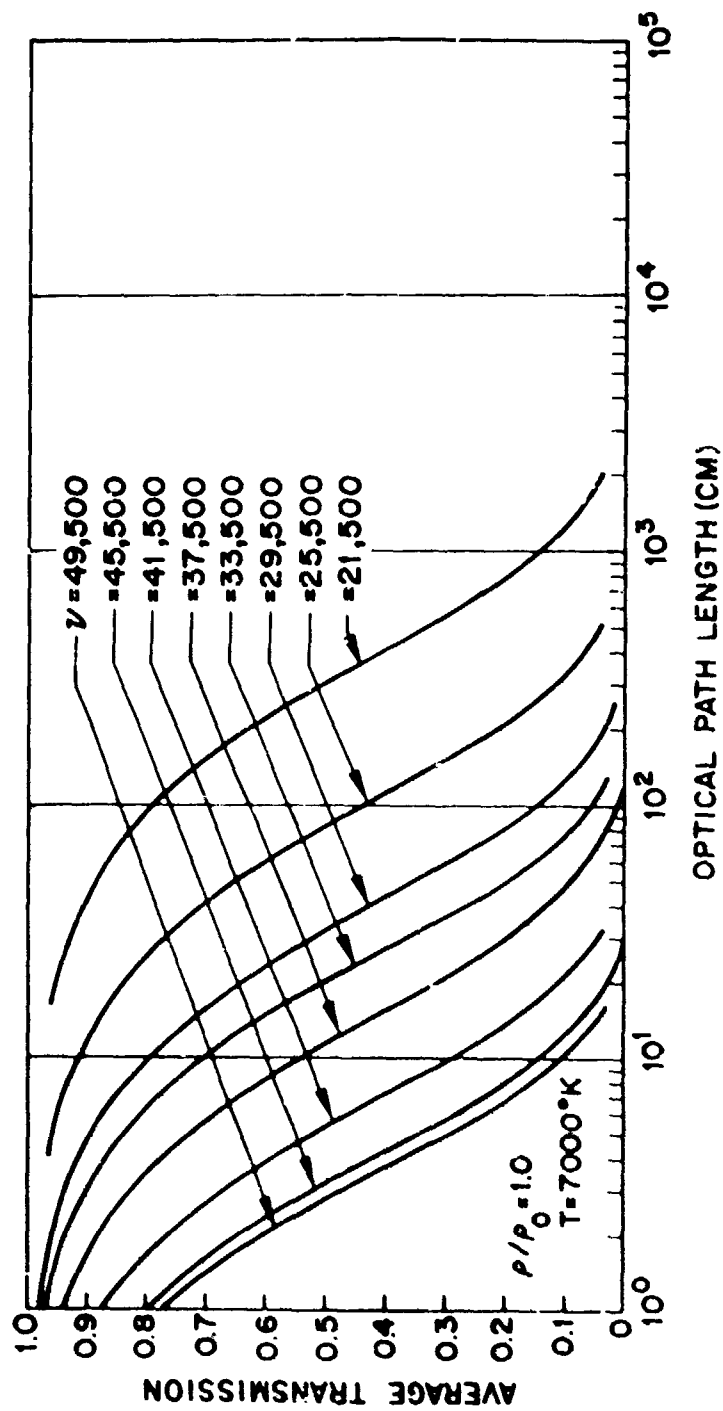
Fig. 12 Average transmission of optical radiation through a slab of heated air as a function of optical path length.
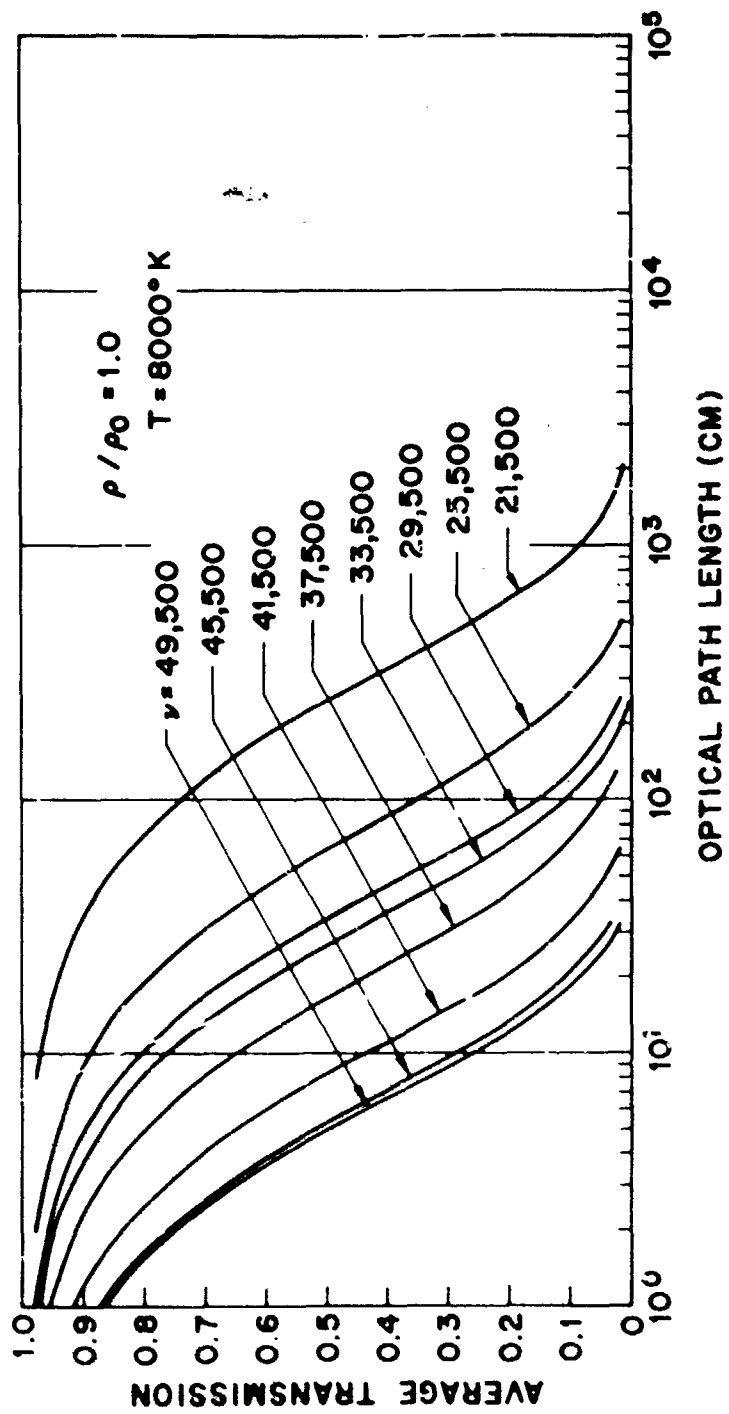
Fig. 14 Average transmission of optical radiation through a slab of heated air as a function of optical path length.

52
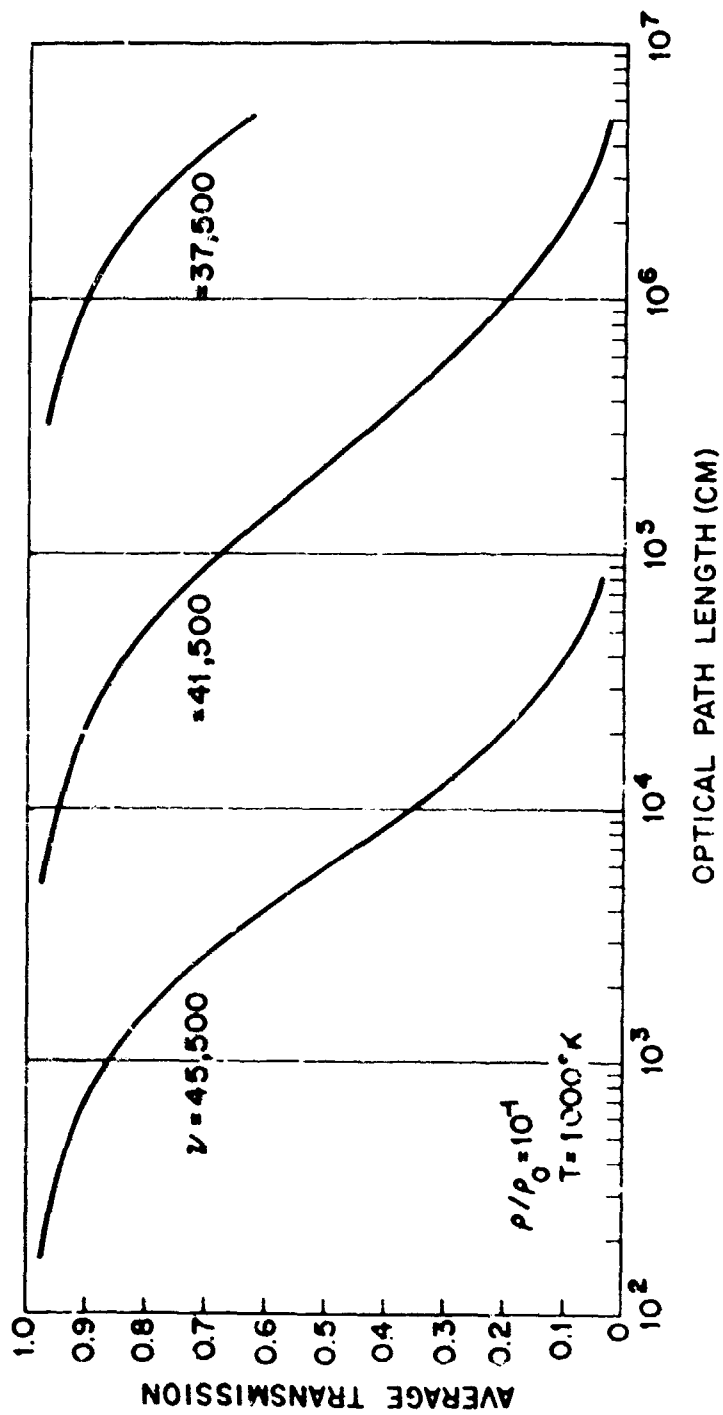
Fig. 15 Average transmission of optical radiation through a slab of heated air as a function of optical path length.
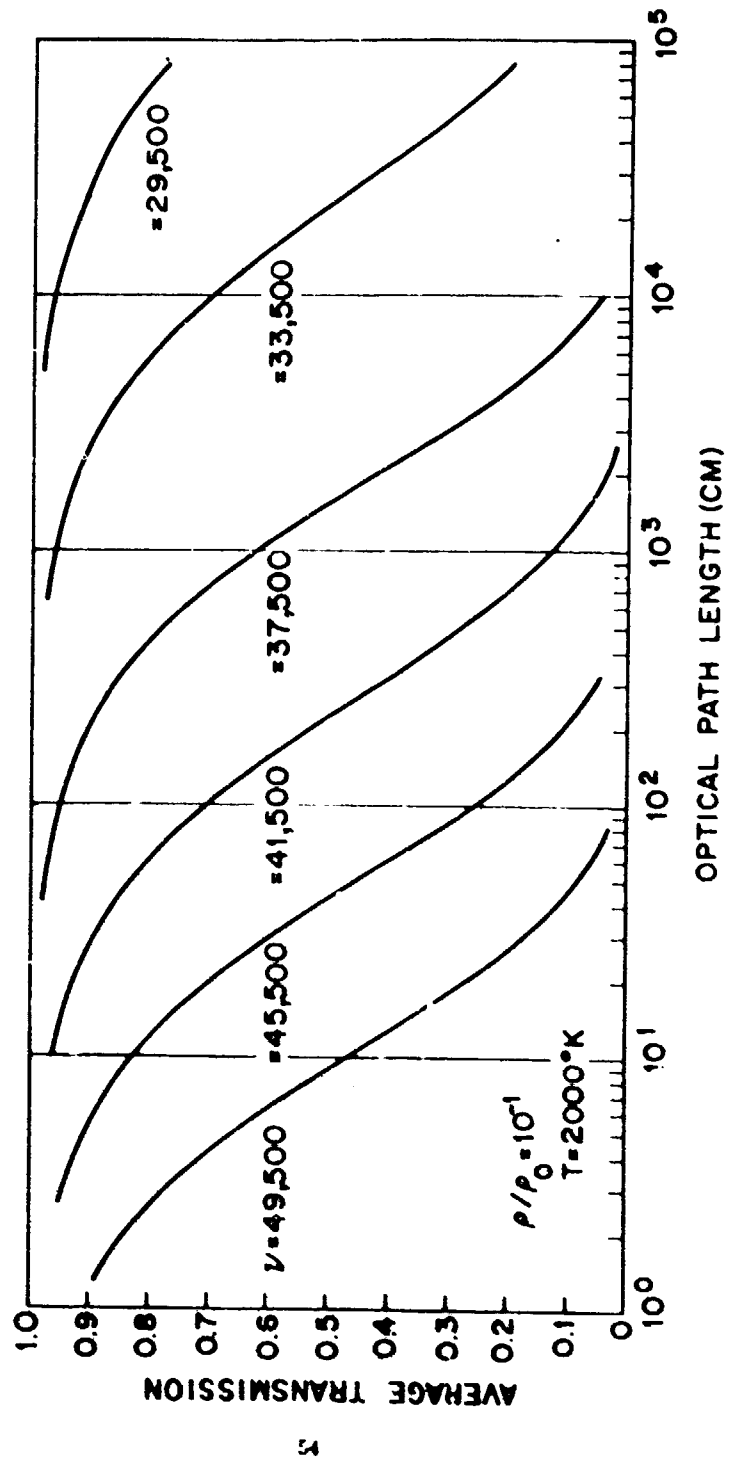
Fig. 16 Average transmission of optical radiation through a slab of heated air as a function of optical path length.
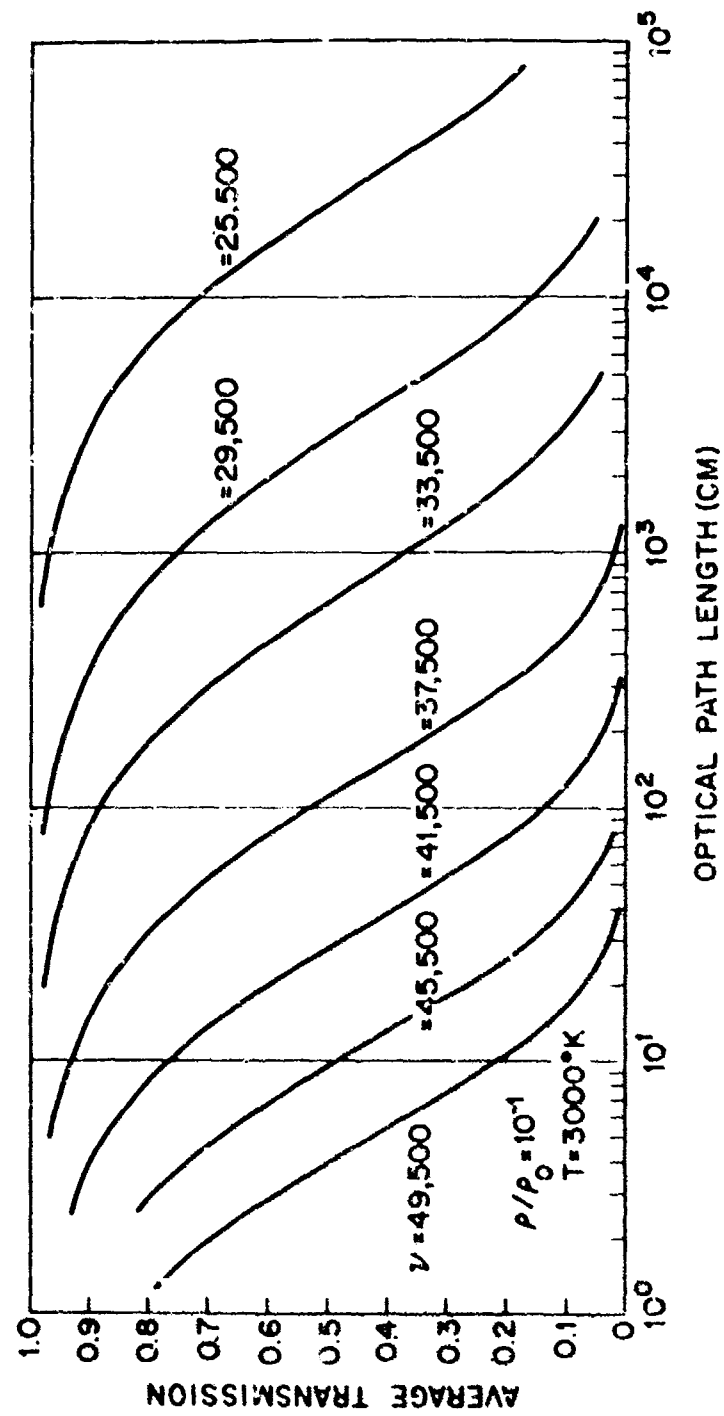
Fig. 17 Average transmission of optical radiation through a slab of heated air as a function of optical path length.

55
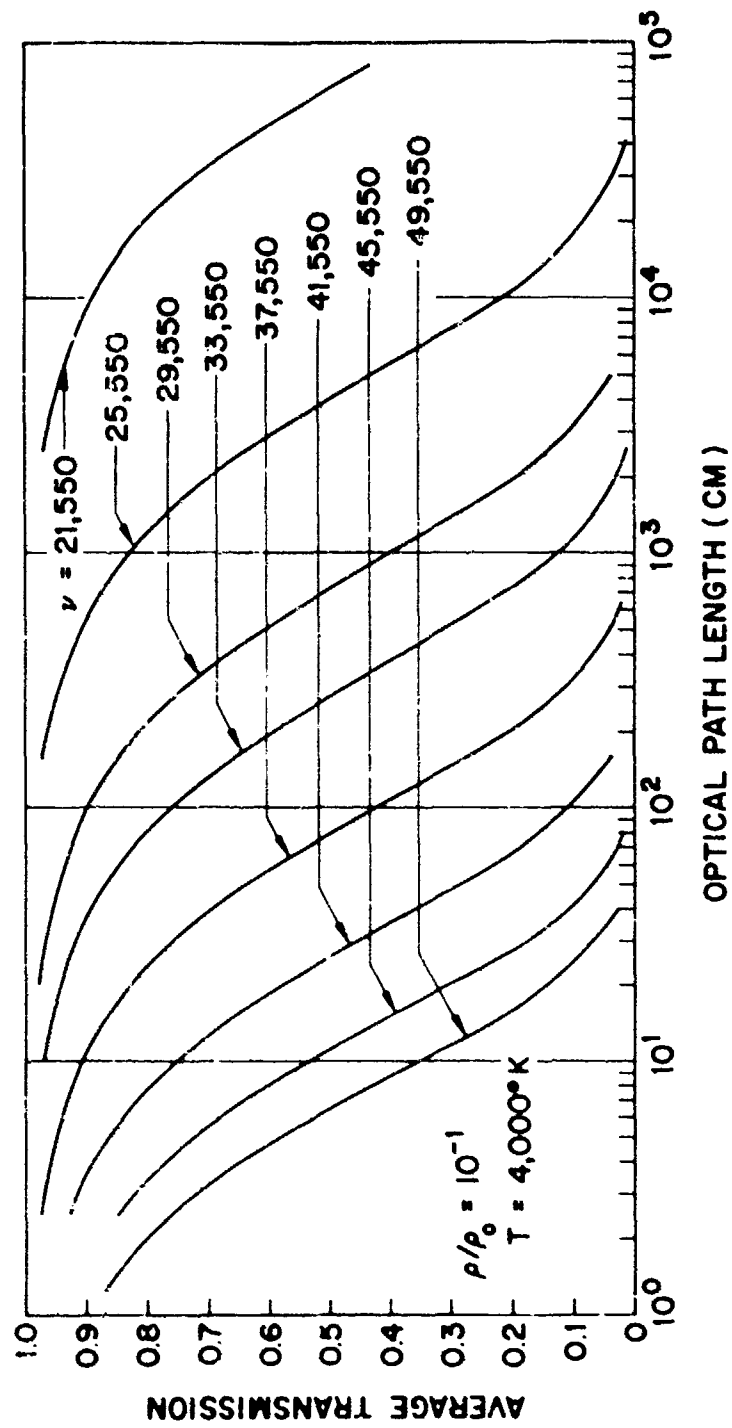
Fig. 18 Average transmission of optical radiation through a slab of heated air as a function of optical path length.

56
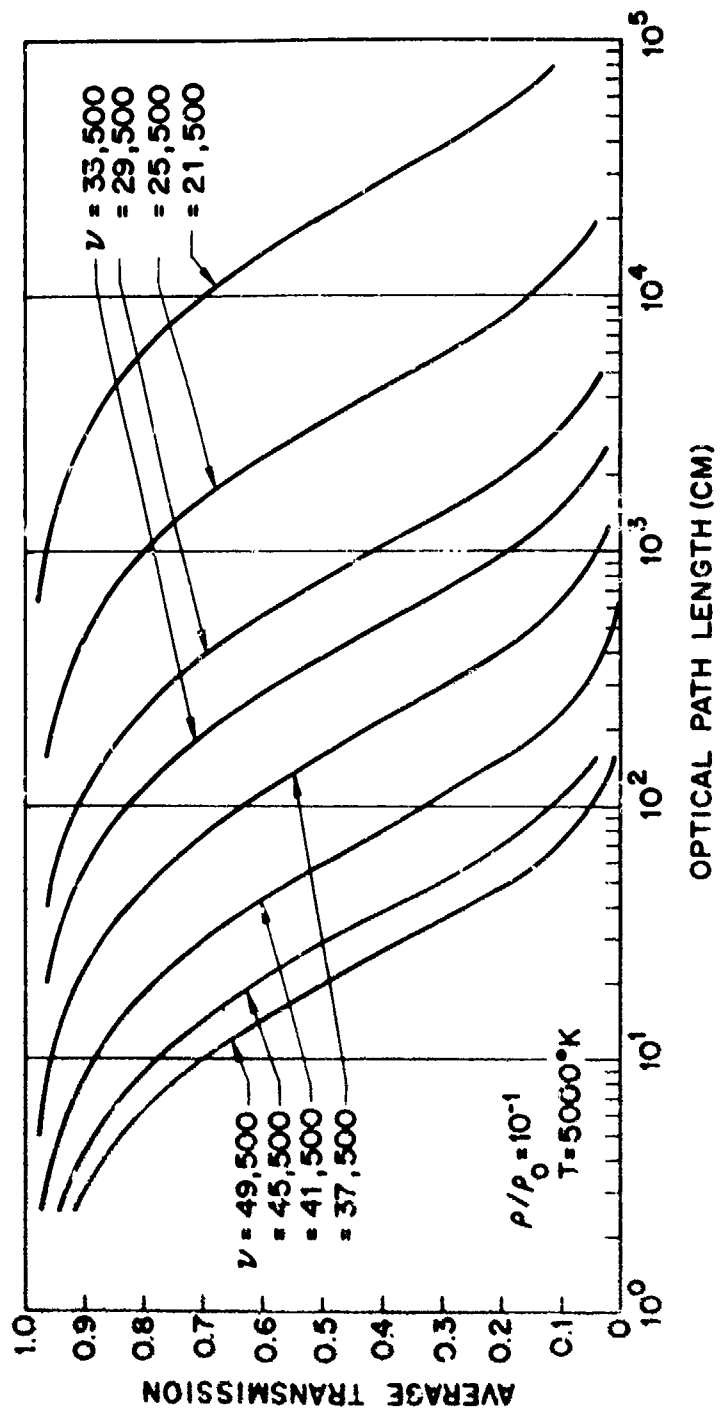
Fig. 19 Average transmission of optical radiation through a slab of heated air as a function of optical path length.

57
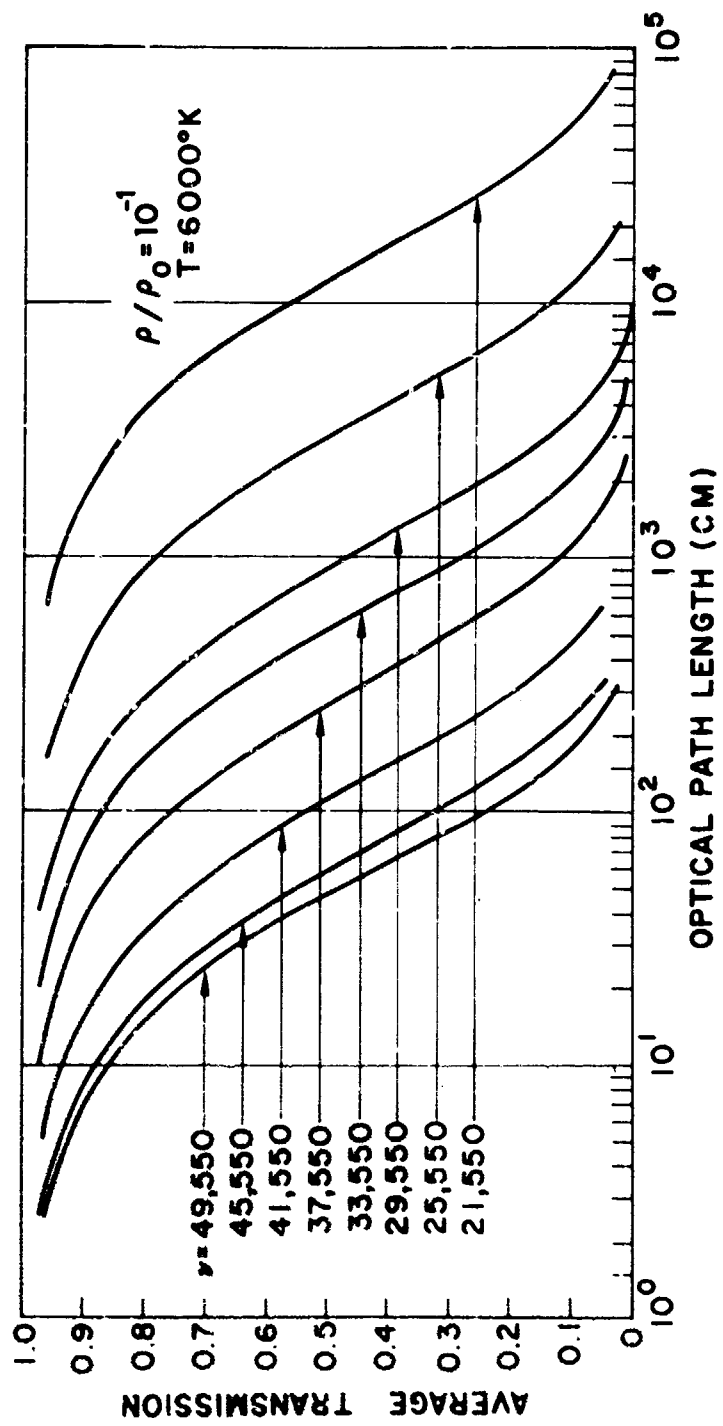
Fig. 20 Average transmission of optical radiation through a slab of heated air as a function of optical path length.

58
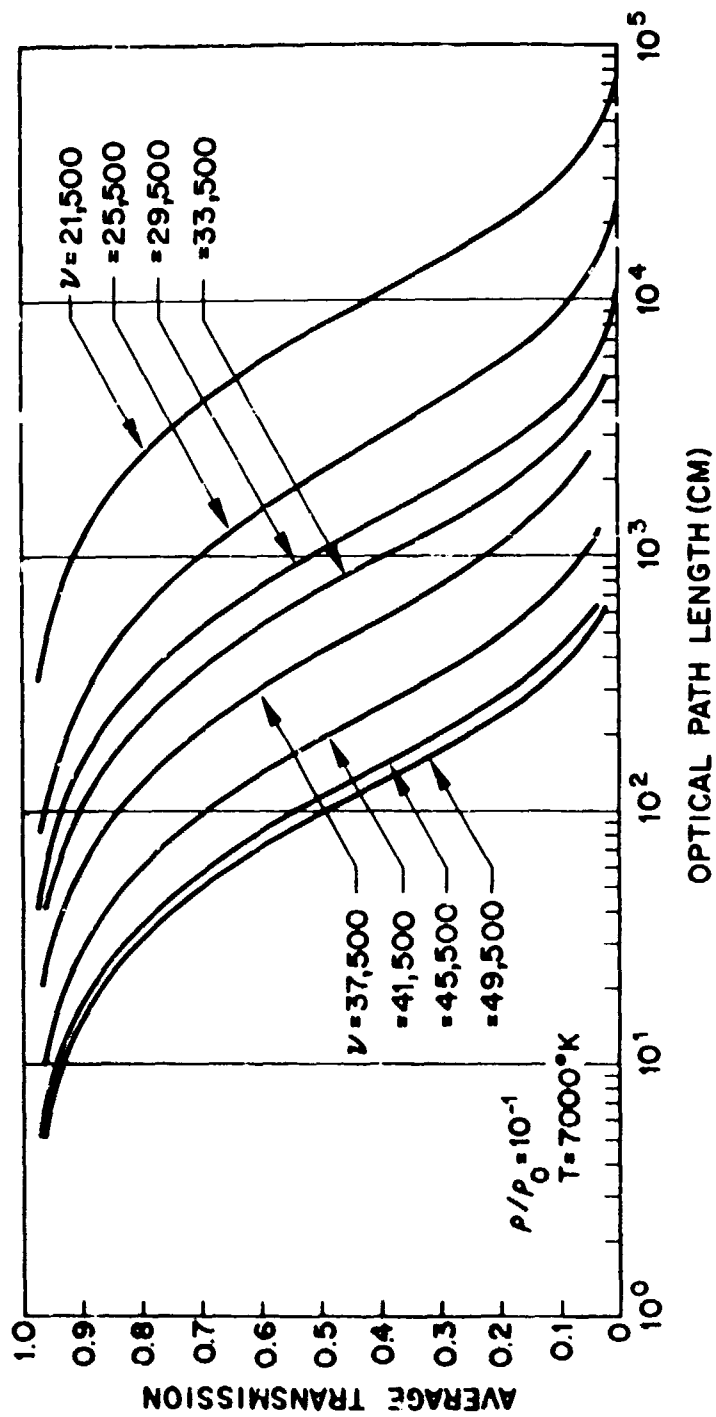
Fig. 21 Average transmission of optical radiation through a slab of heated air as a function of optical path length.

Fig. 22 Average transmission of optical radiation through a slab of heated air as a function of optical path length.

$\rho/\rho_0 = 10^{-1}$

$T = 8000°K$

$\nu = 49,550$
45,550
41,550
37,550
29,550
33,550
25,550
21,550

OPTICAL PATH LENGTH (CM)

AVERAGE TRANSMISSION

60

Fig. 23 Average transmission of optical radiation through a slab of heated air as a function of optical path length.

61
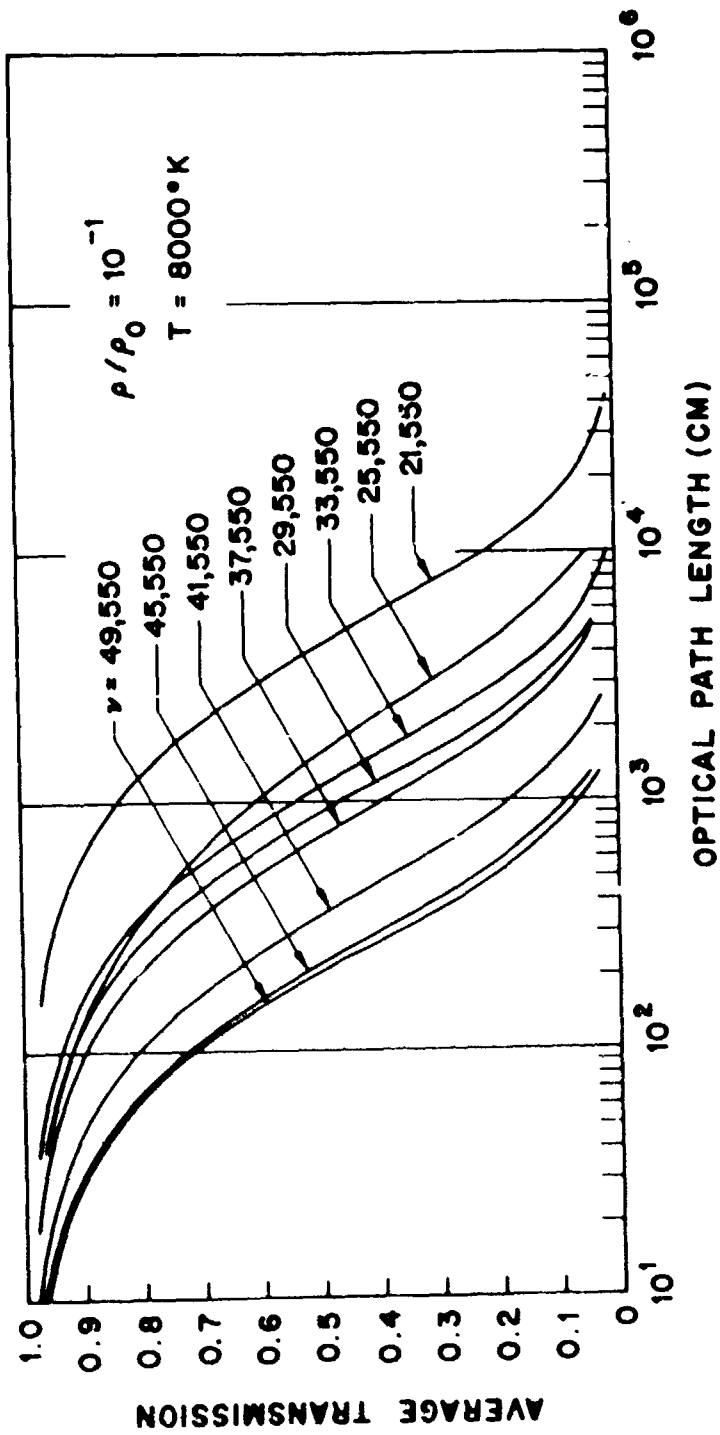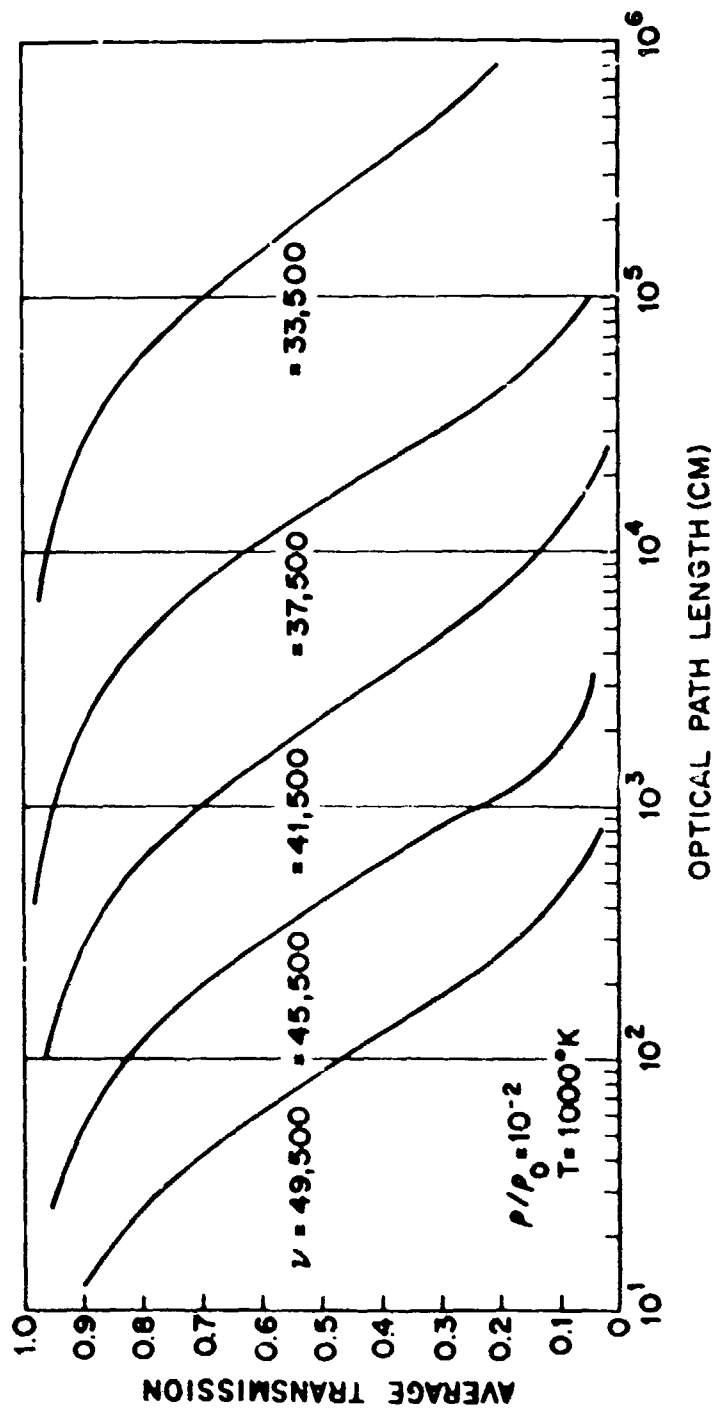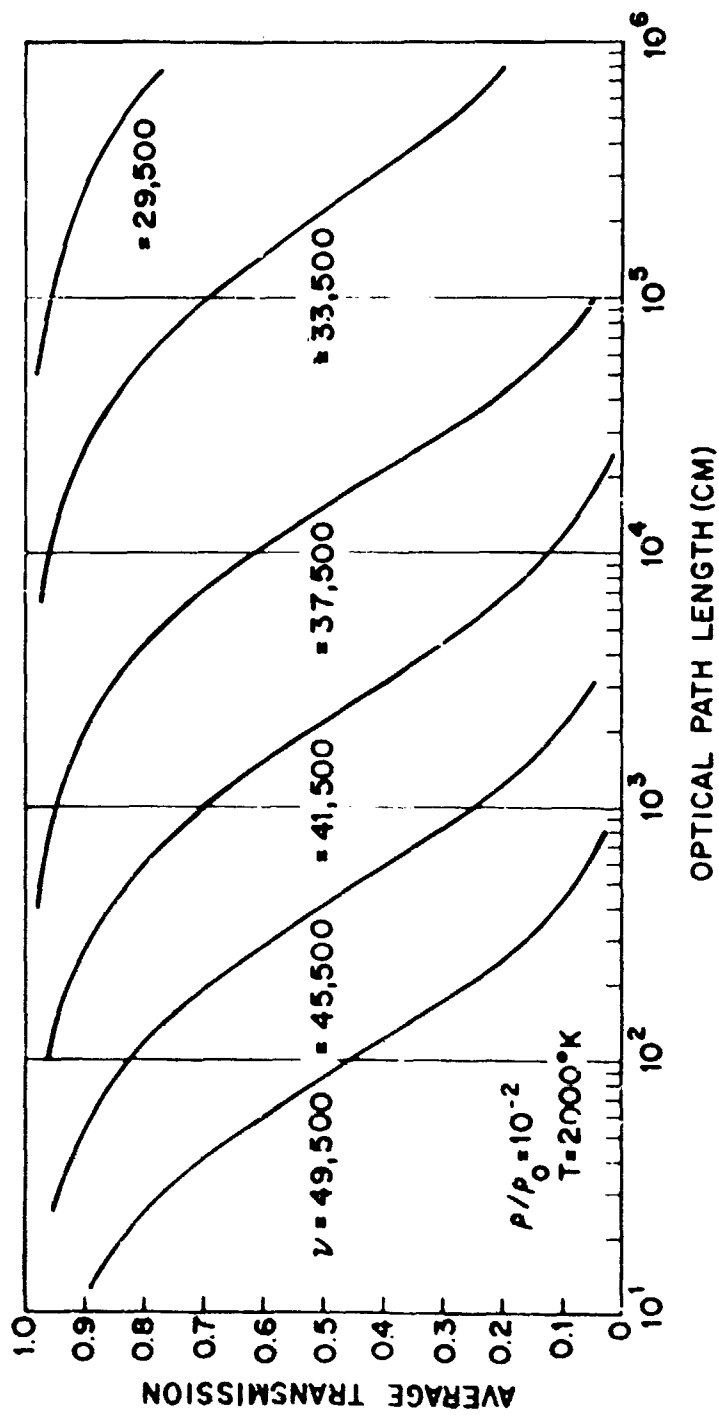
Fig. 24 Average transmission of optical radiation through a slab of heated air as a function of optical path length.

62

Fig. 23 Average transmission of optical radiation through a slab of heated air as a function of optical path length.

63

Fig. 26 Average transmission of optical radiation through a slab of heated air as a function of optical path length.

64

AVERAGE TRANSMISSION

OPTICAL PATH LENGTH (CM)

10^1 10^2 10^3 10^4 10^5 10^6

1.0 0.9 0.8 0.7 0.6 0.5 0.4 0.3 0.2 0.1 0

21,500

25,500

29,500

$\nu = 35,500$

37,500

41,500

45,500

49,500

$\rho/\rho_0 = 10^{-2}$

$T = 5000°K$
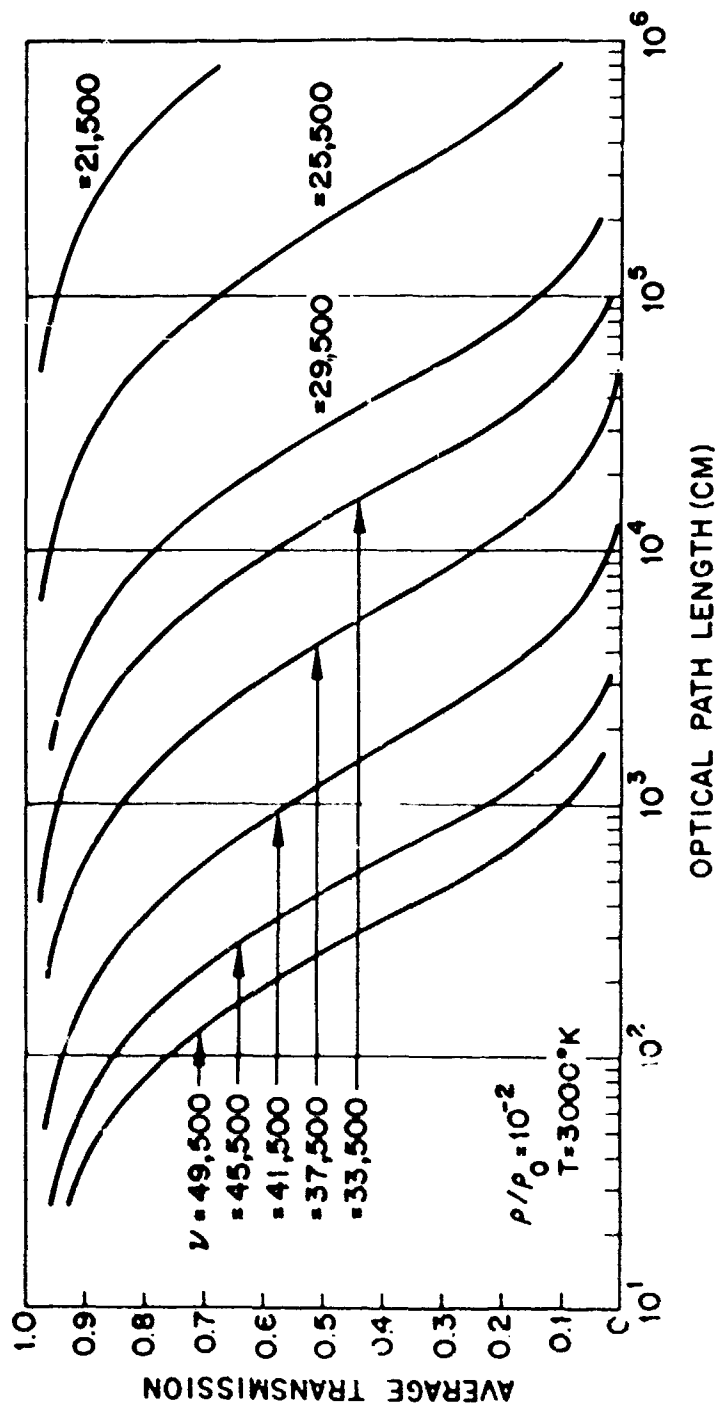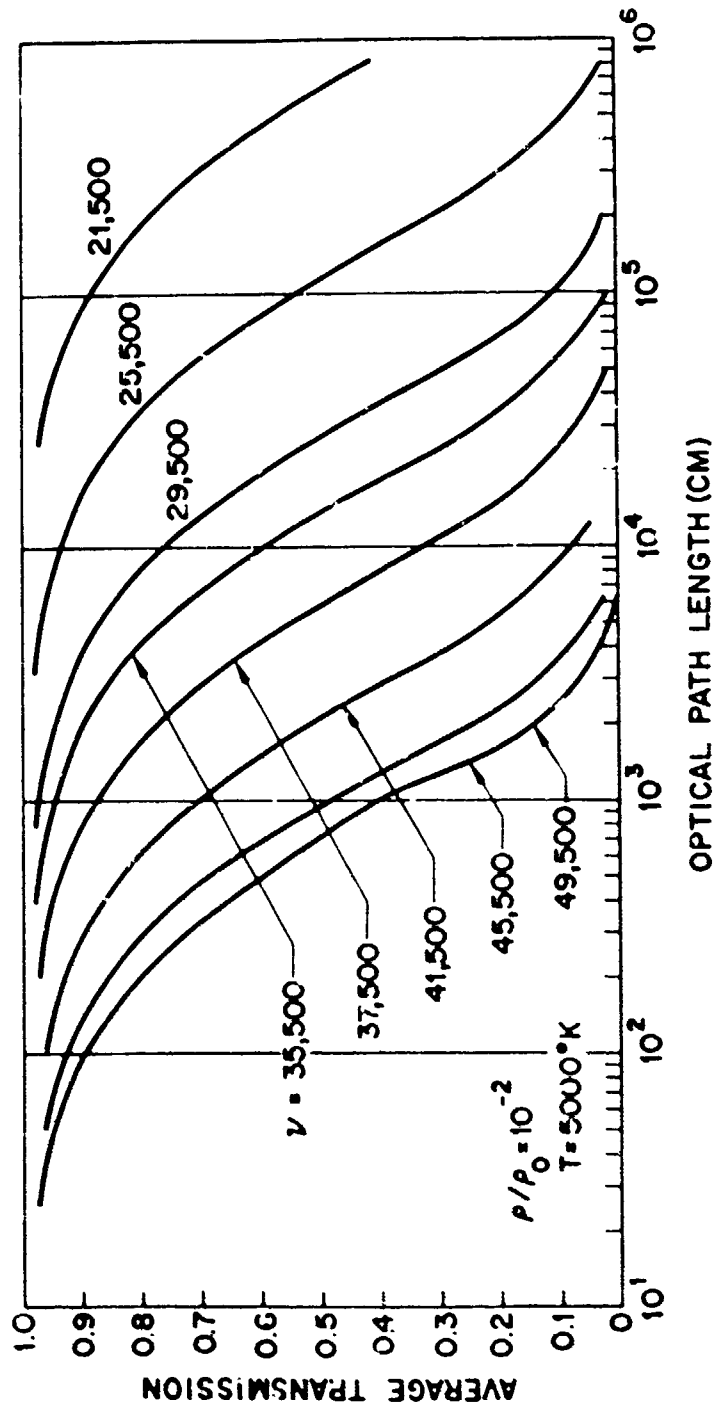
Fig. 27 Average transmission of optical radiation through a slab of heated air as a function of optical path length.
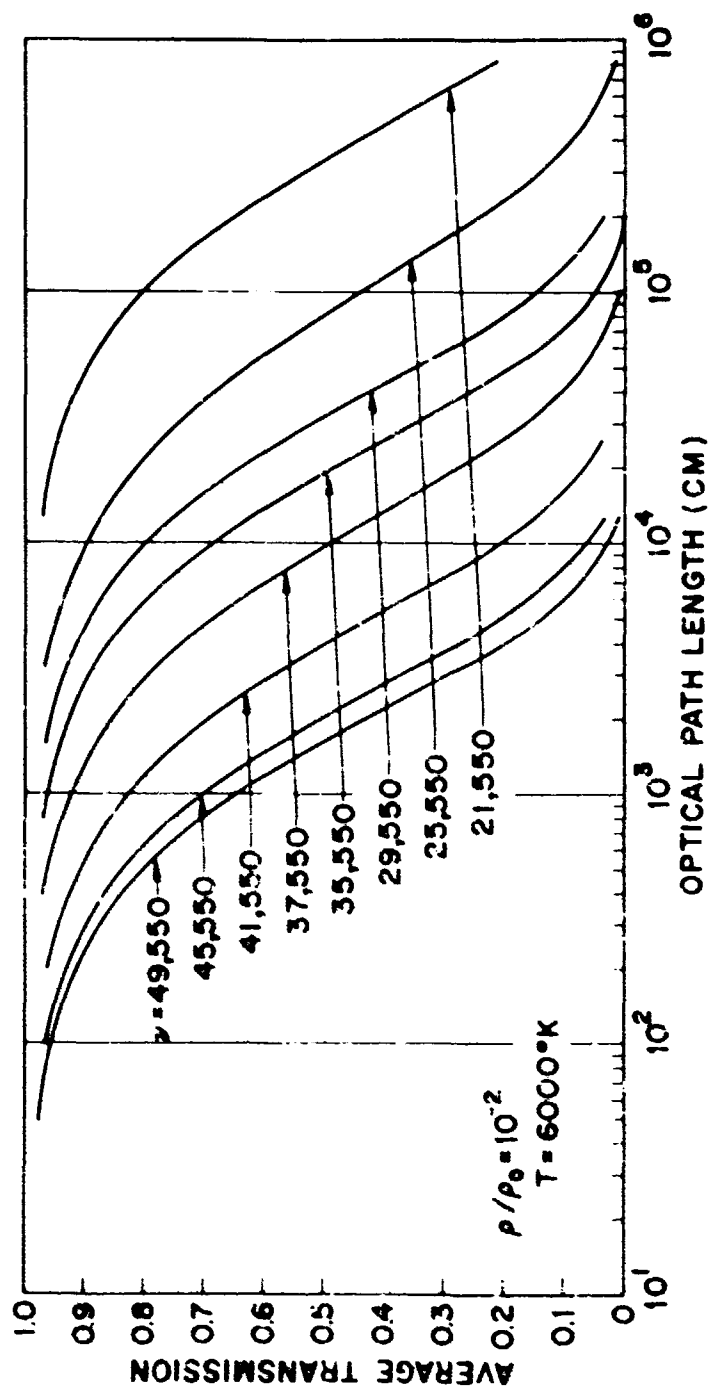
Fig. 28 Average transmission of optical radiation through a slab of heated air as a function of optical path length.
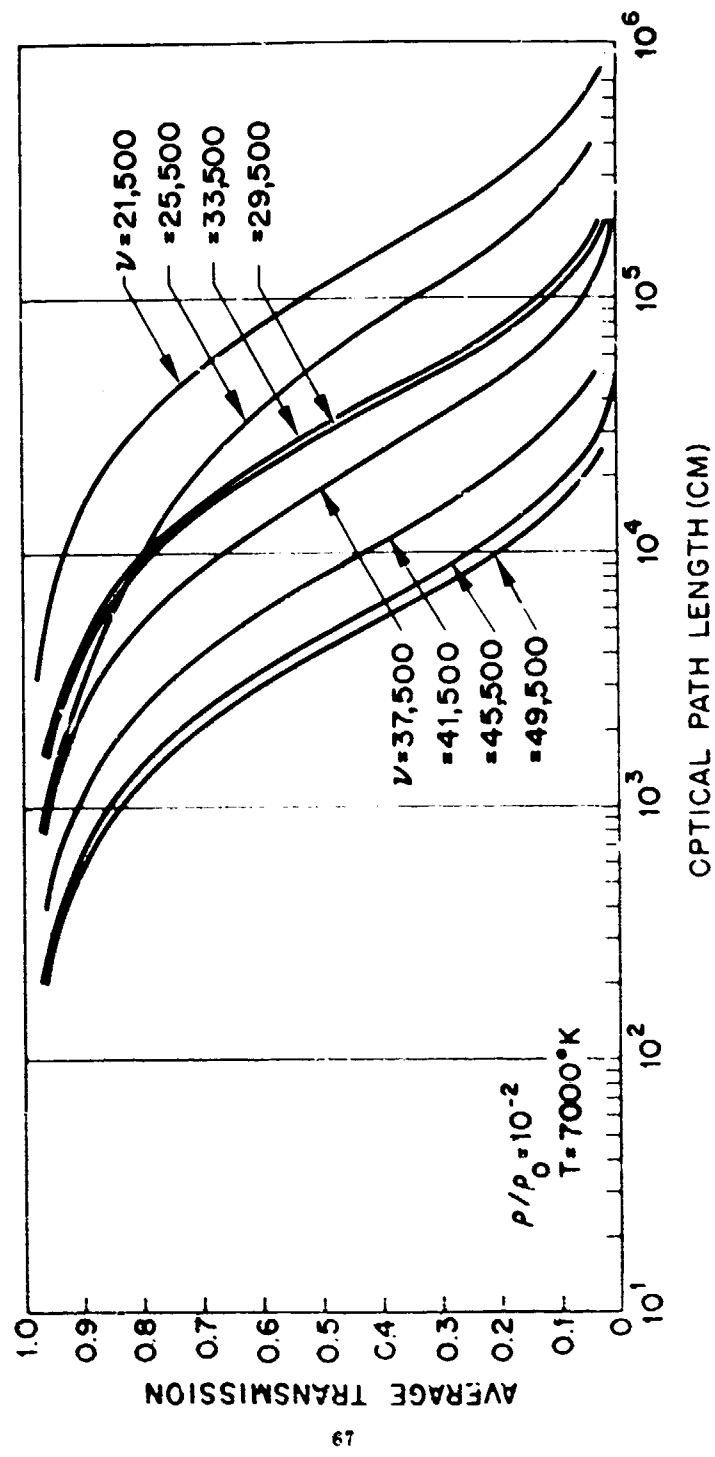
Fig. 29 Average transmission of optical radiation through a slab of heated air as a function of optical path length.

67
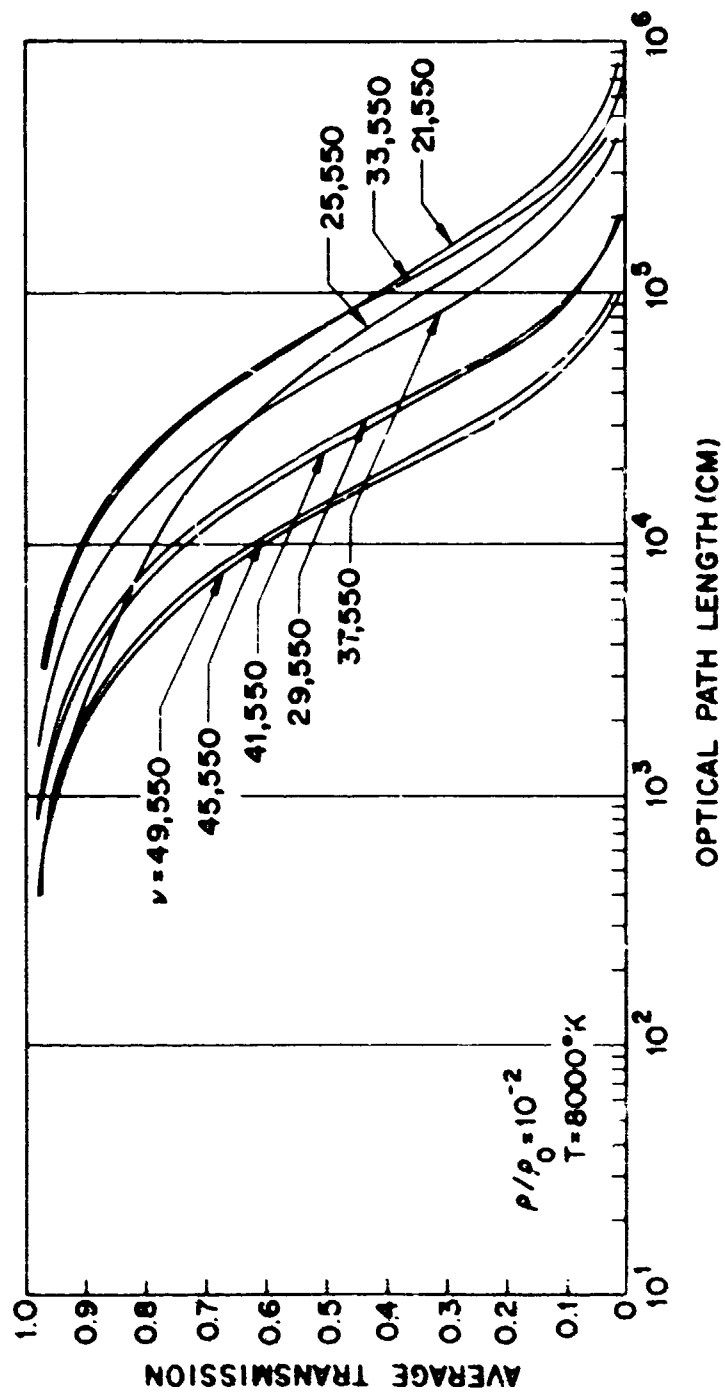
Fig. 30 Average transmission of optical radiation through a slab of heated air as a function of optical path length.
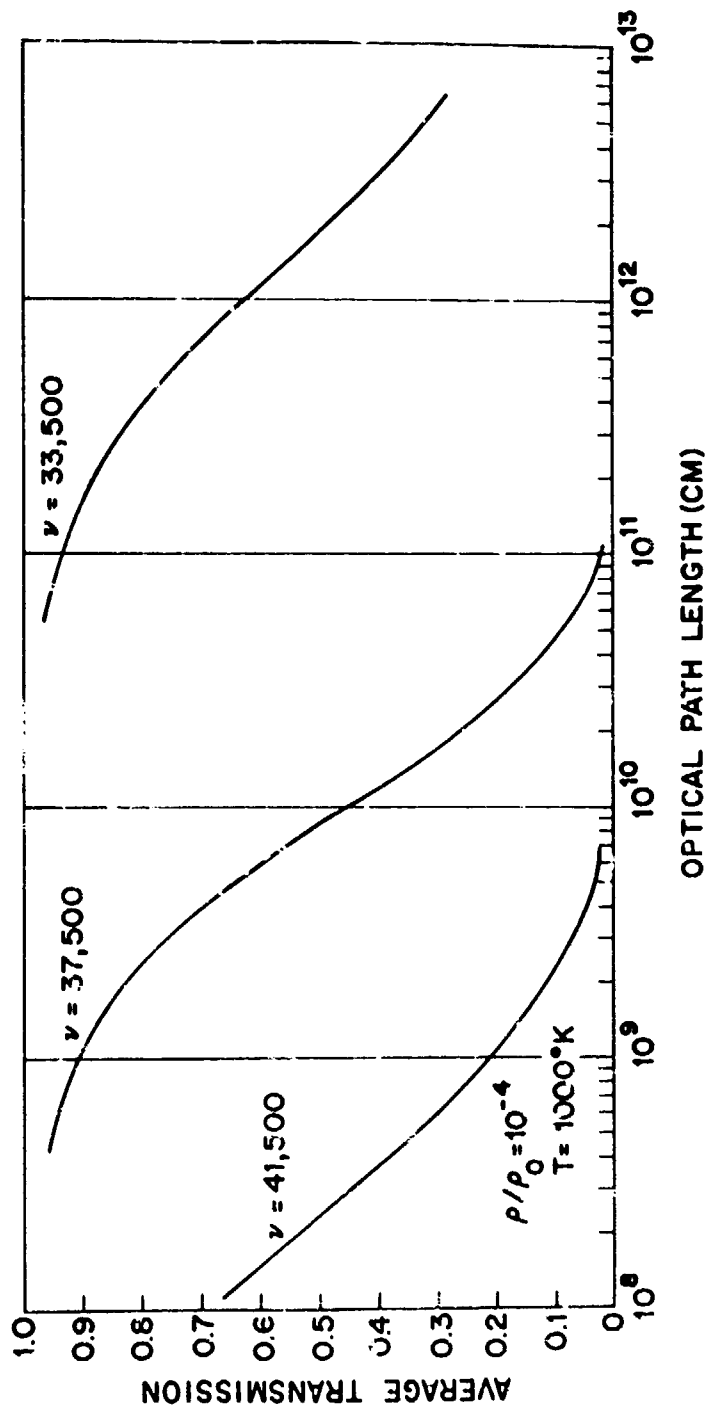
Fig. 31 Average transmission of optical radiation through a slab of heated air as a function of optical path length.

69
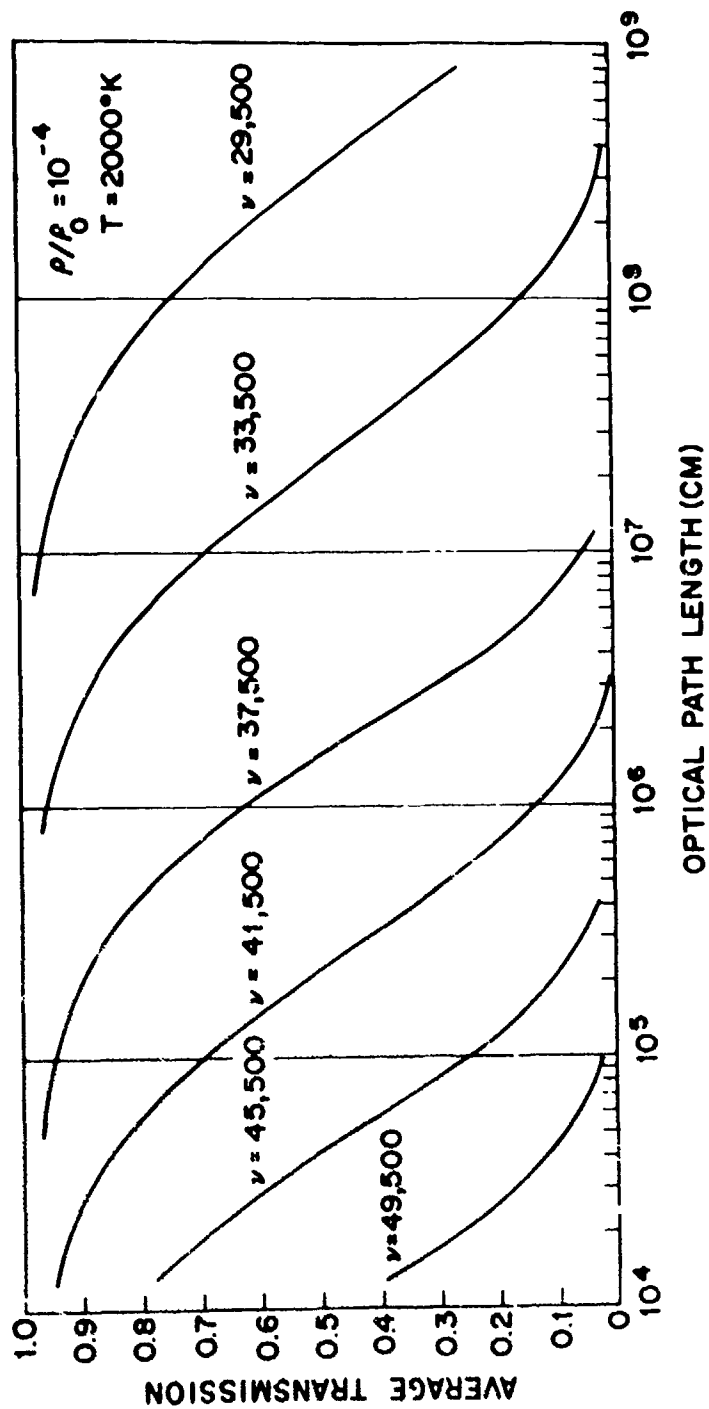
Fig. 32 Average transmission of optical radiation through a slab of heated air as a function of optical path length.

70
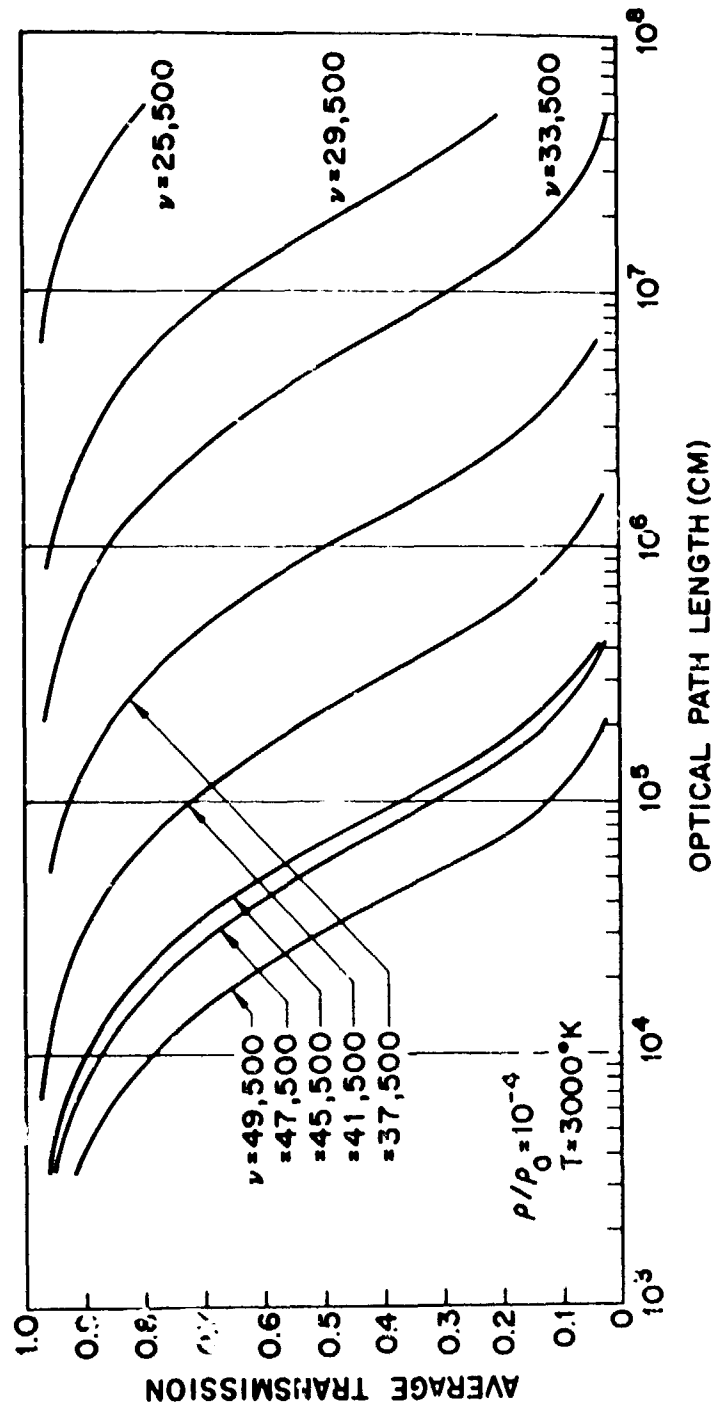
Fig. 33 Average transmission of optical radiation through a slab of heated
air as a function of optical path length.

71
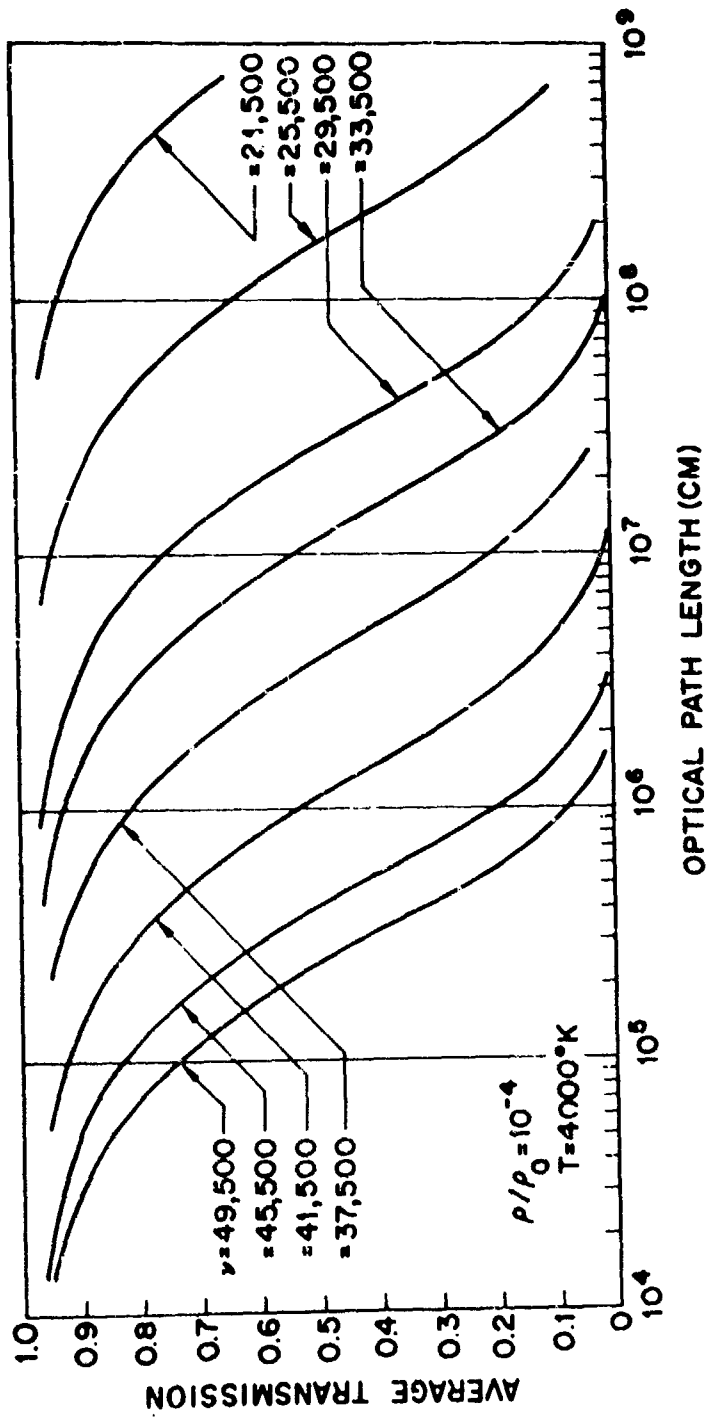
Fig. 34   Average transmission of optical radiation through a slab of heated air as a function of optical path length.
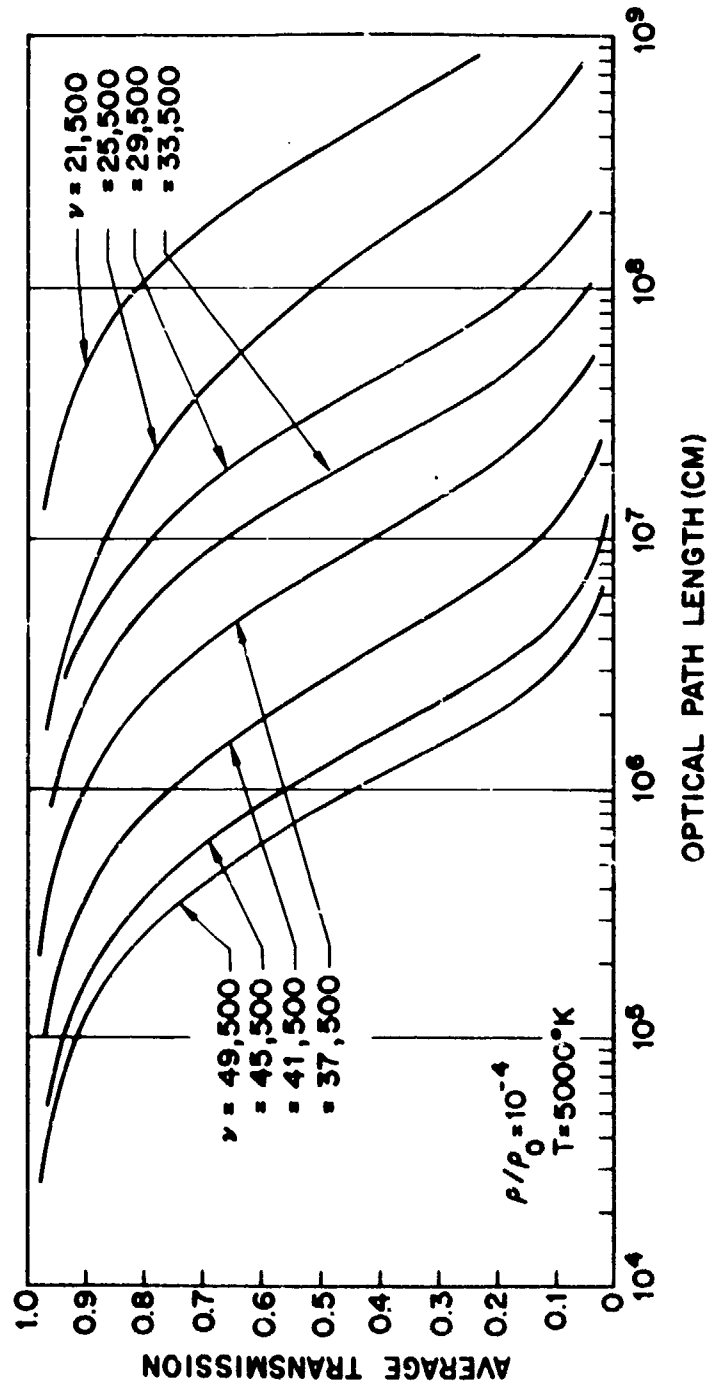
Fig. 35   Average transmission of optical radiation through a slab of heated air as a function of optical path length.

73
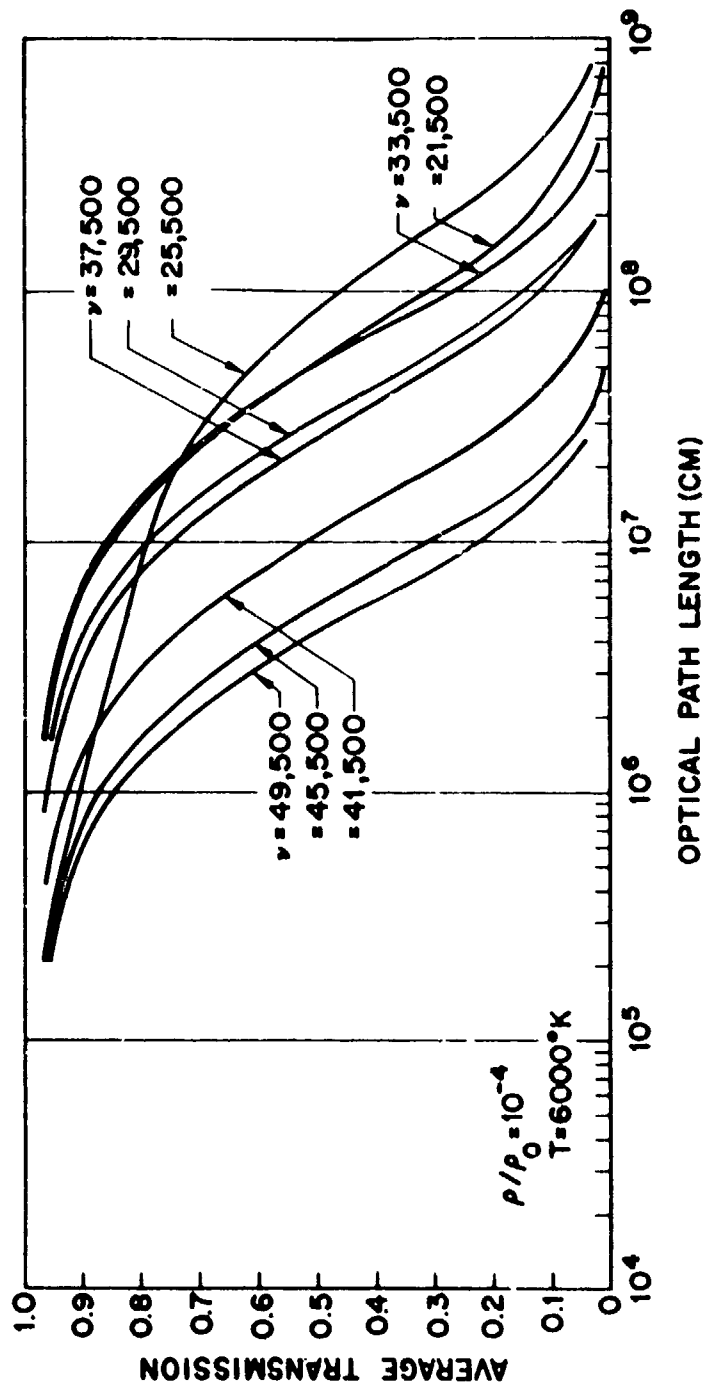
Fig. 36 Average transmission of optical radiation through a slab of heated air as a function of optical path length.
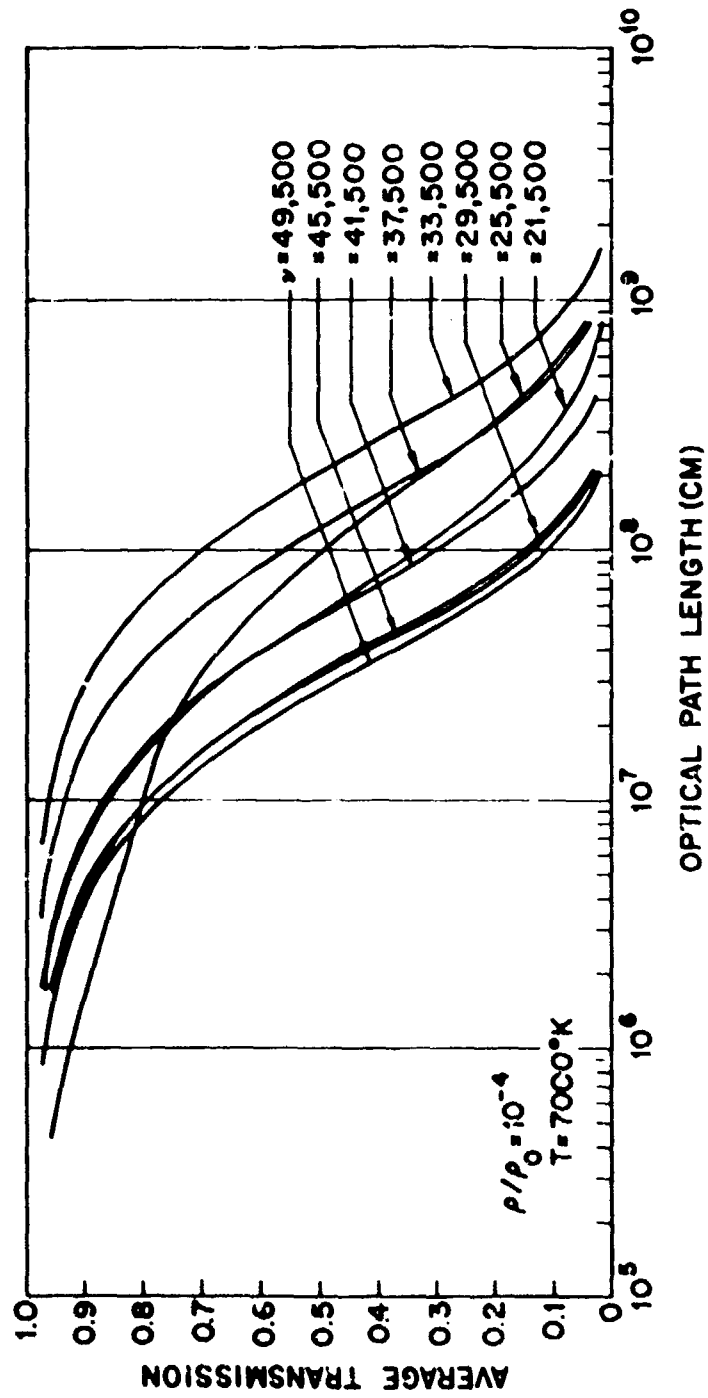
Fig. 37   Average transmission of optical radiation through a slab of heated
air as a function of optical path length.

75
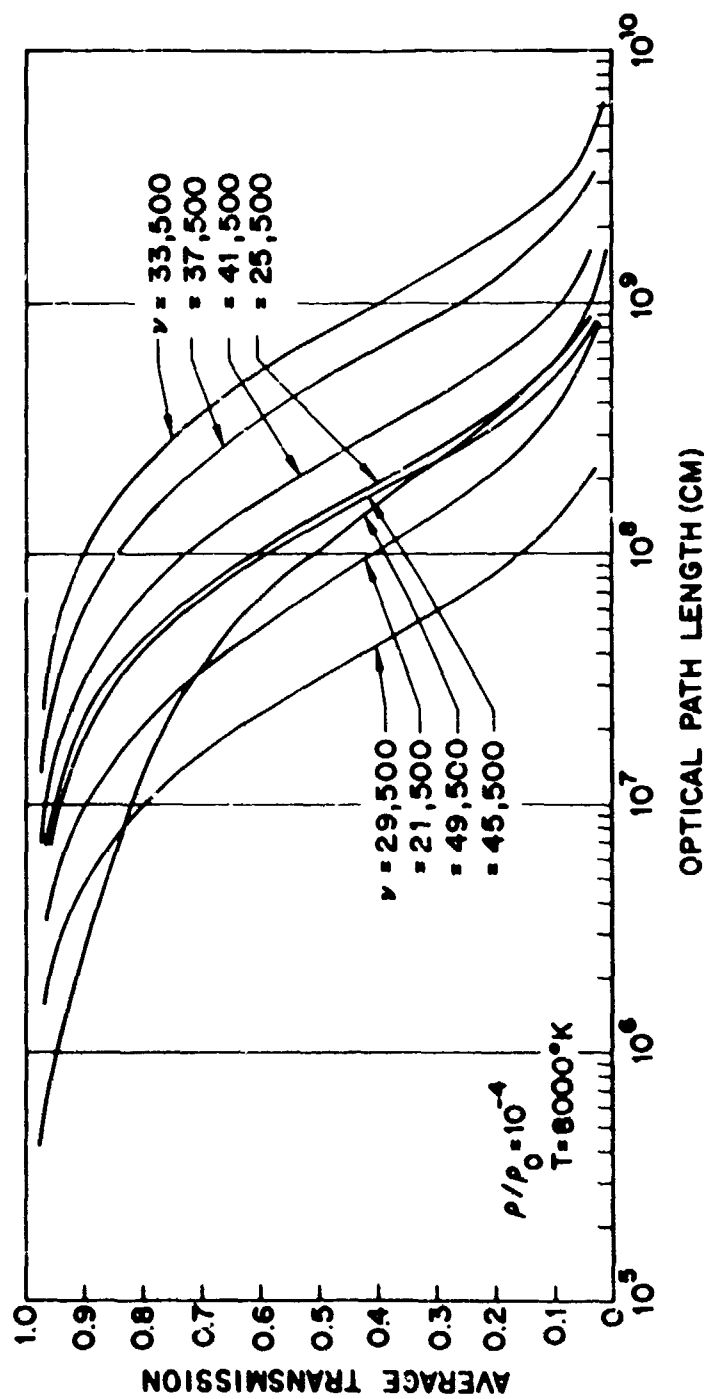
Fig. 38   Average transmission of optical radiation through a slab of heated air as a function of optical path length.

76
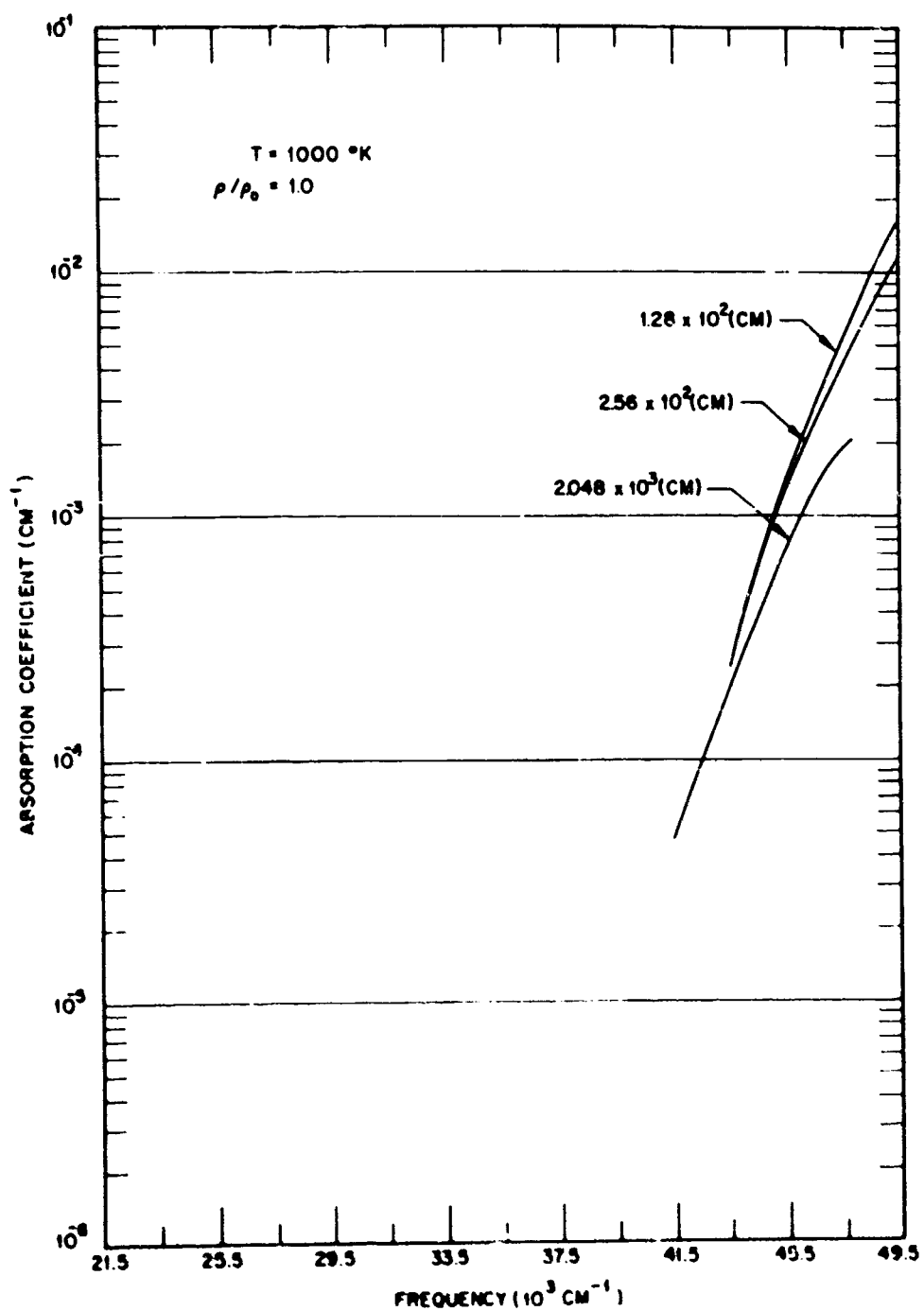
Fig. 39 The average absorption coefficient of heated air as a function of frequency for various optical path lengths.

77
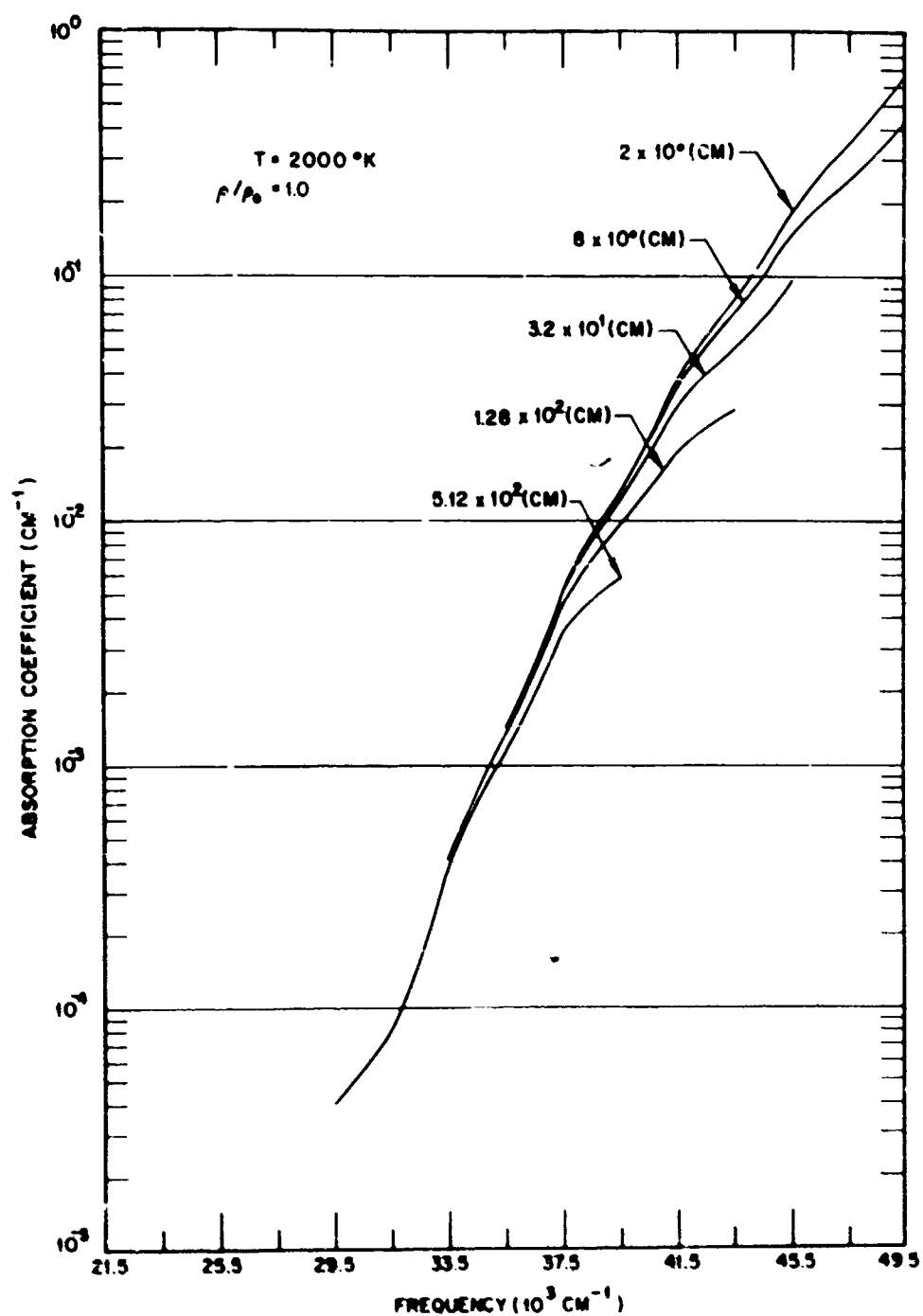
Fig. 40   The average absorption coefficient of heated air as a function of
frequency for various optical path lengths.

78
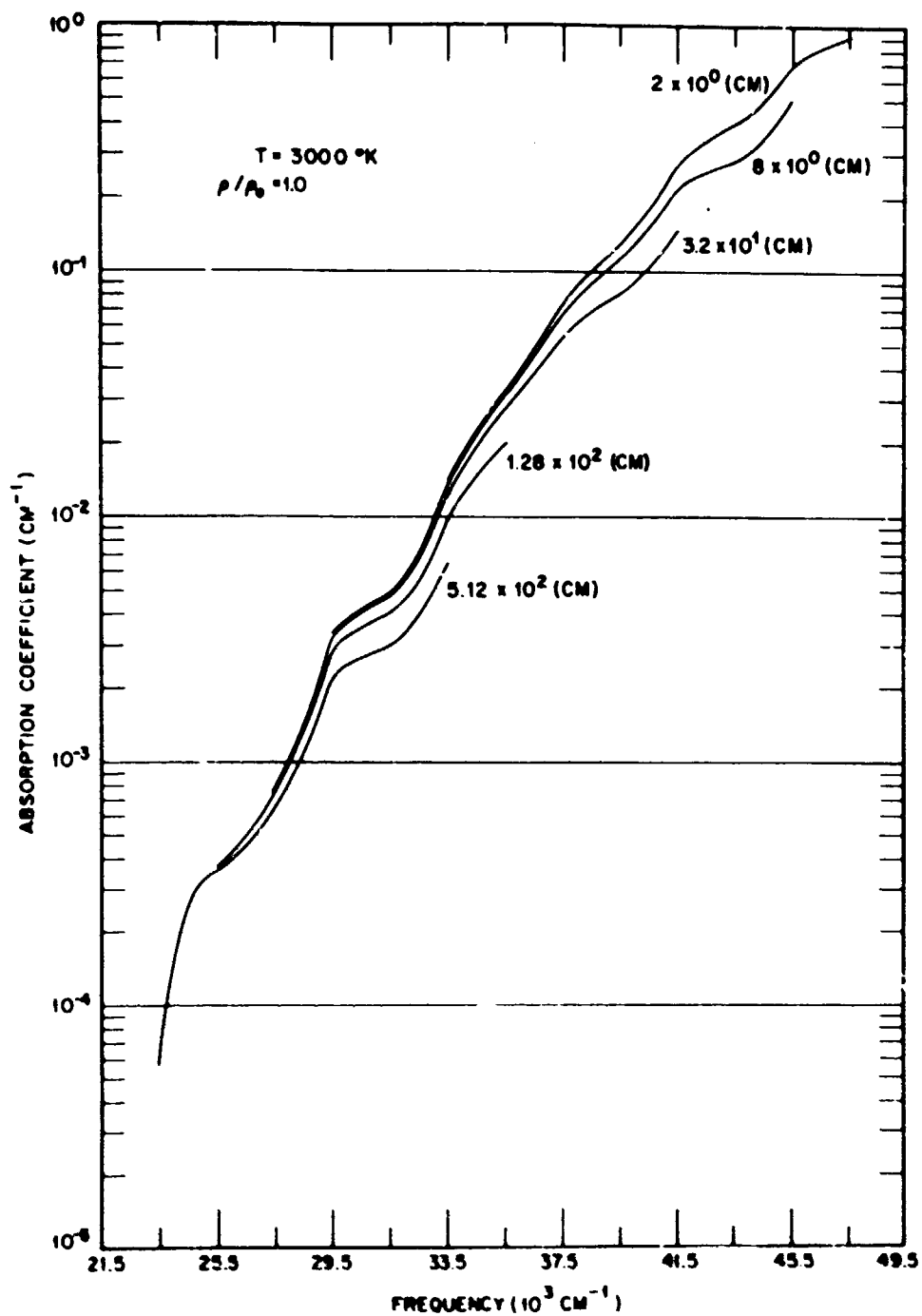
Fig. 41 The average absorption coefficient of heated air as a function of frequency for various optical path lengths.

79
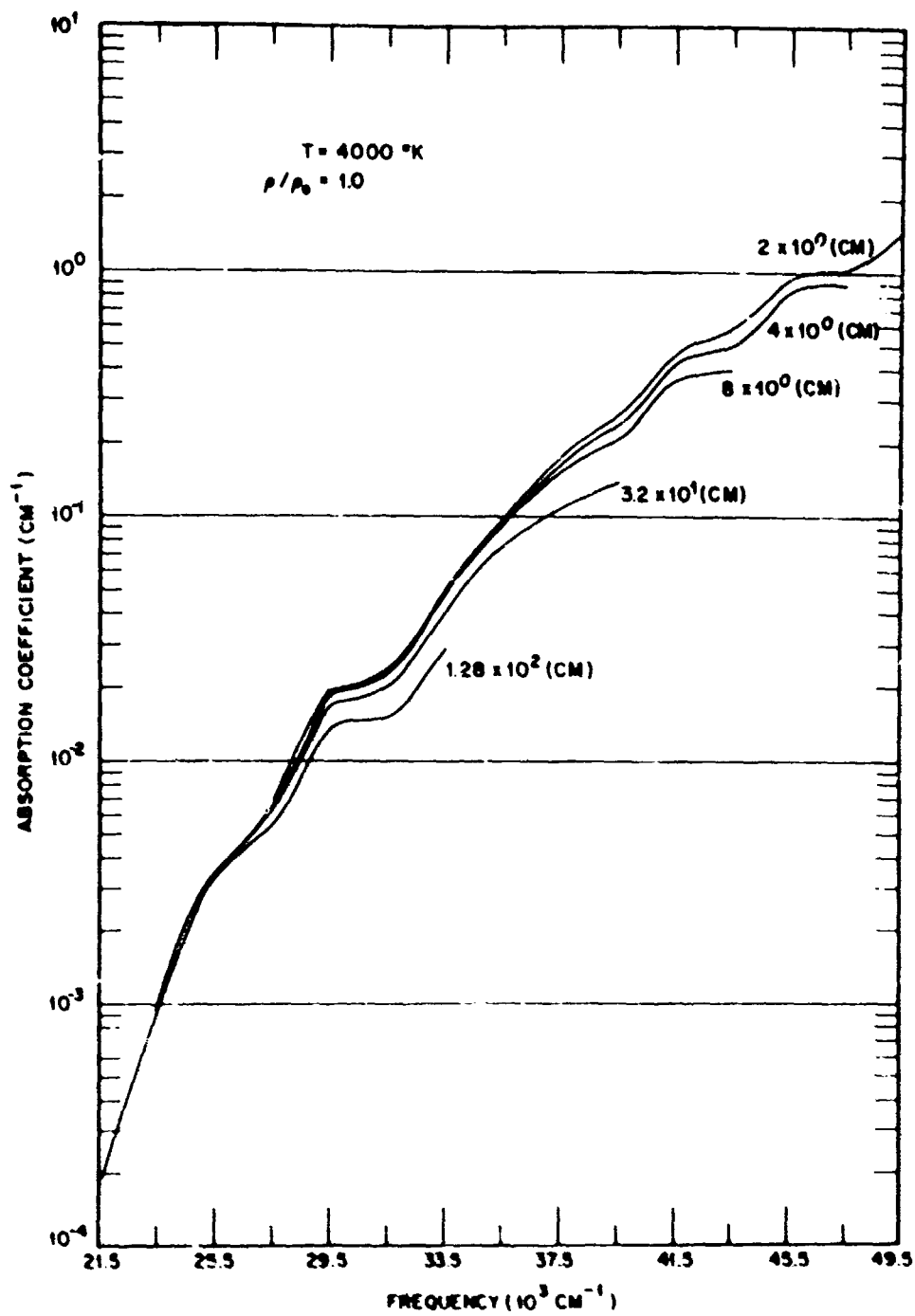
Fig. 42 The average absorption coefficient of heated air as a function of frequency for various optical path lengths.

80
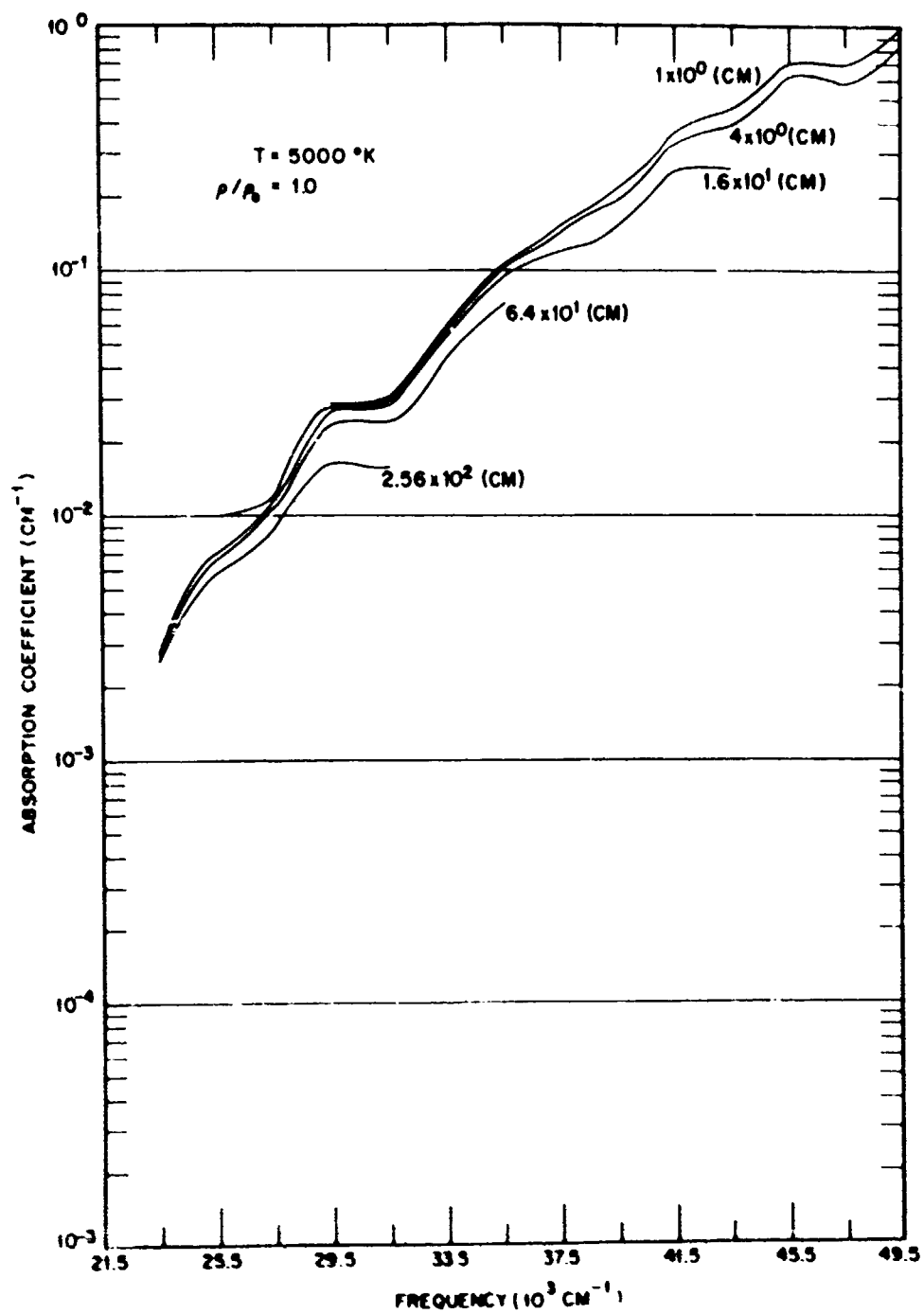
Fig. 43 The average absorption coefficient of heated air as a function of frequency for various optical path lengths.

81
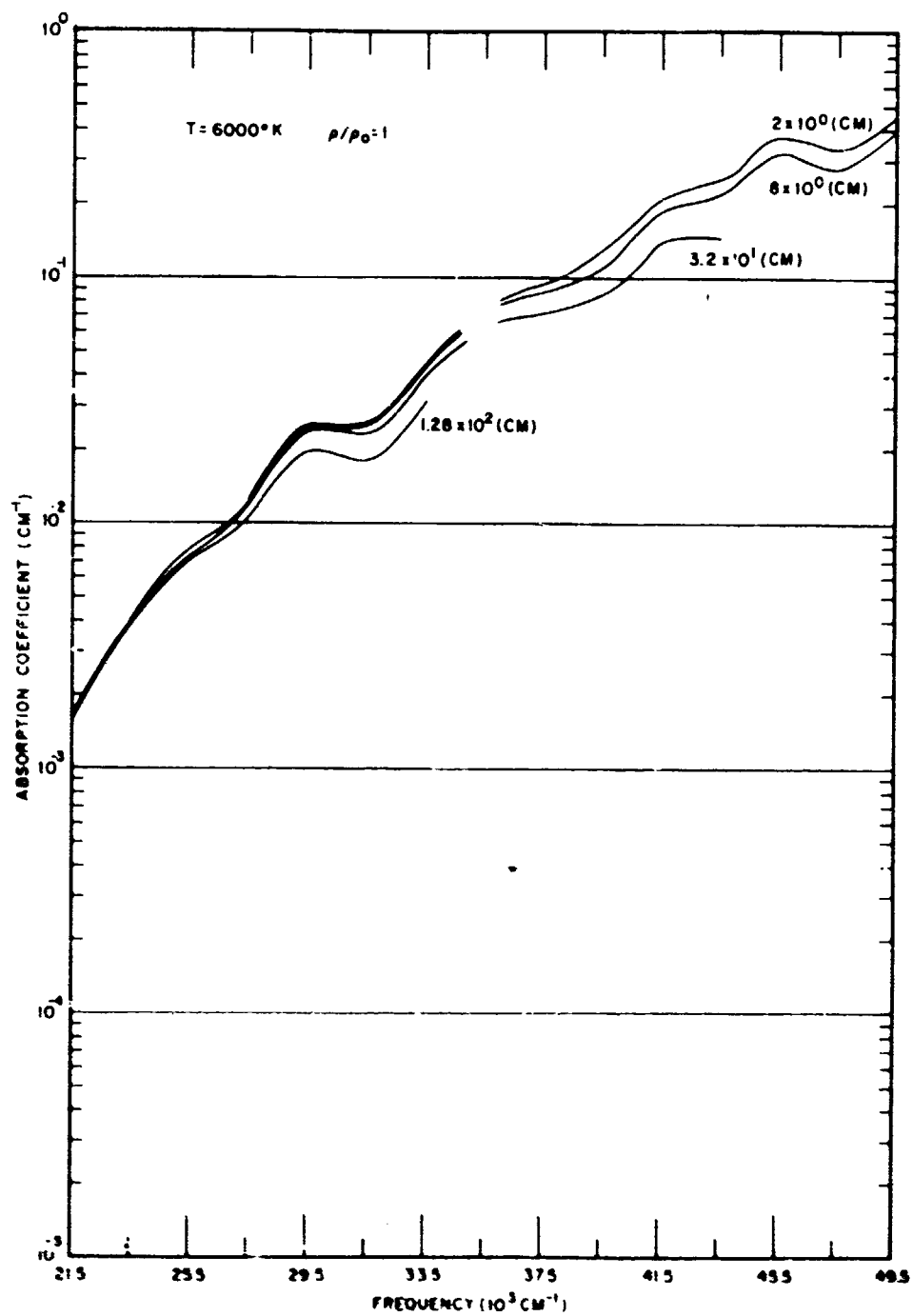
Fig. 44 The average absorption coefficient of heated air as a function of frequency for various optical path lengths.

82
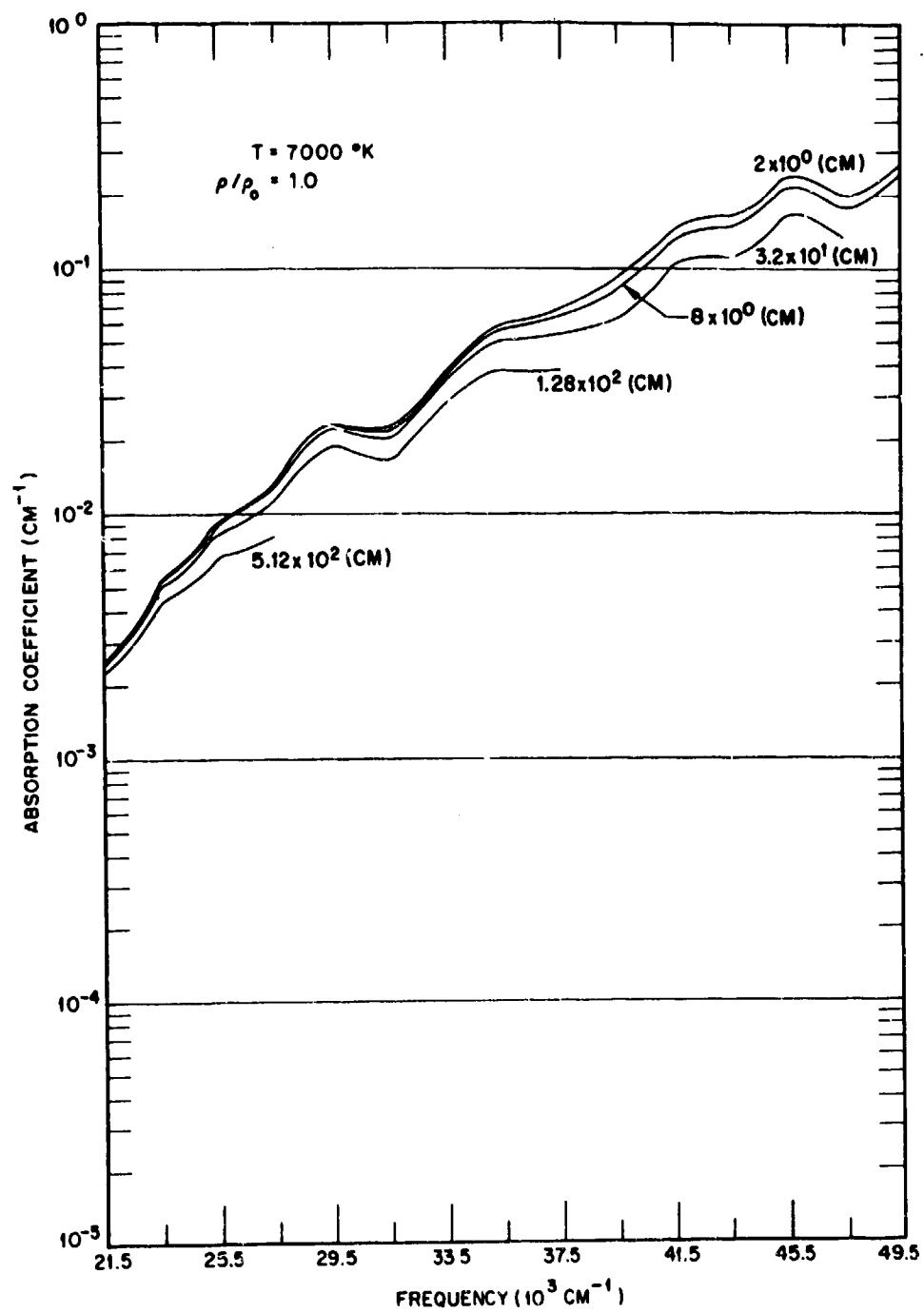
Fig. 45   The average absorption coefficient of heated air as a function of frequency for various optical path lengths.

83
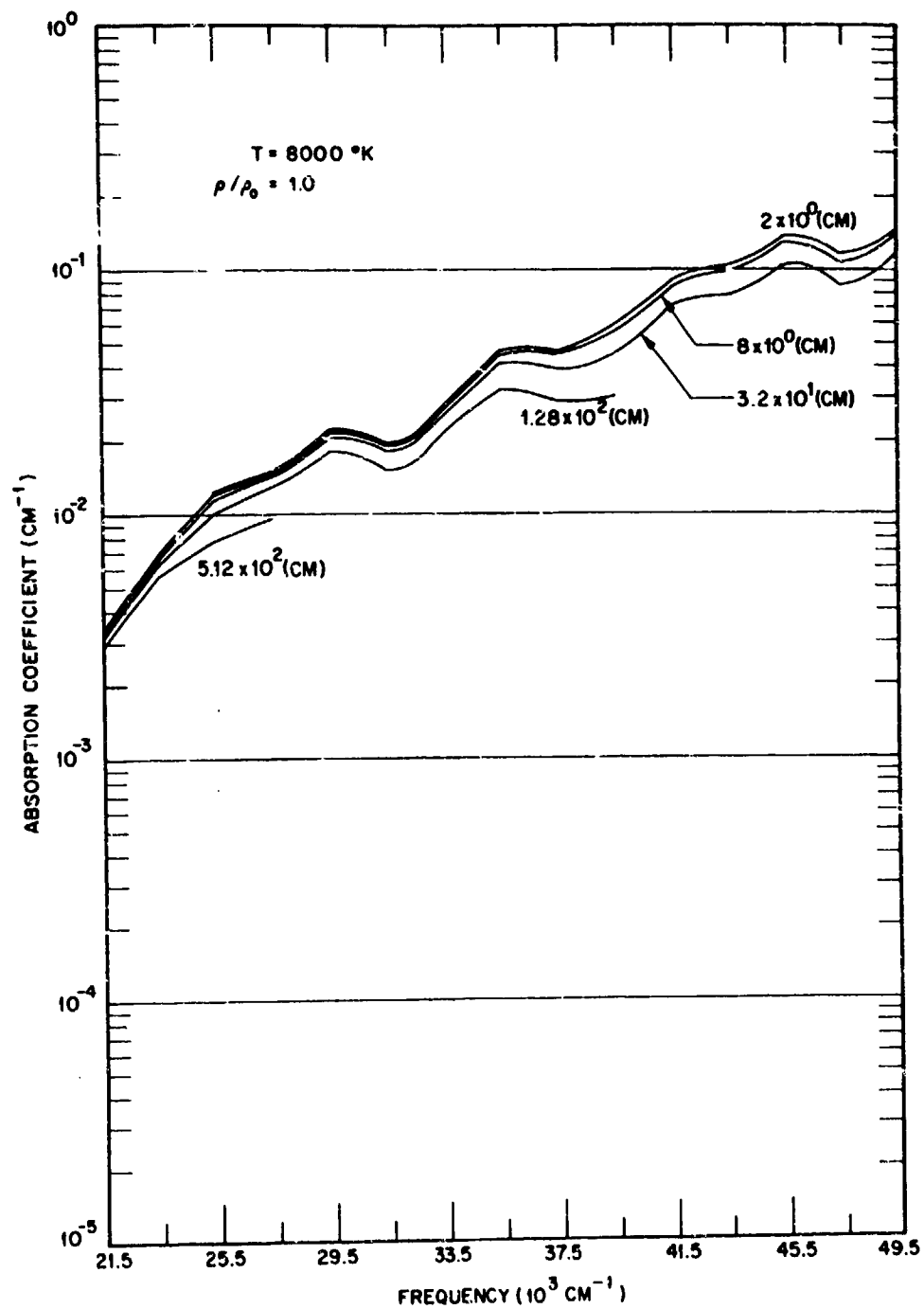
Fig. 46   The average absorption coefficient of heated air as a function of frequency for various optical path lengths.
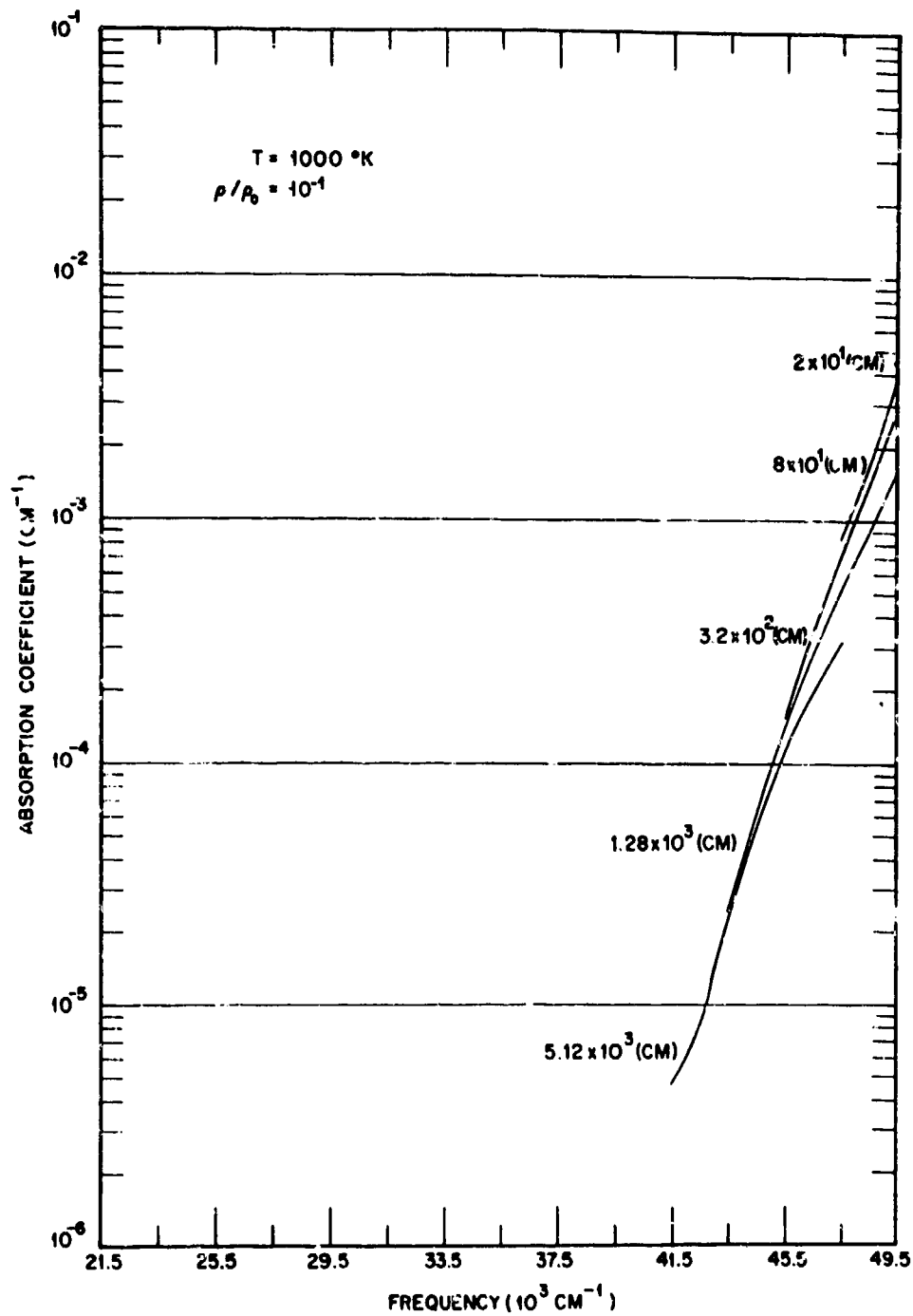
Fig. 47 The average absorption coefficient of heated air as a function of frequency for various optical path lengths.

85
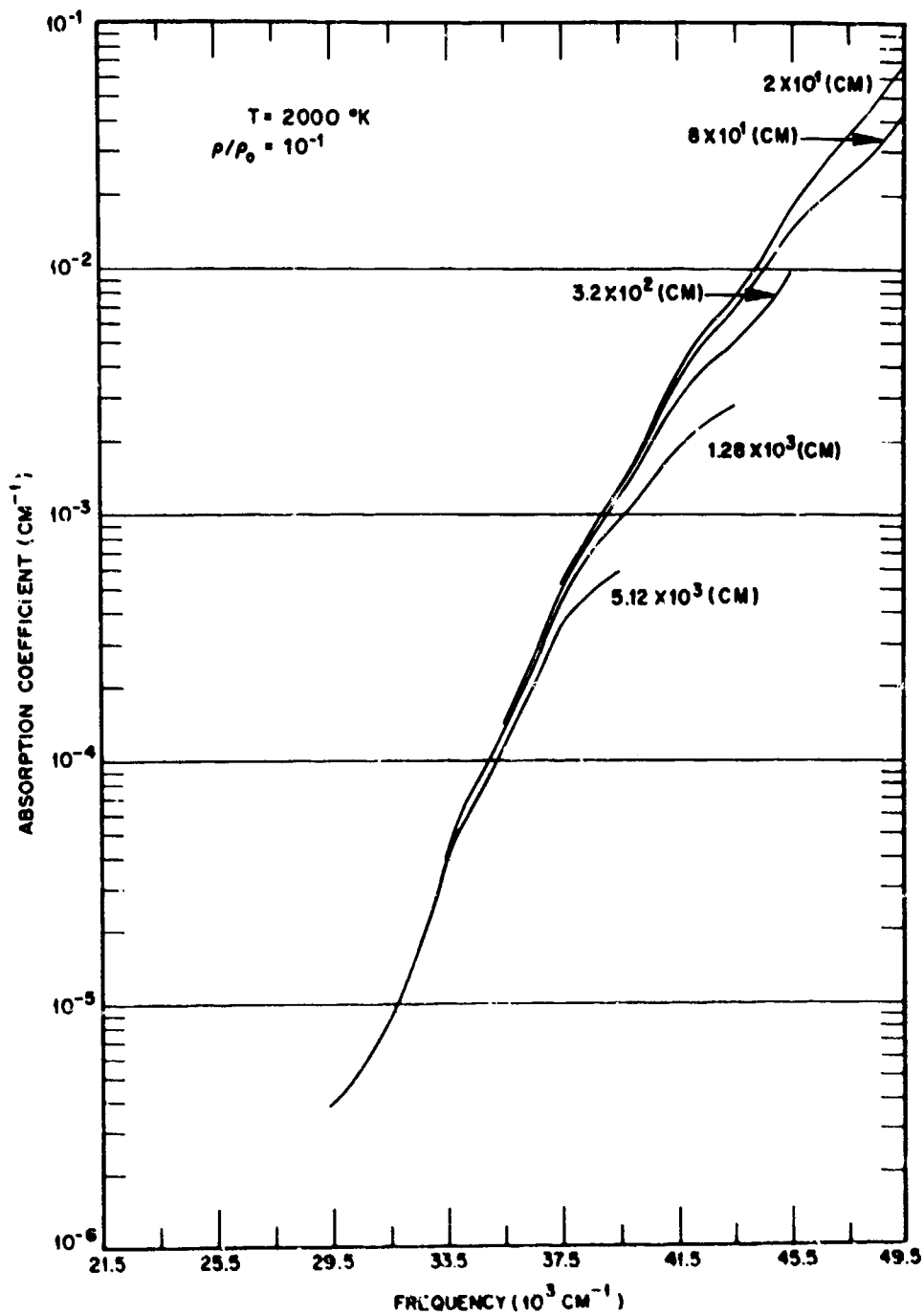
Fig. 48   The average absorption coefficient of heated air as a function of frequency for various optical path lengths.

86
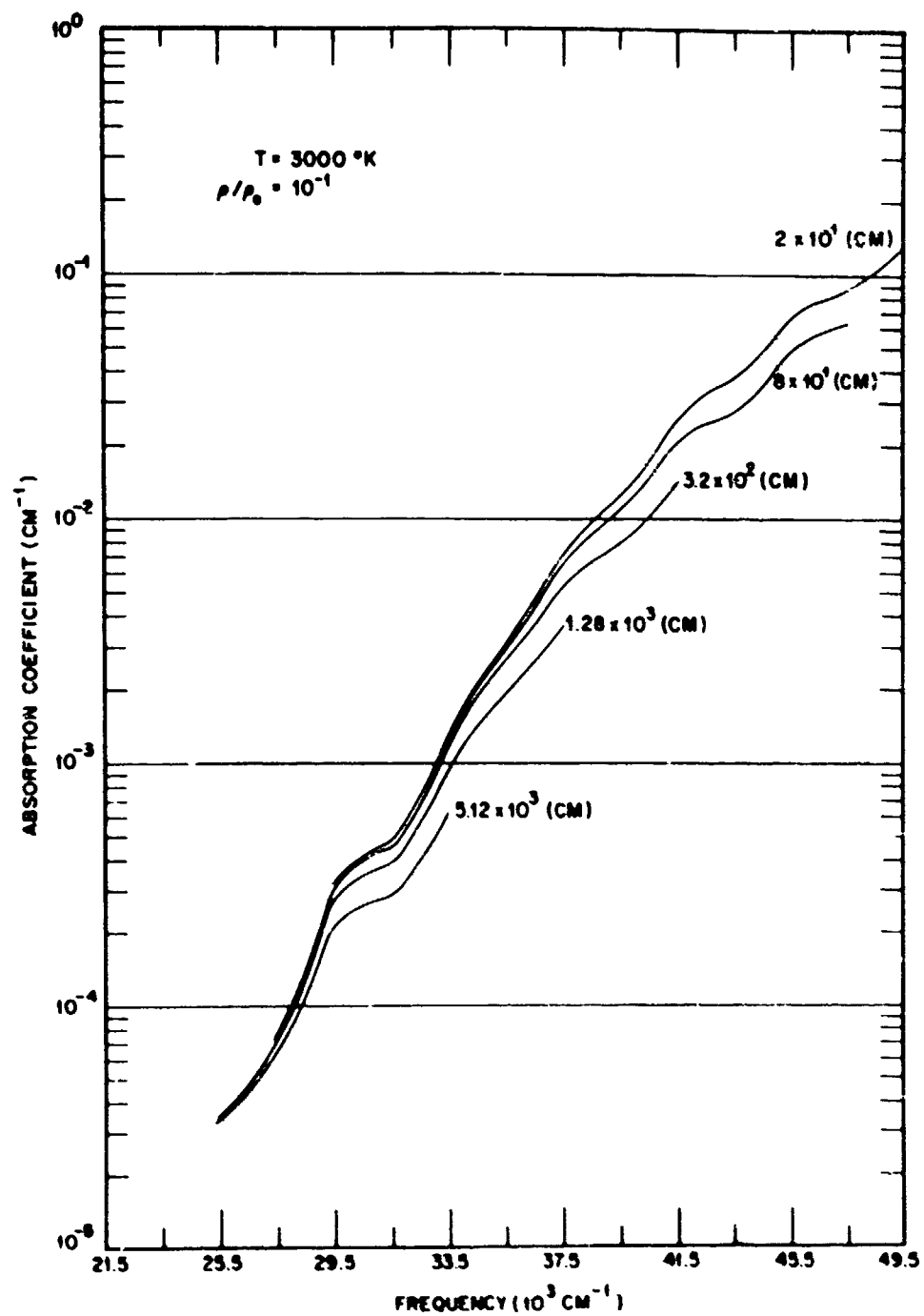
Fig. 49   The average absorption coefficient of heated air as a function of
frequency for various optical path lengths.

87
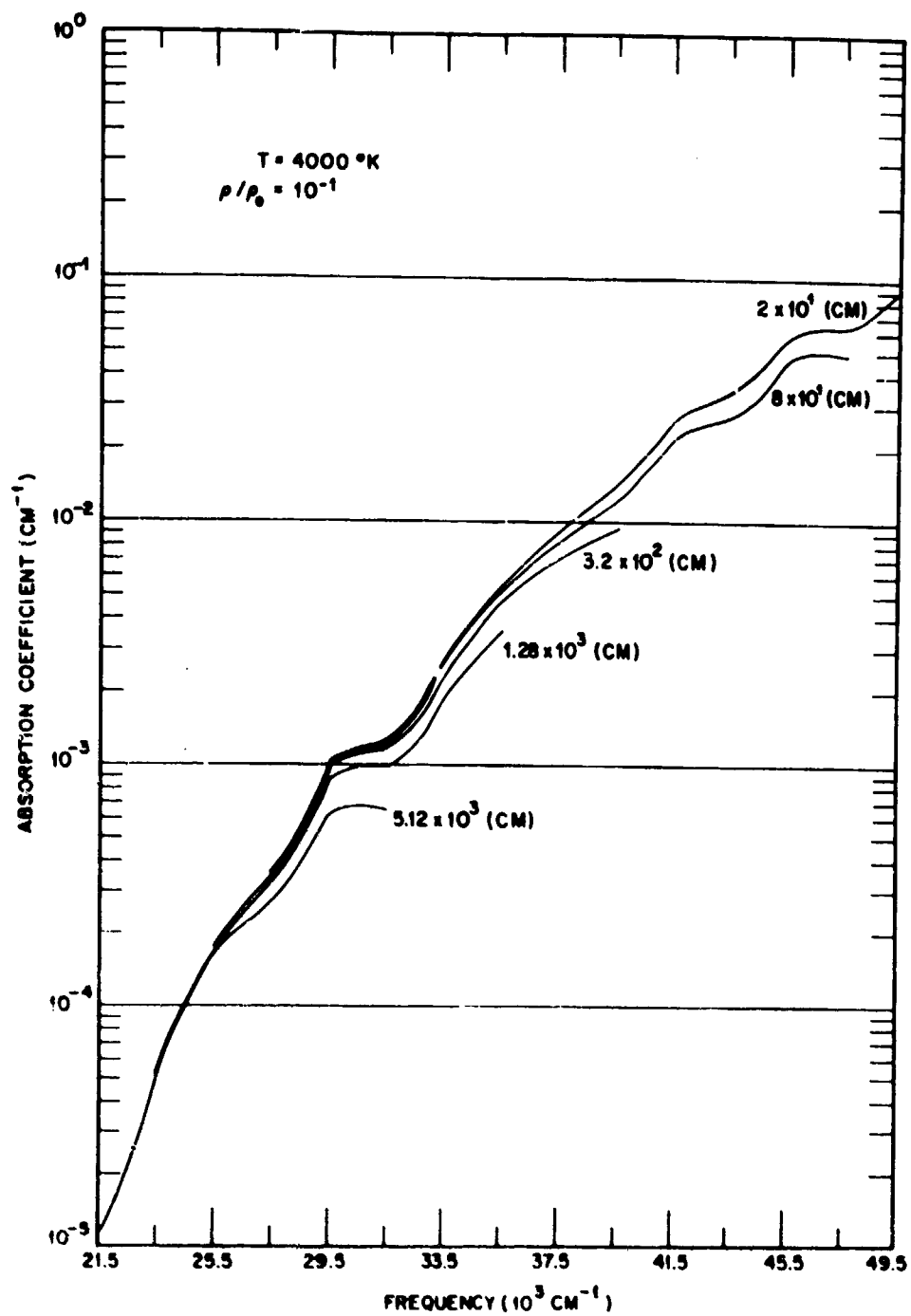
Fig. 50 The average absorption coefficient of heated air as a function of frequency for various optical path lengths.

88
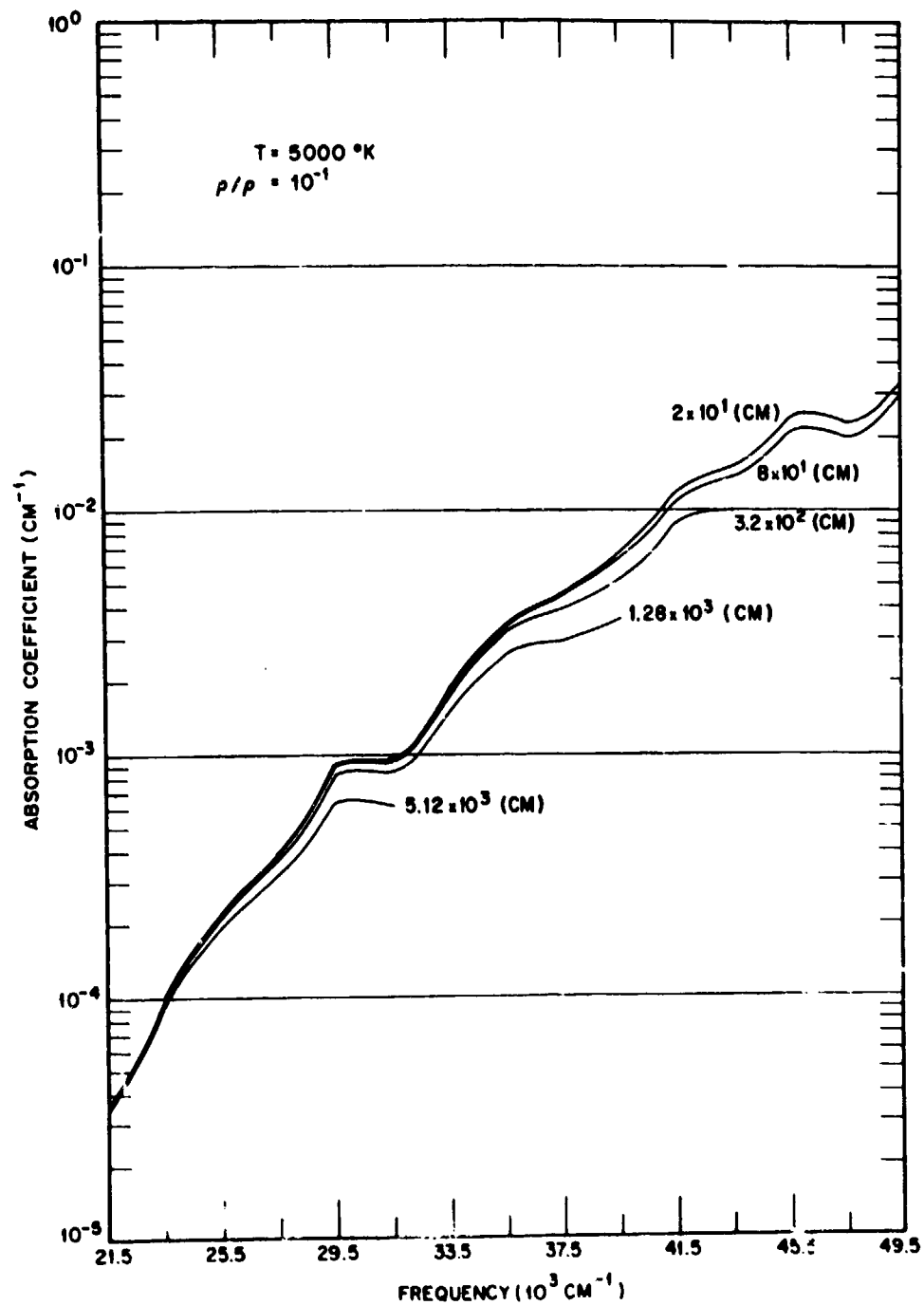
Fig. 51   The average absorption coefficient of heated air as a function of
frequency for various optical path lengths.

89
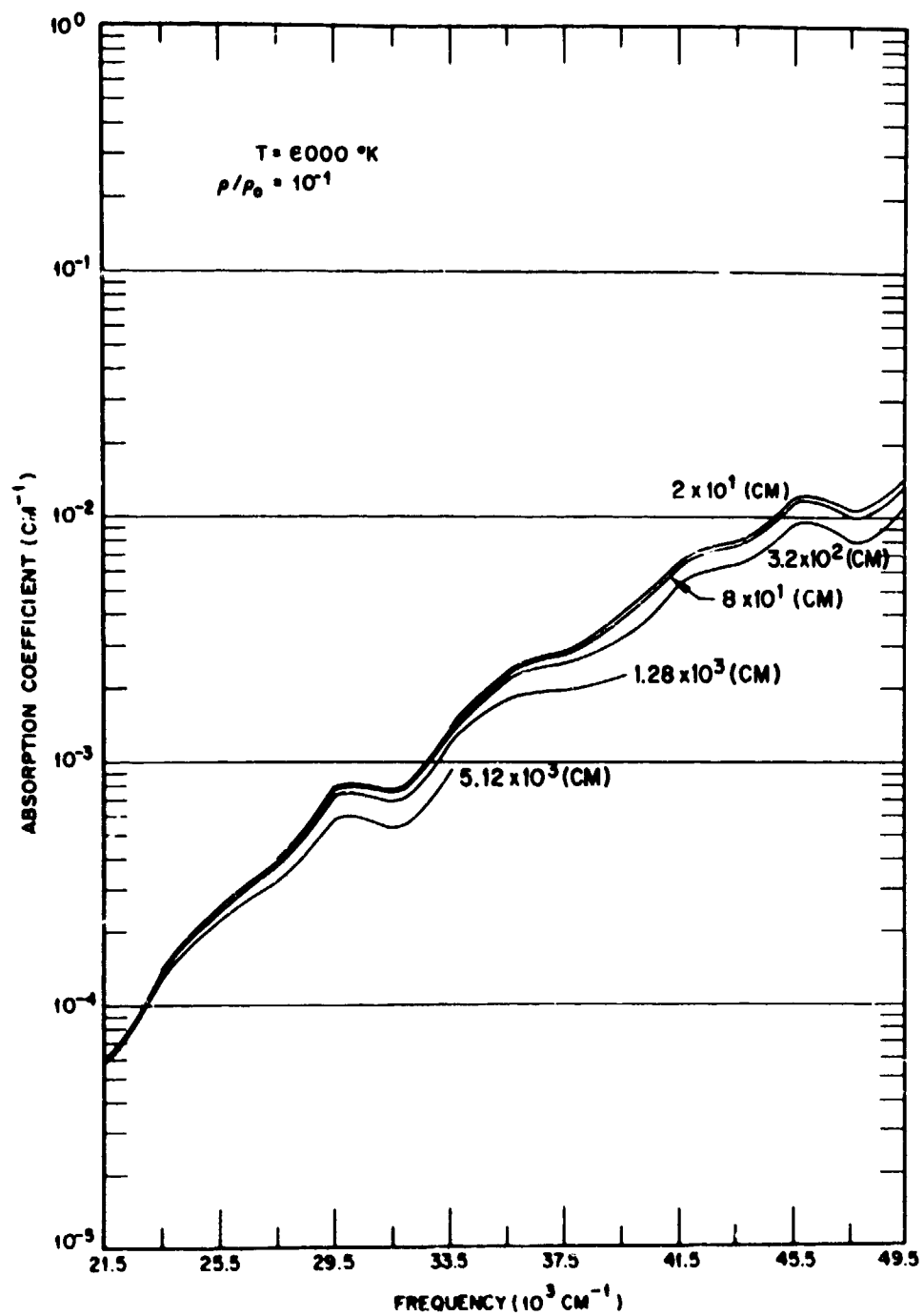
Fig. 52 The average absorption coefficient of heated air as a function of
frequency for various optical path lengths.

90
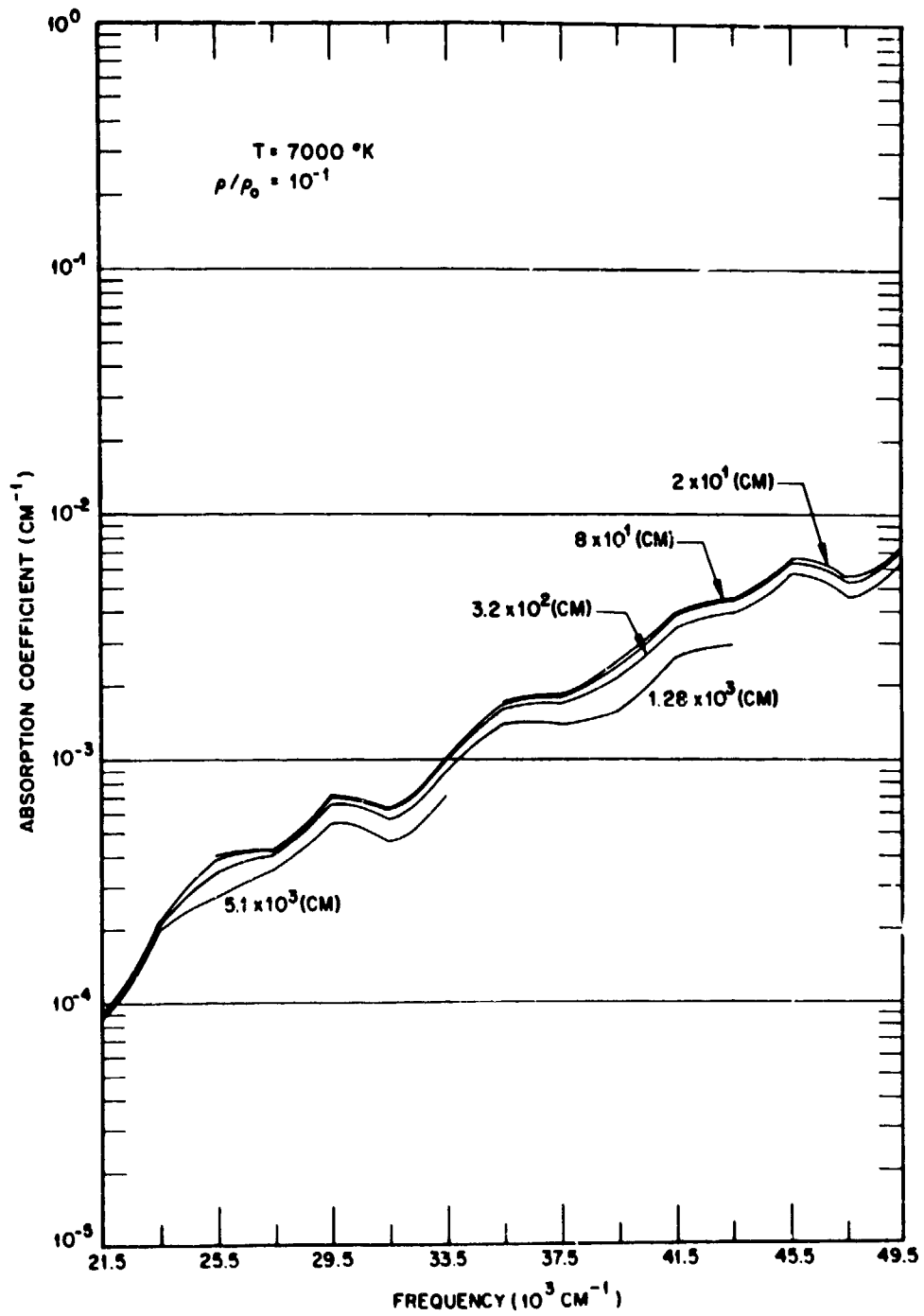
Fig. 53 The average absorption coefficient of heated air as a function of
frequency for various optical path lengths.

91
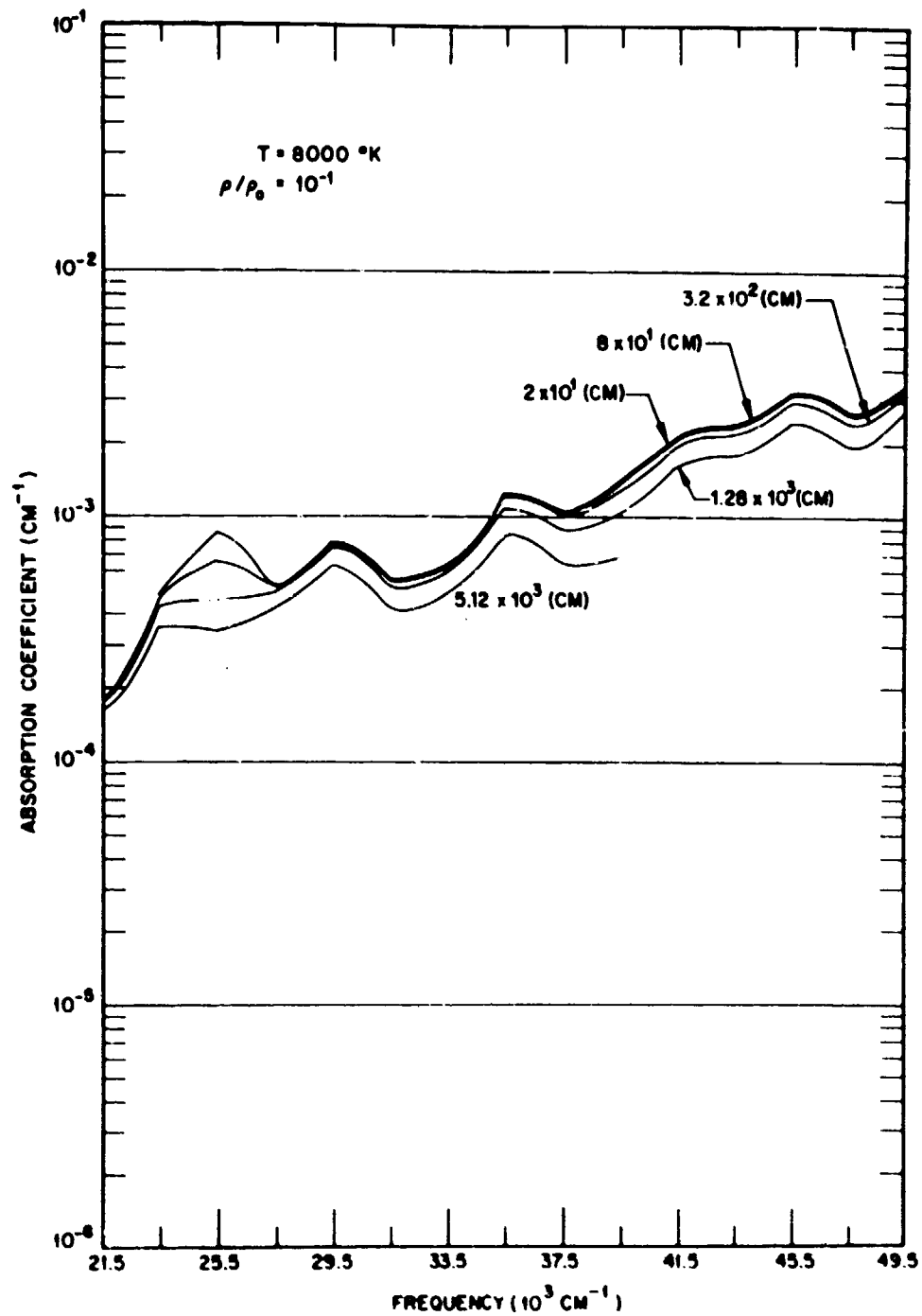
Fig. 54 The average absorption coefficient of heated air as a function of
frequency for various optical path lengths.

92
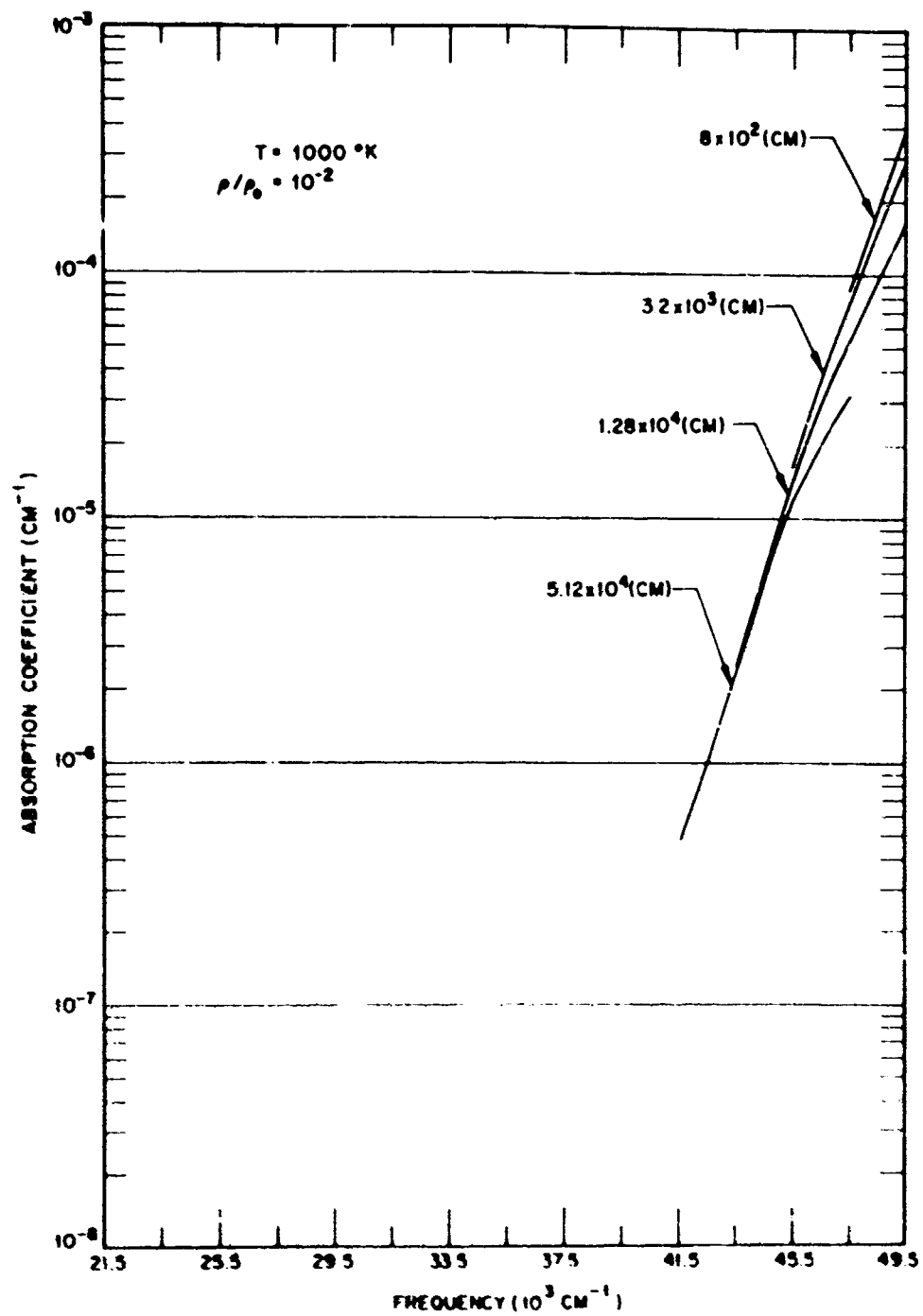
Fig. 55 The average absorption coefficient of heated air as a function of frequency for various optical path lengths.
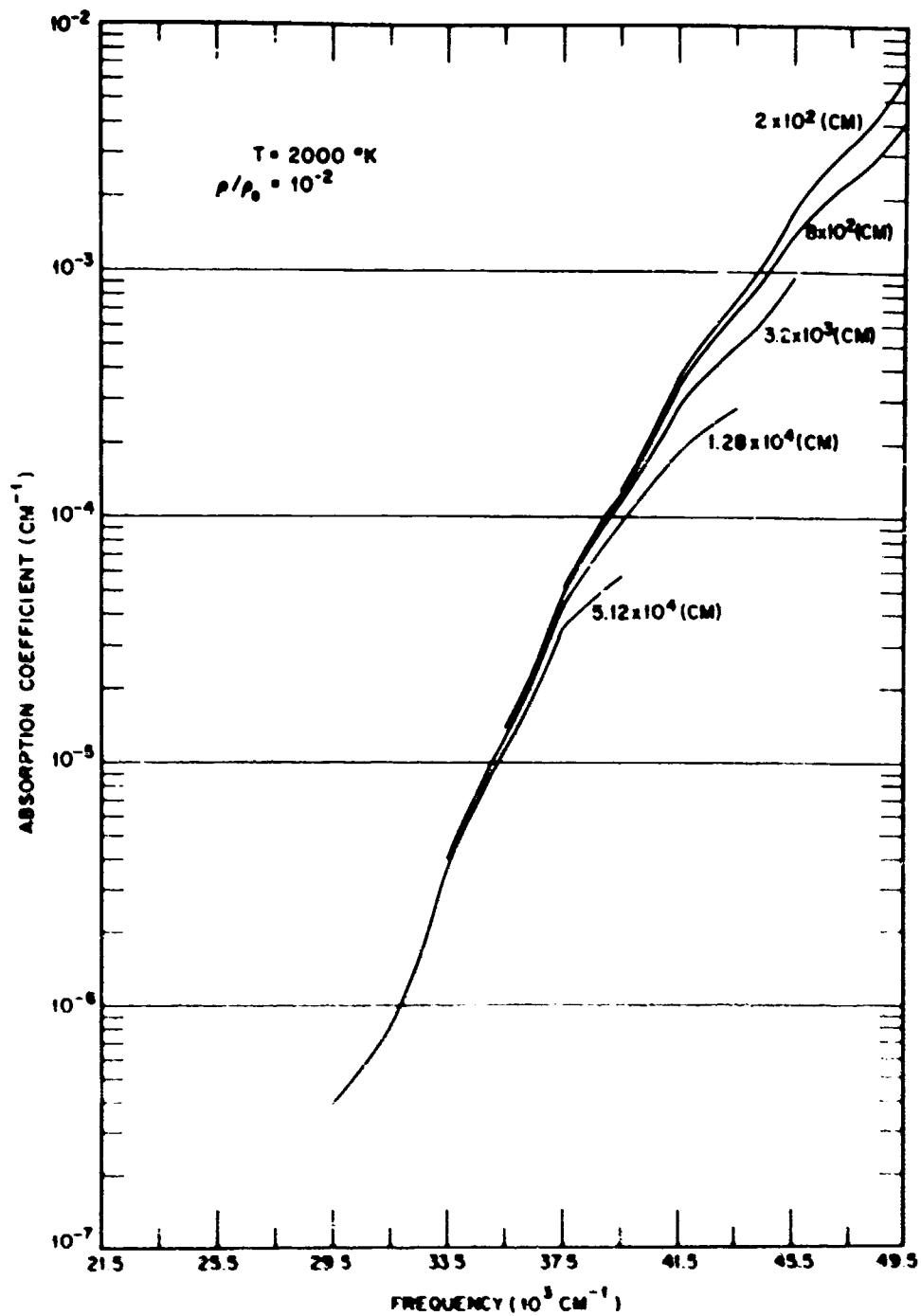
Fig. 56 The average absorption coefficient of heated air as a function of
frequency for various optical path lengths.
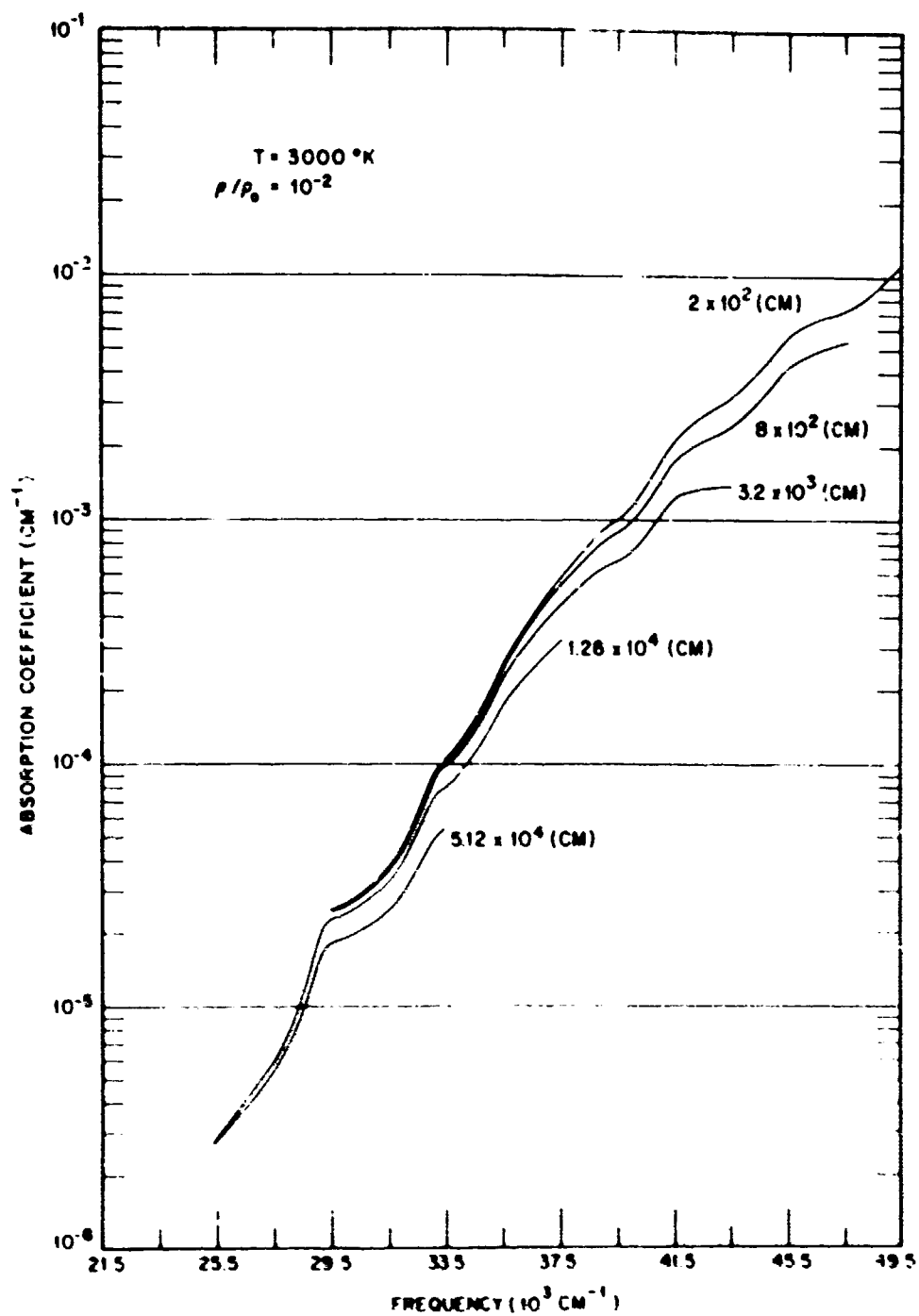
Fig. 57 The average absorption coefficient of heated air as a function of frequency for various optical path lengths.
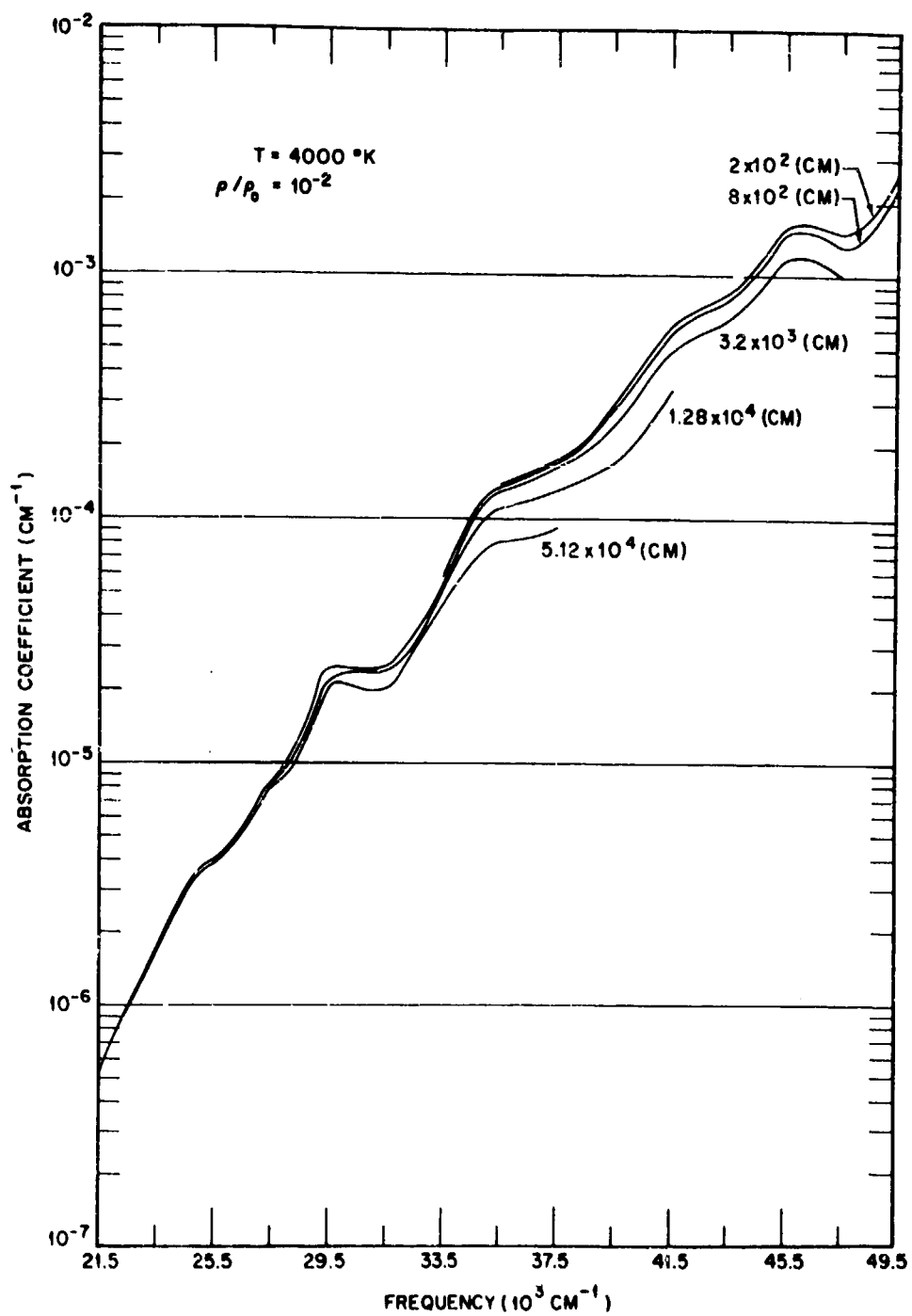
Fig. 58   The average absorption coefficient of heated air as a function of
frequency for various optical path lengths.

96
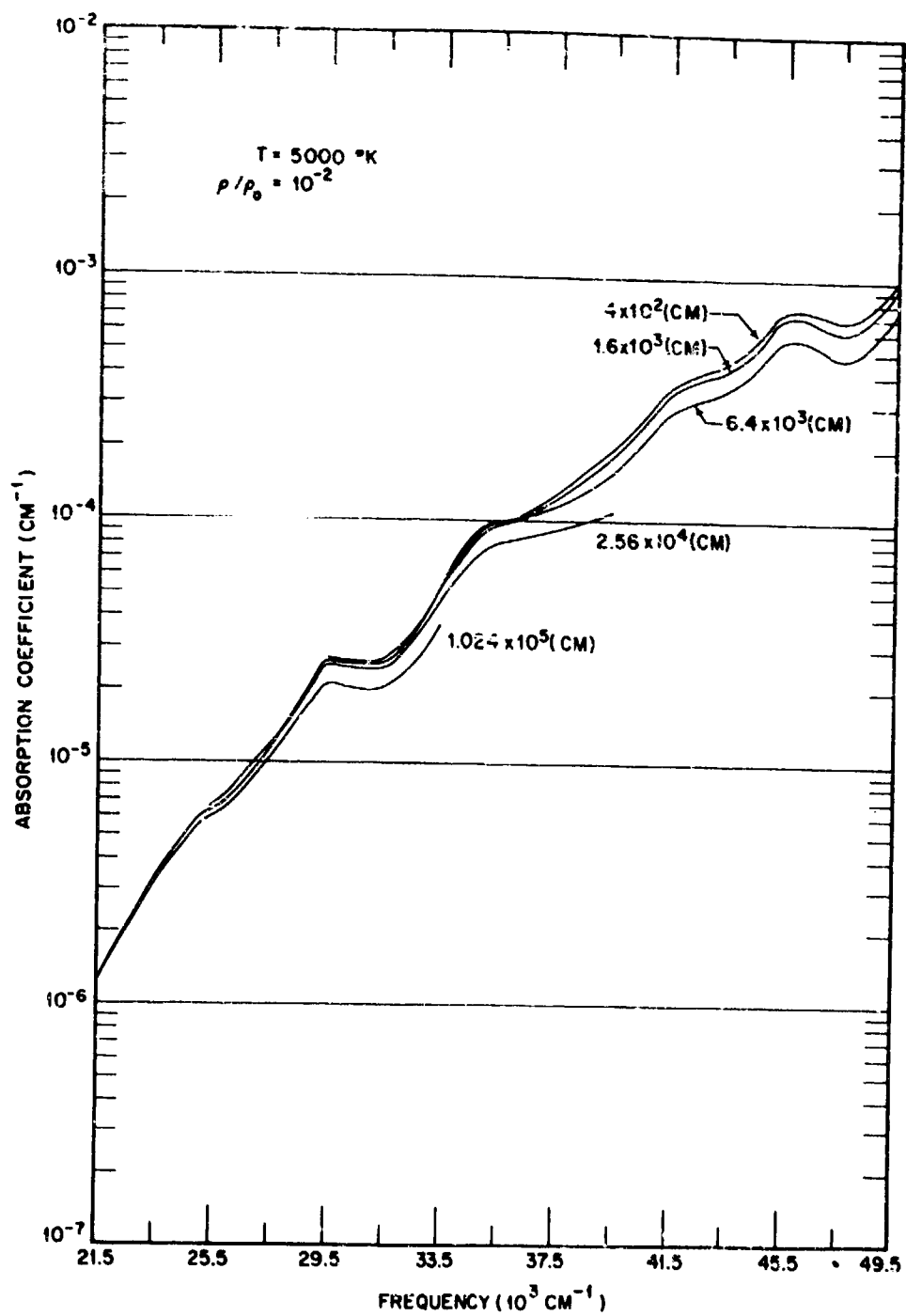
Fig. 59 The average absorption coefficient of heated air as a function of frequency for various optical path lengths.

97
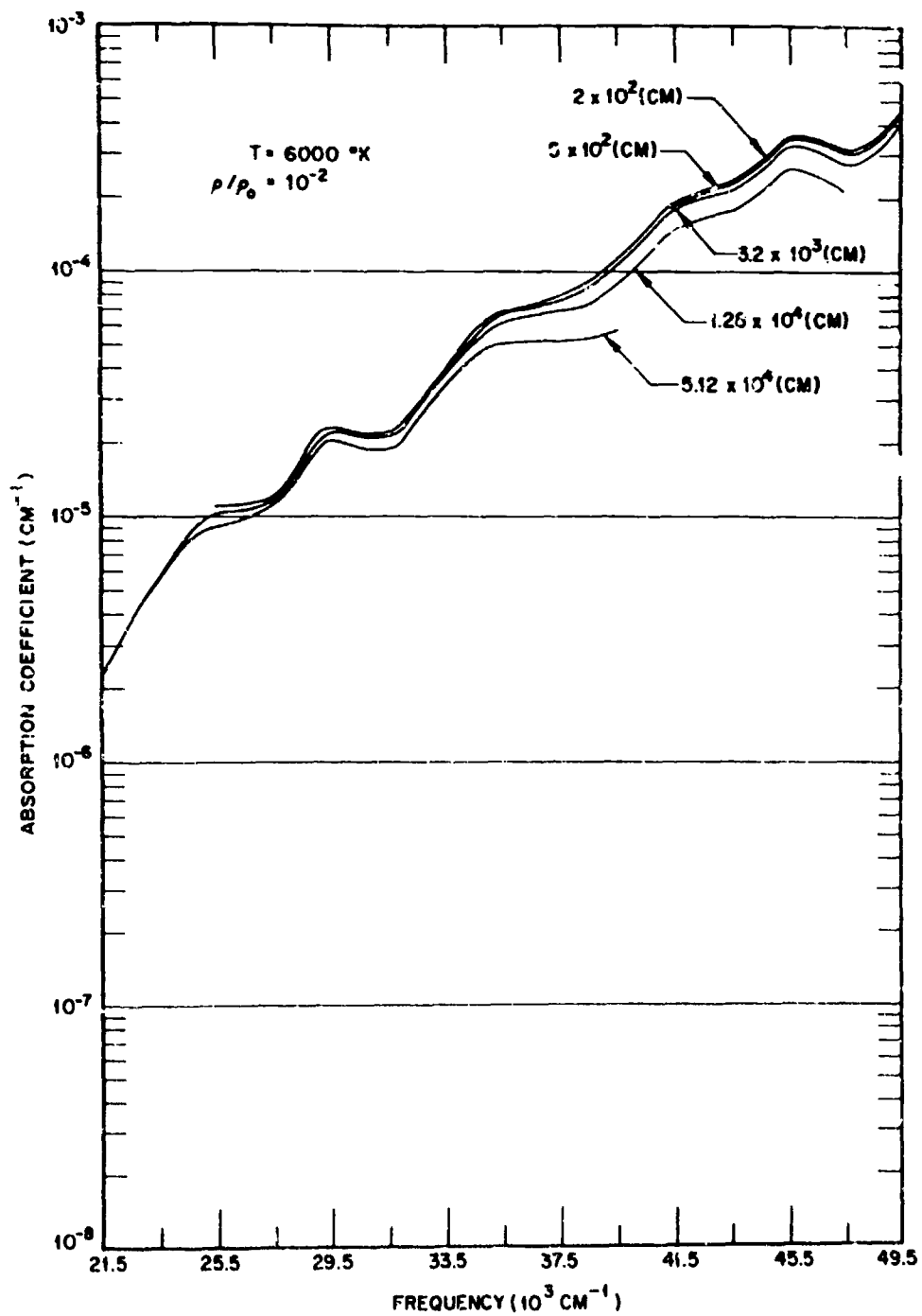
Fig. 60 The average absorption coefficient of heated air as a function of frequency for various optical path lengths.

98
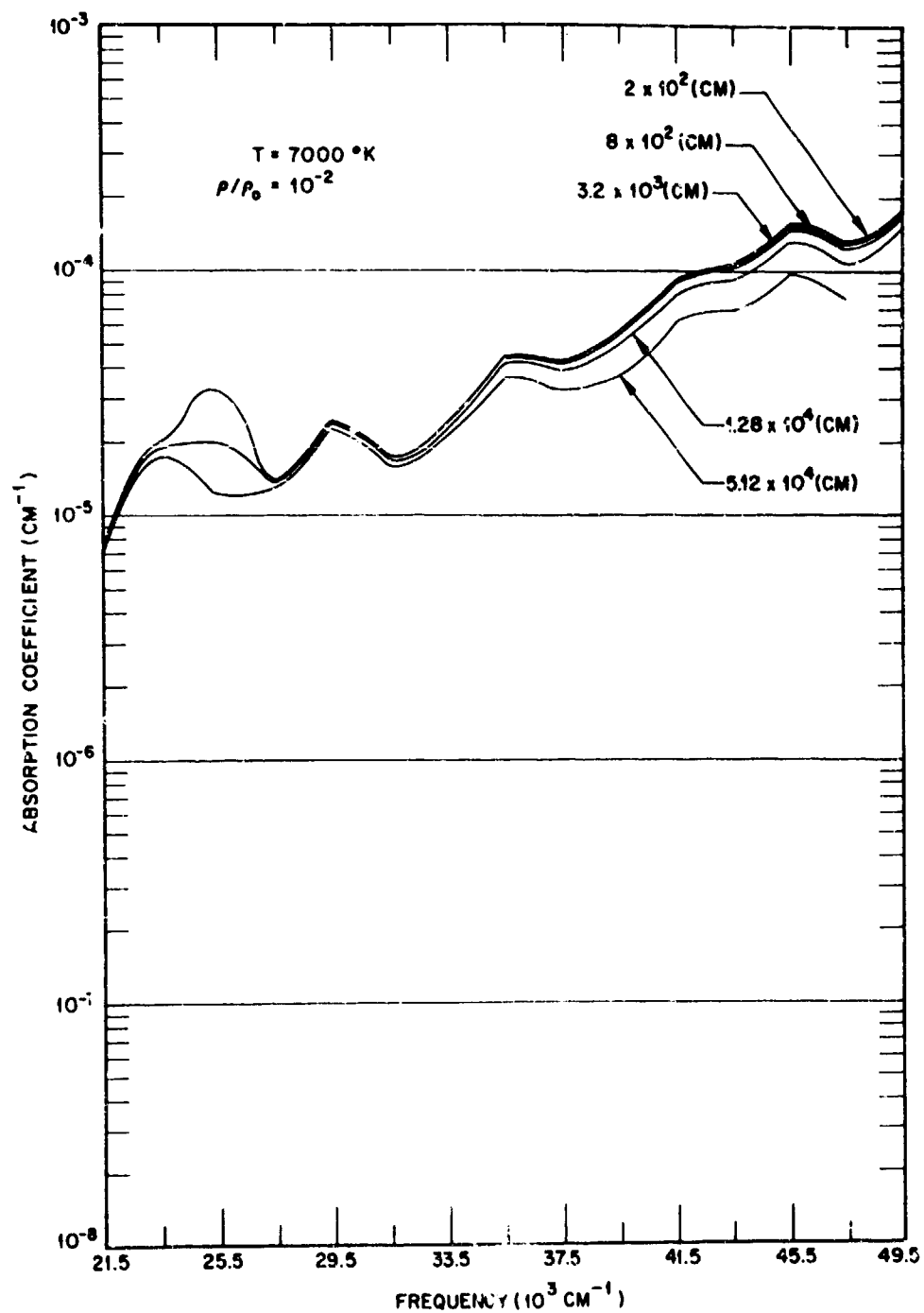
Fig. 61 The average absorption coefficient of heated air as a function of frequency for various optical path lengths.
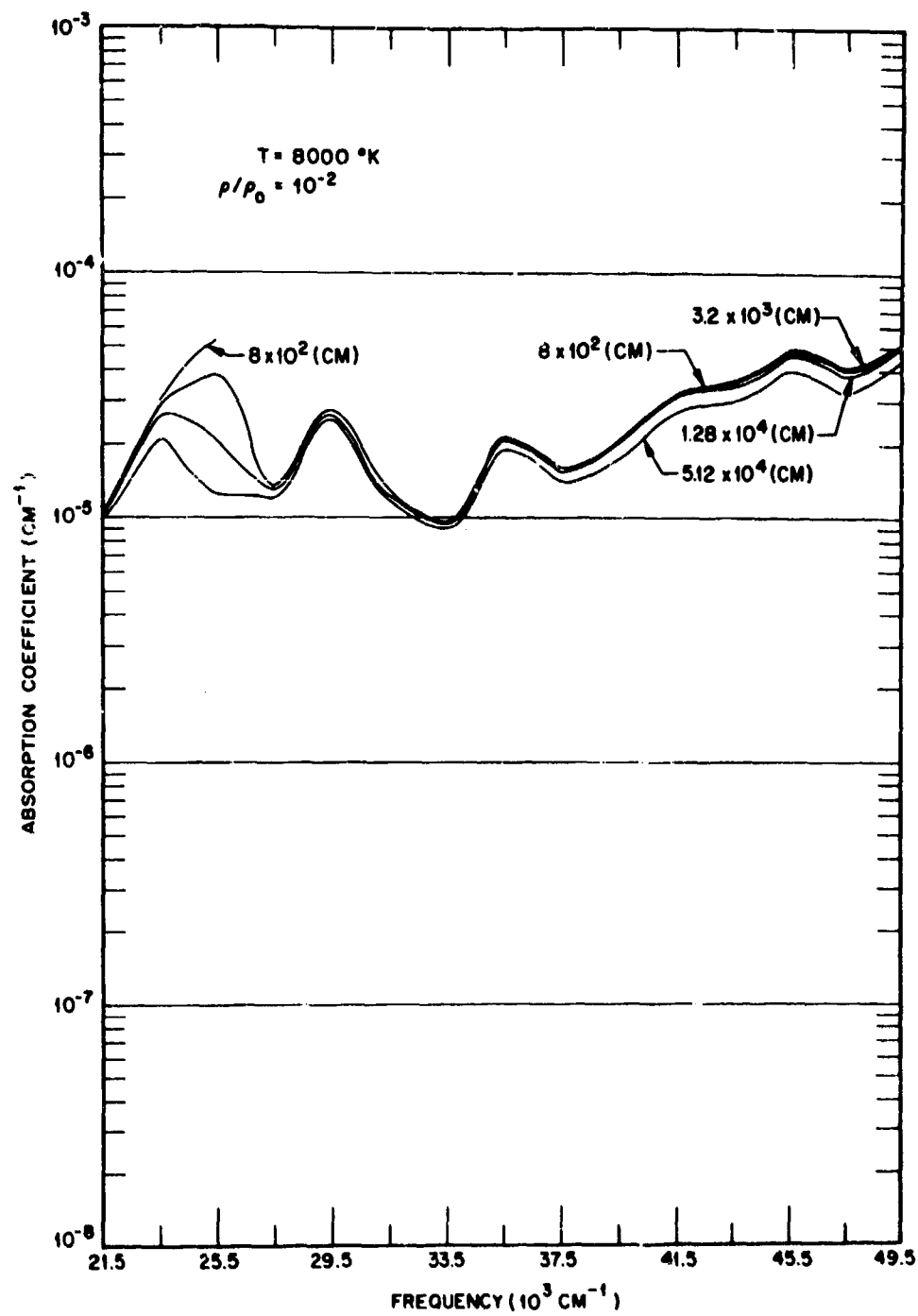
Fig. 62 The average absorption coefficient of heated air as a function of frequency for various optical path lengths.

100
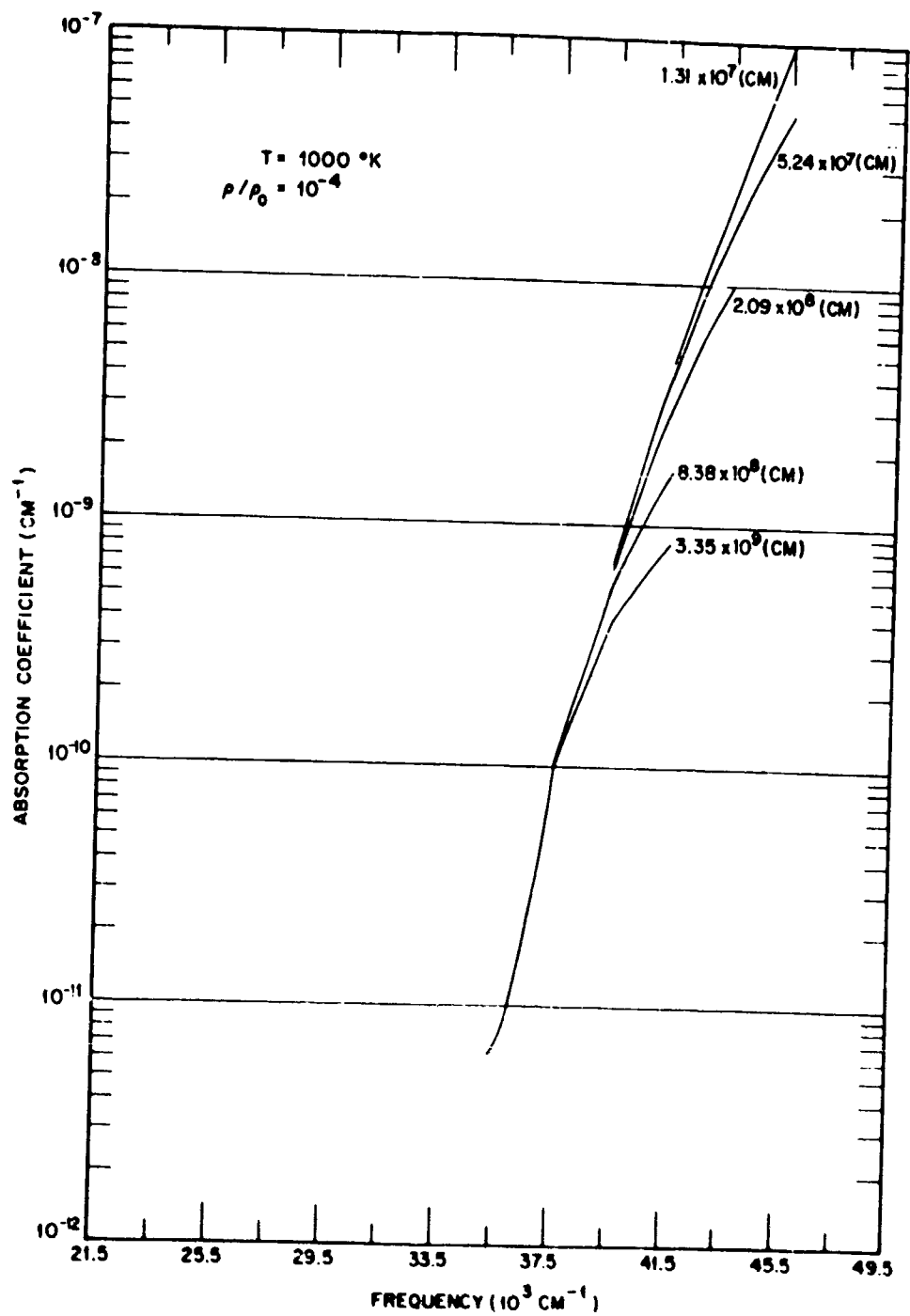
Fig. 63 The average absorption coefficient of heated air as a function of frequency for various optical path lengths.

101
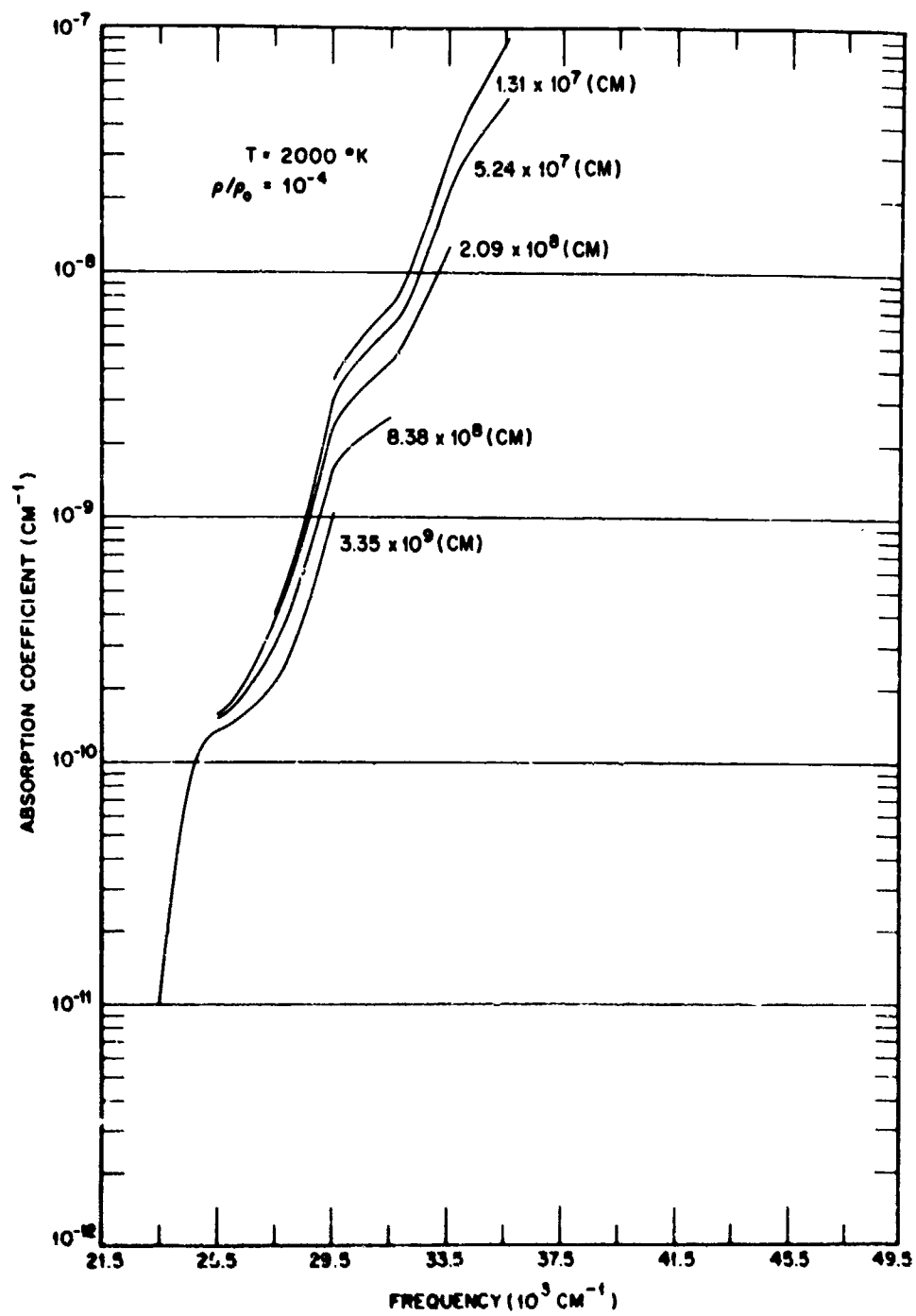
Fig. 64 The average absorption coefficient of heated air as a function of frequency for various optical path lengths.

102

Fig. 65   The average absorption coefficient of heated air as a function of
frequency for various optical path lengths.

103

T = 4000 °K
$\rho/\rho_0 = 10^{-4}$

$1.31 \times 10^7 (CM)$

$5.24 \times 10^7 (CM)$

$2.09 \times 10^8 (CM)$

$8.39 \times 10^8 (CM)$

ABSORPTION COEFFICIENT (CM^{-1})

FREQUENCY ($10^3 CM^{-1}$)
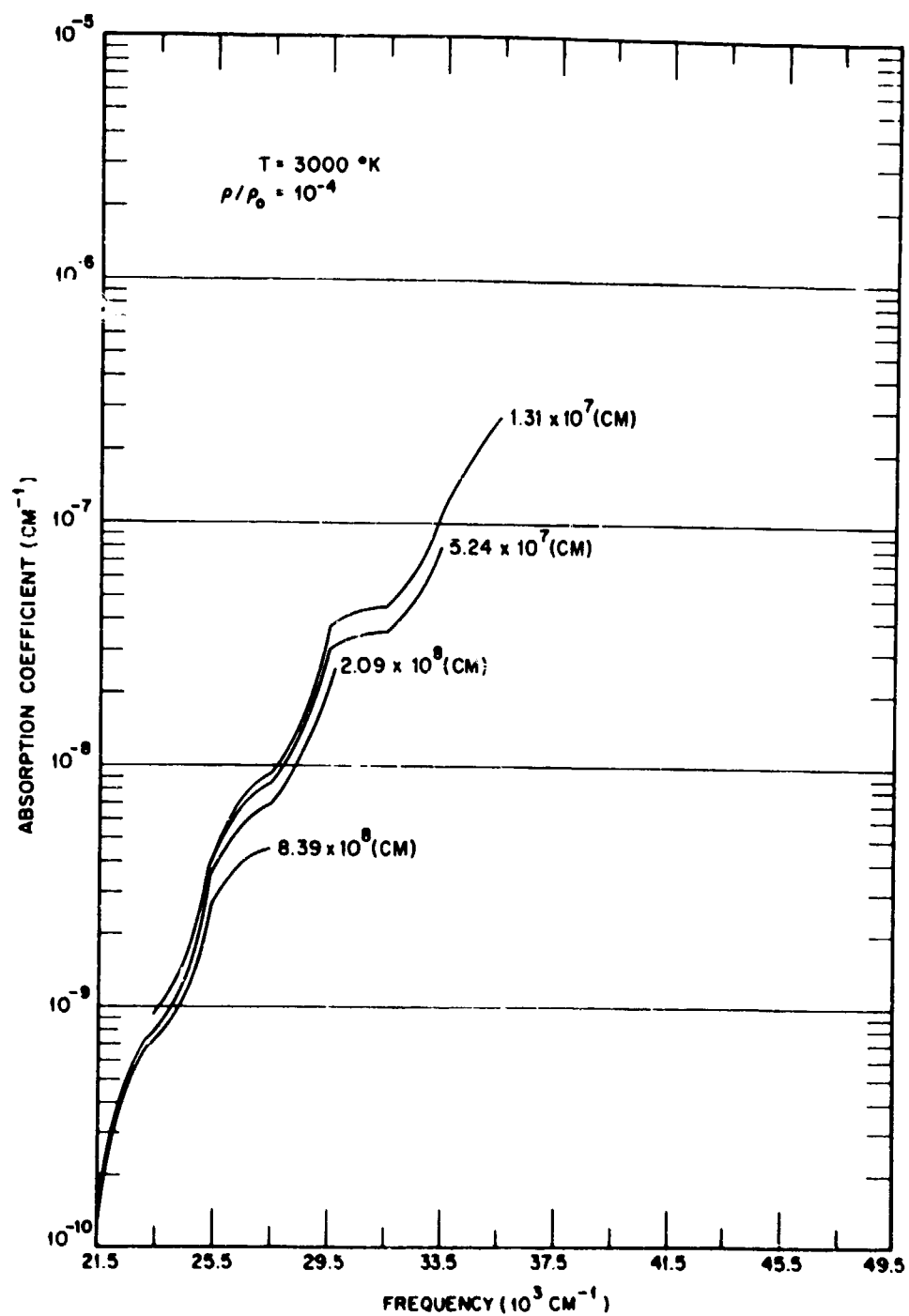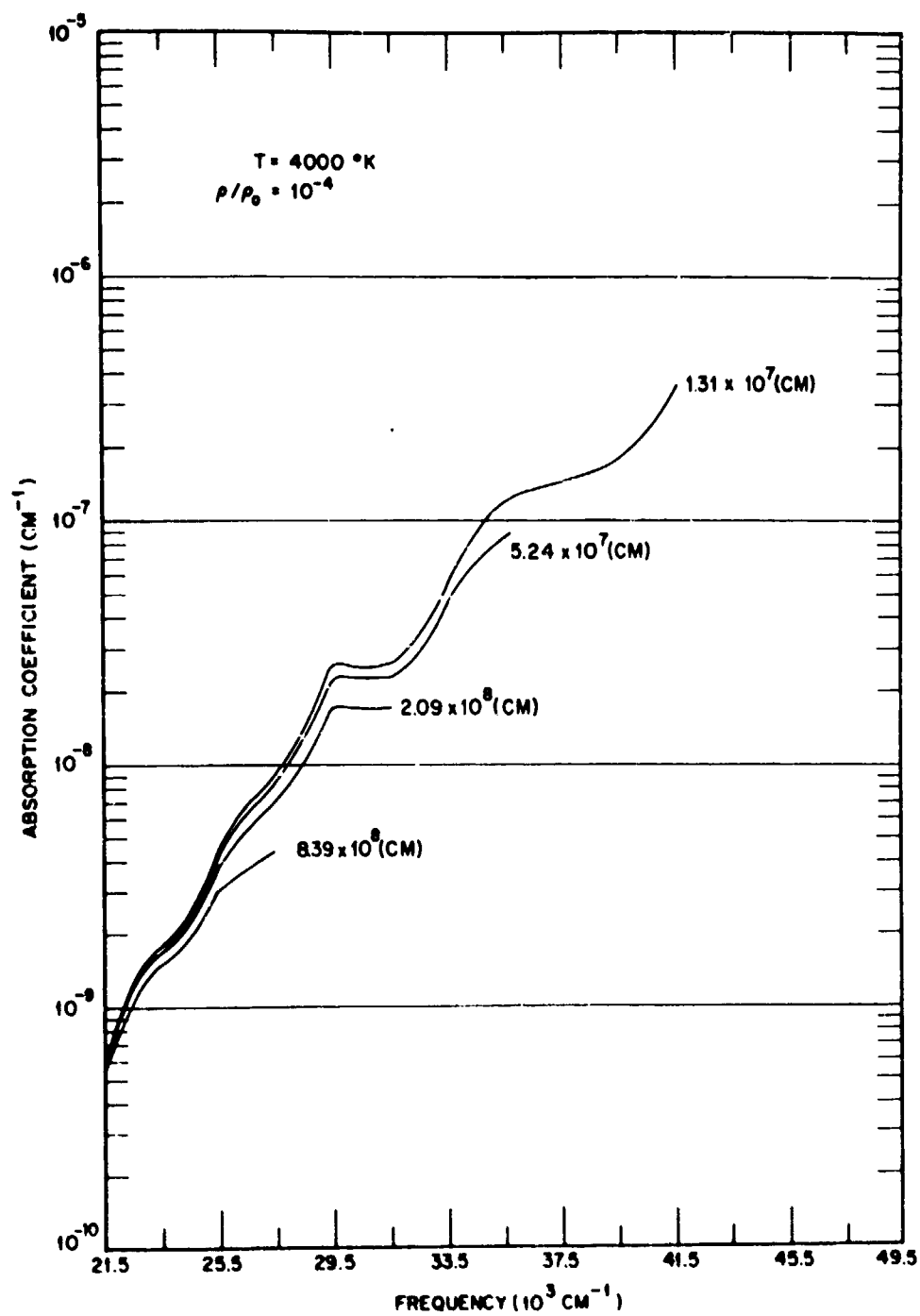
Fig. 66   The average absorption coefficient of heated air as a function of
frequency for various optical path lengths.

104
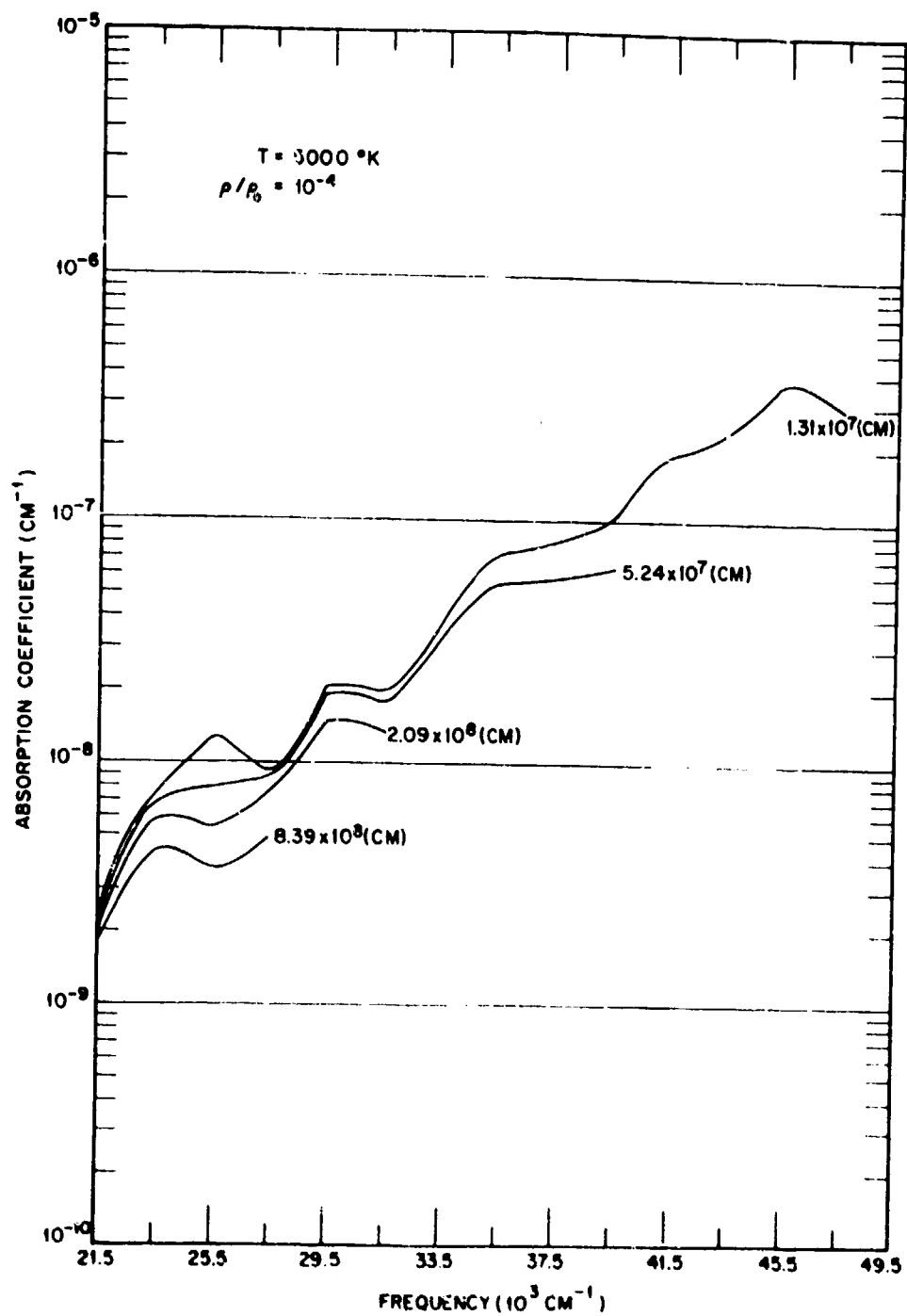
Fig. 67 The average absorption coefficient of heated air as a function of frequency for various optical path lengths.

105
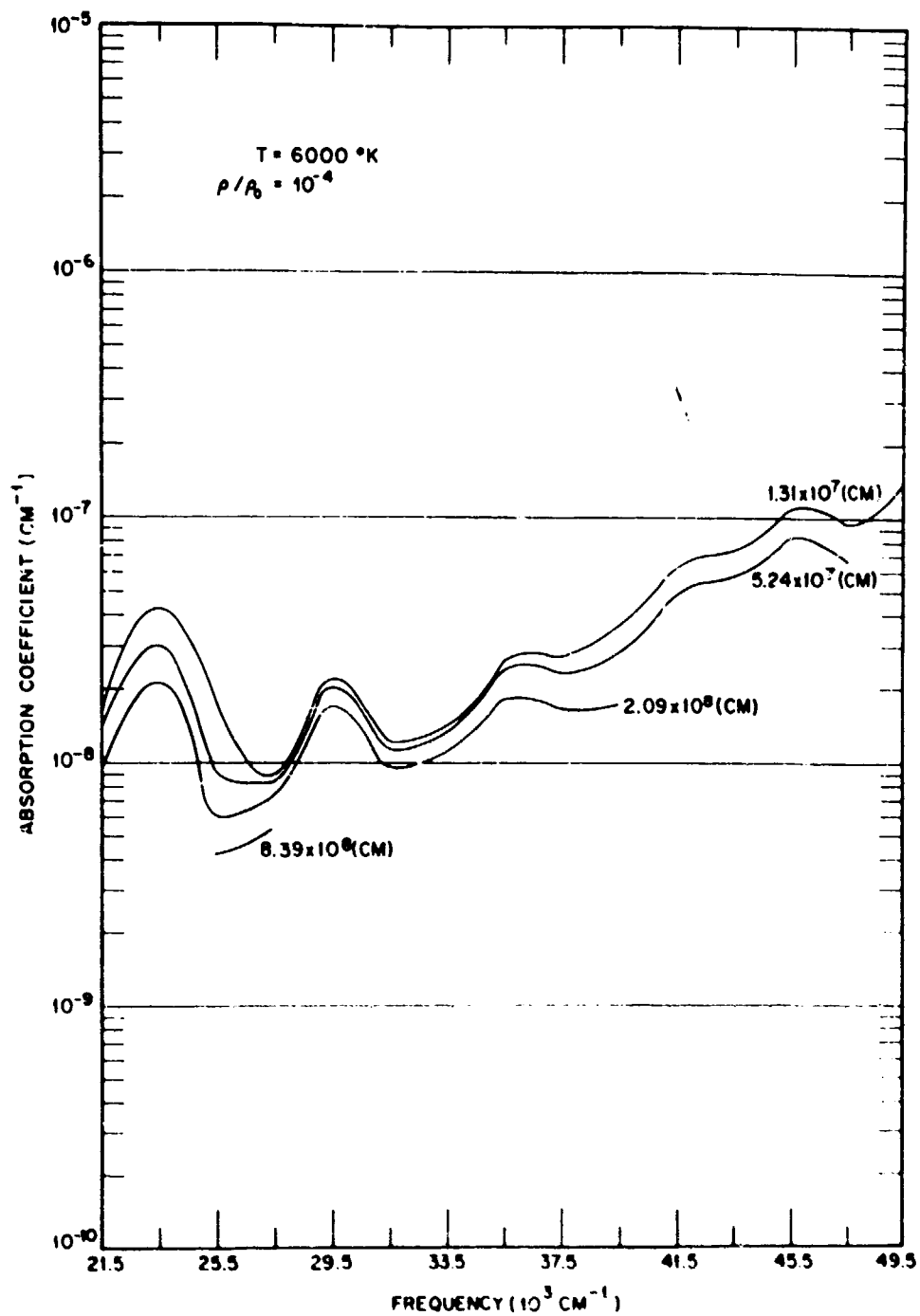
Fig. 68   The average absorption coefficient of heated air as a function of
frequency for various optical path lengths.

106
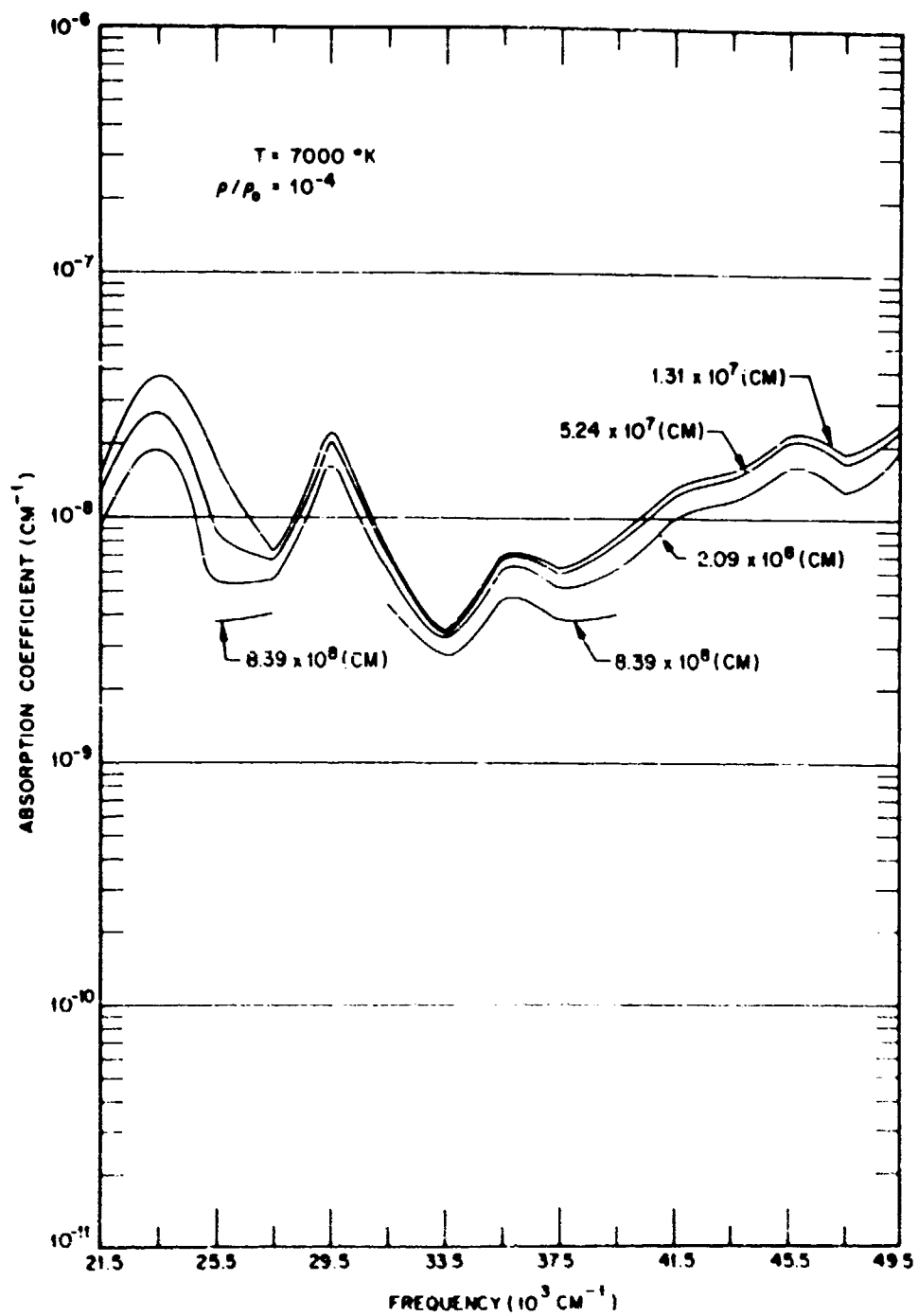
Fig. 69 The average absorption coefficient of heated air as a function of frequency for various optical path lengths.

107
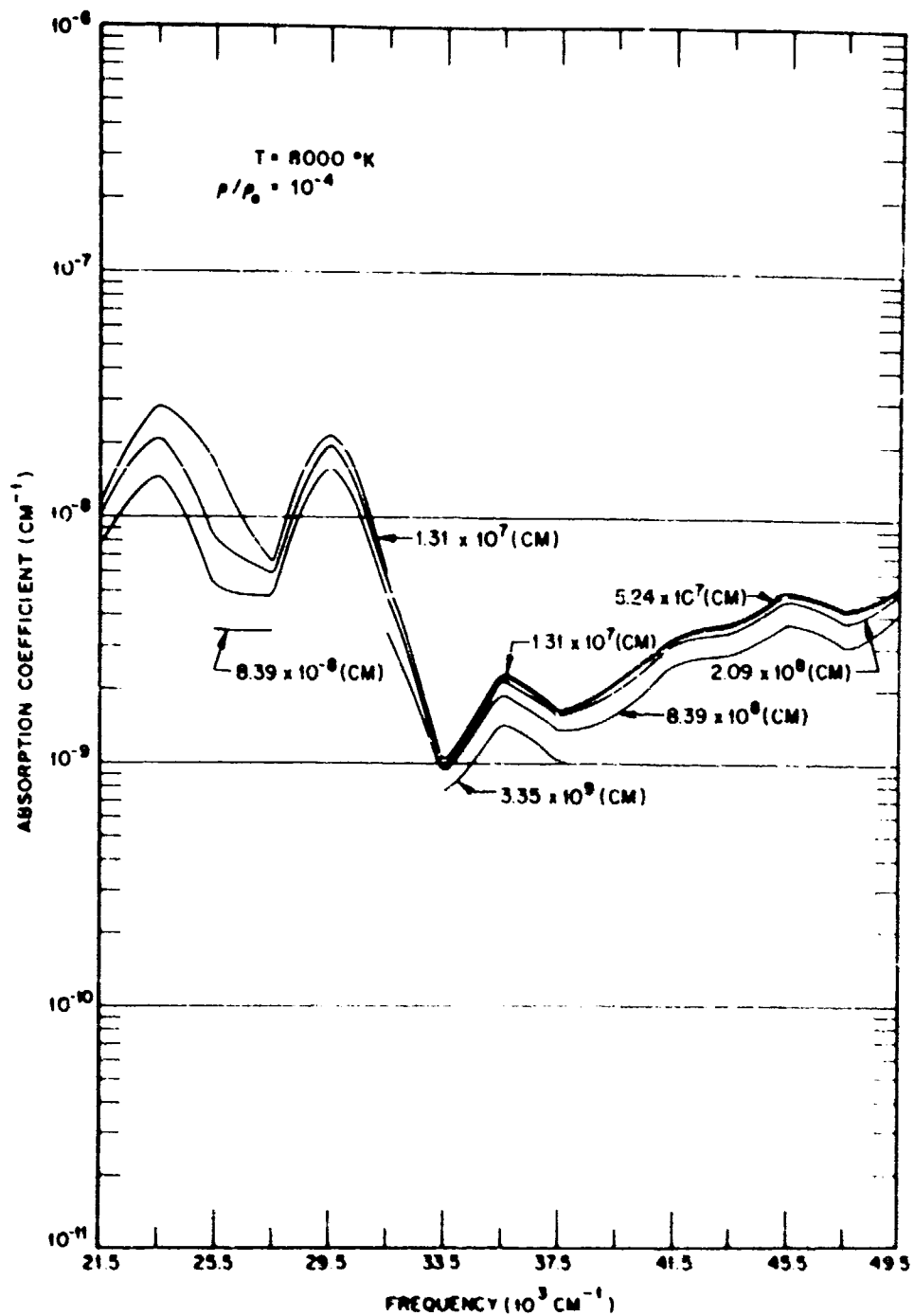
Fig. 70 The average absorption coefficient of heated air as a function of
frequency for various optical path lengths.

108
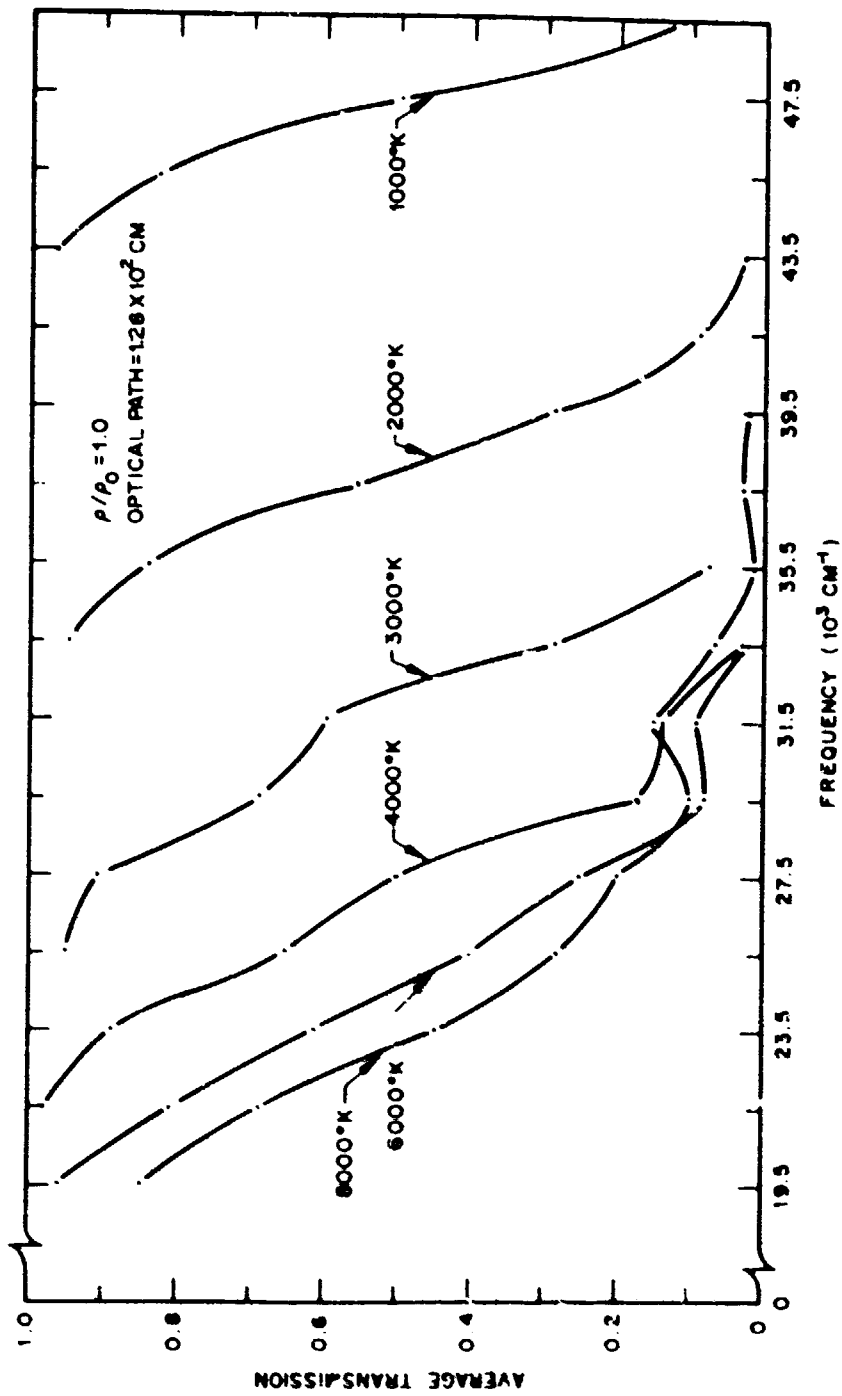
Fig. 71 Average transmission of optical radiation through a slab of heated air as a function of frequency for various temperatures. The optical path length is given in the figure.

109
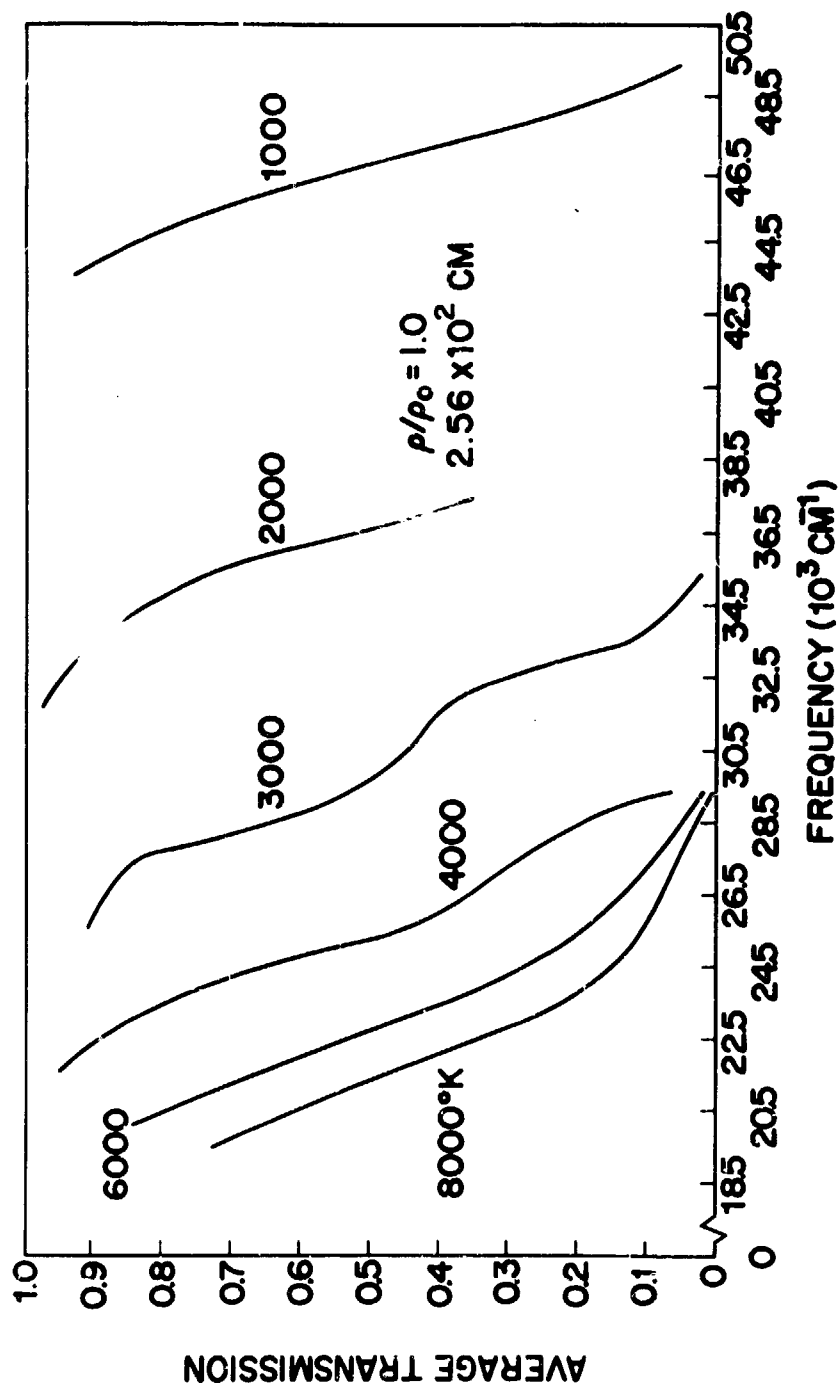
Fig. 72 Average transmission of optical radiation through a slab of
heated air as a function of frequency for various temperatures.
The optical path length is given in the figure.

110
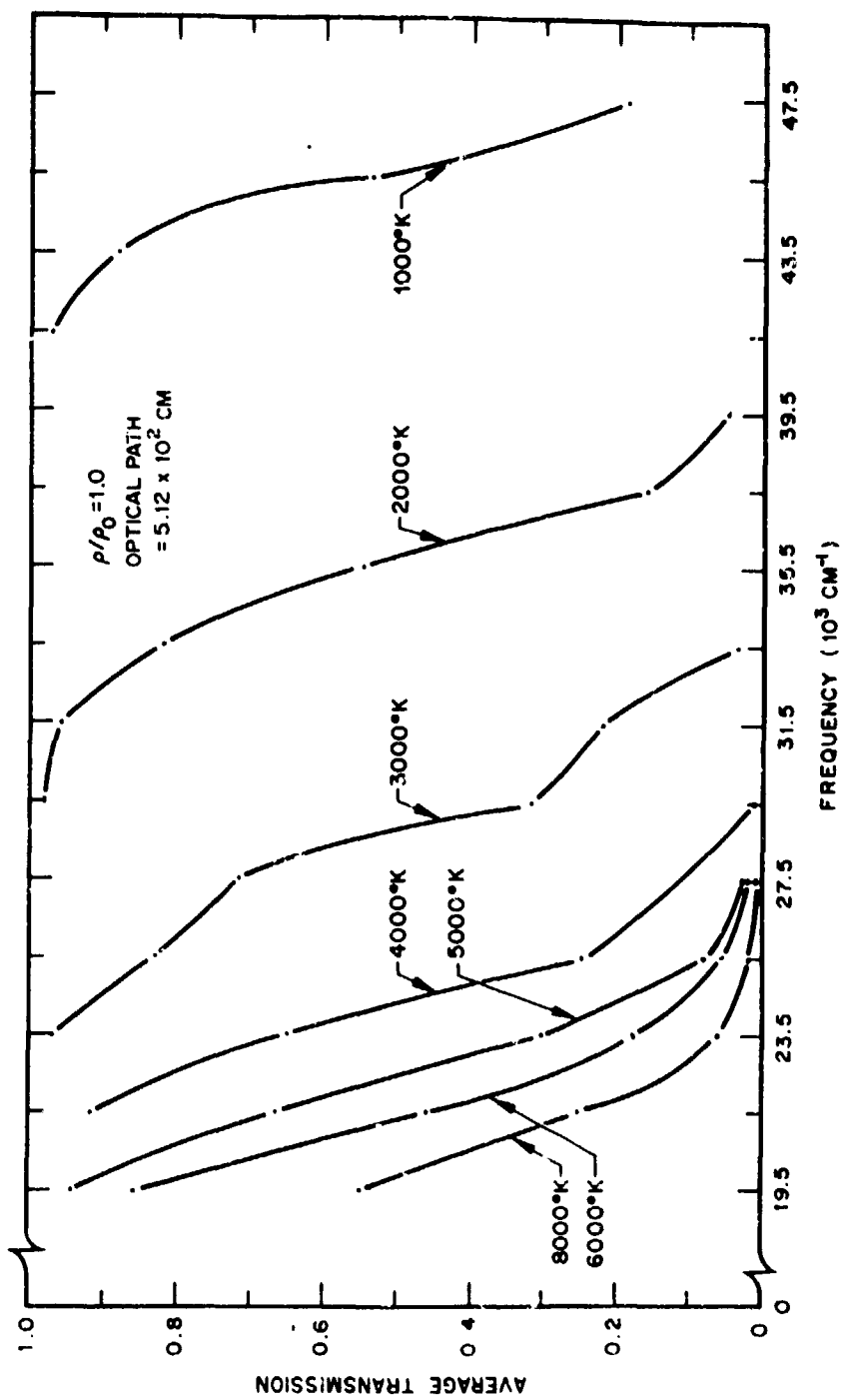
Fig. 73 Average transmission of optical radiation through a slab of heated air as a function of frequency for various temperatures. The optical path length is given in the figure.

111
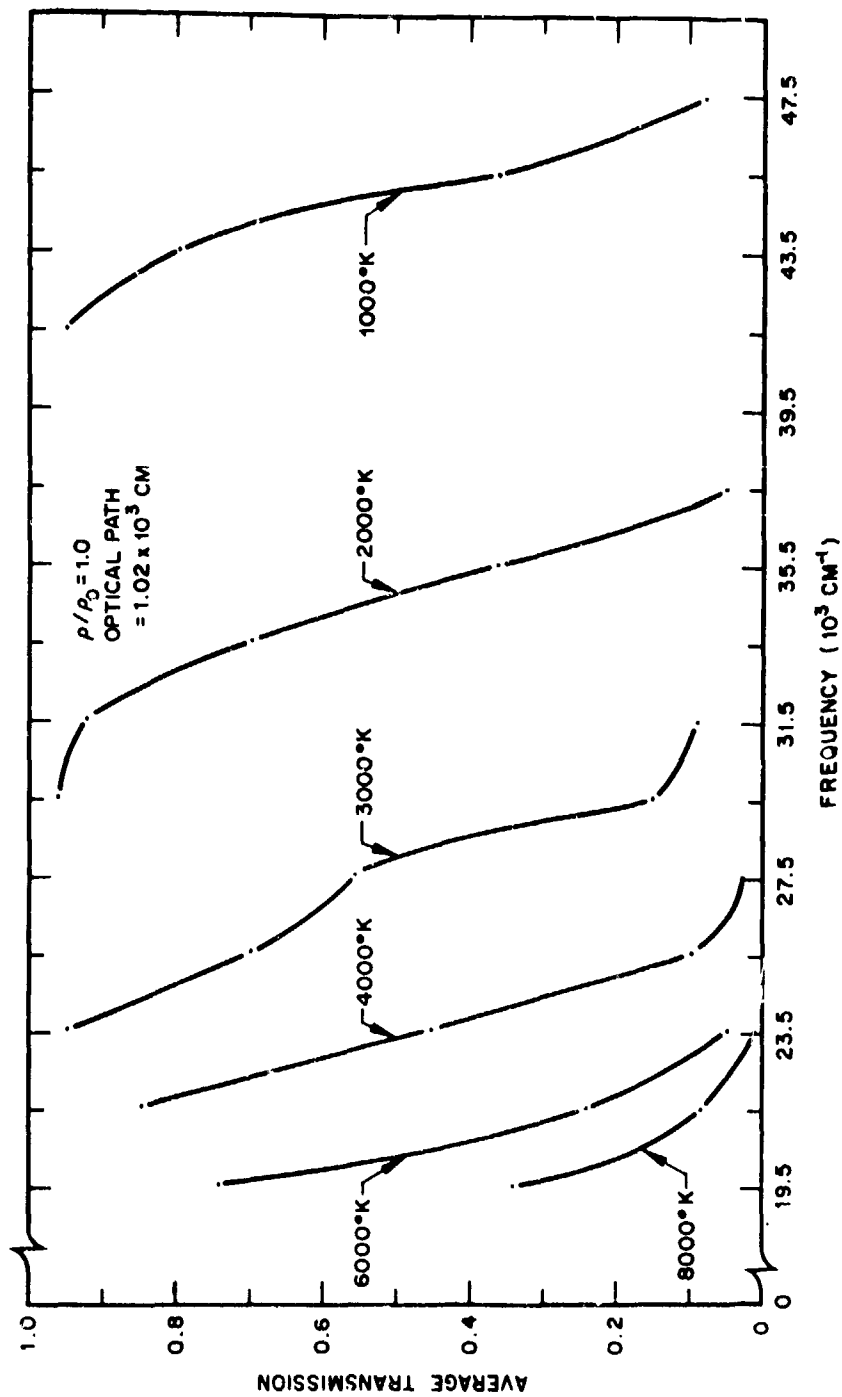
Fig. 74 Average transmission of optical radiation through a slab of heated air as a function of frequency for various temperatures. The optical path length is given in the figure.

112
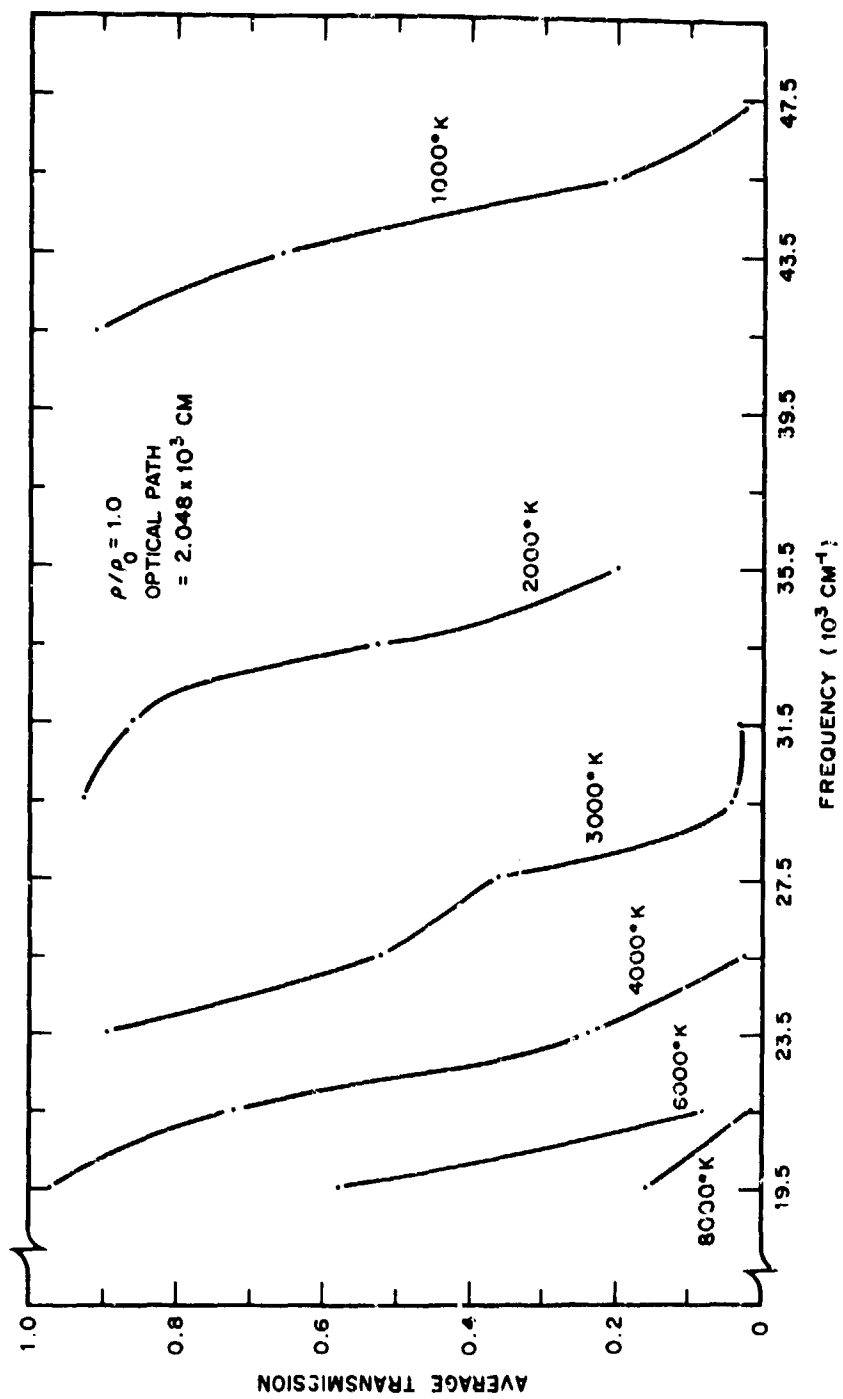
Fig. 75 Average transmission of optical radiation through a slab of heated air as a function of frequency for various temperatures. The optical path length is given in the figure.

113
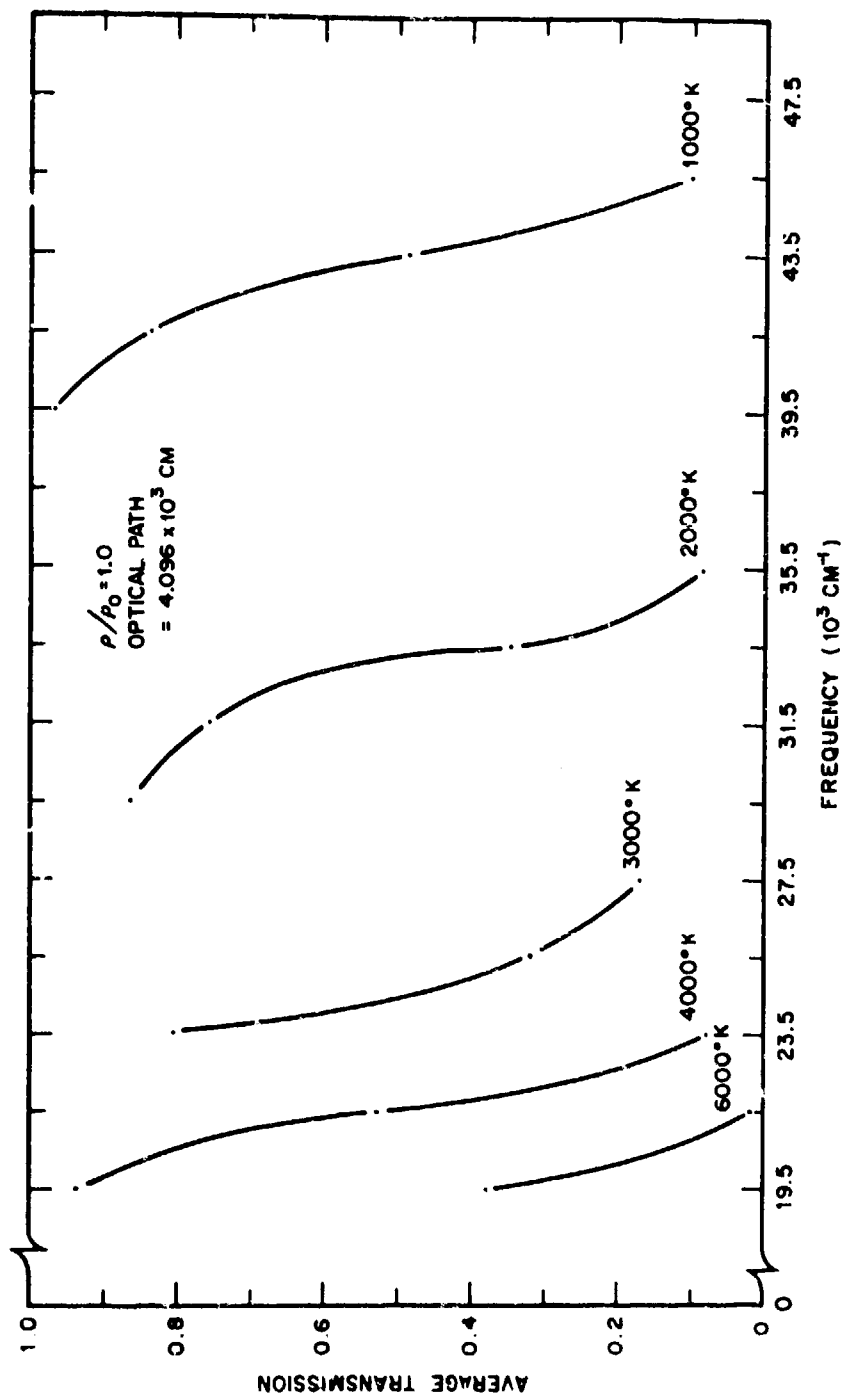
Fig. 76 Average transmission of optical radiation through a slab of heated air as a function of frequency for various temperatures. The optical path length is given in the figure.

114
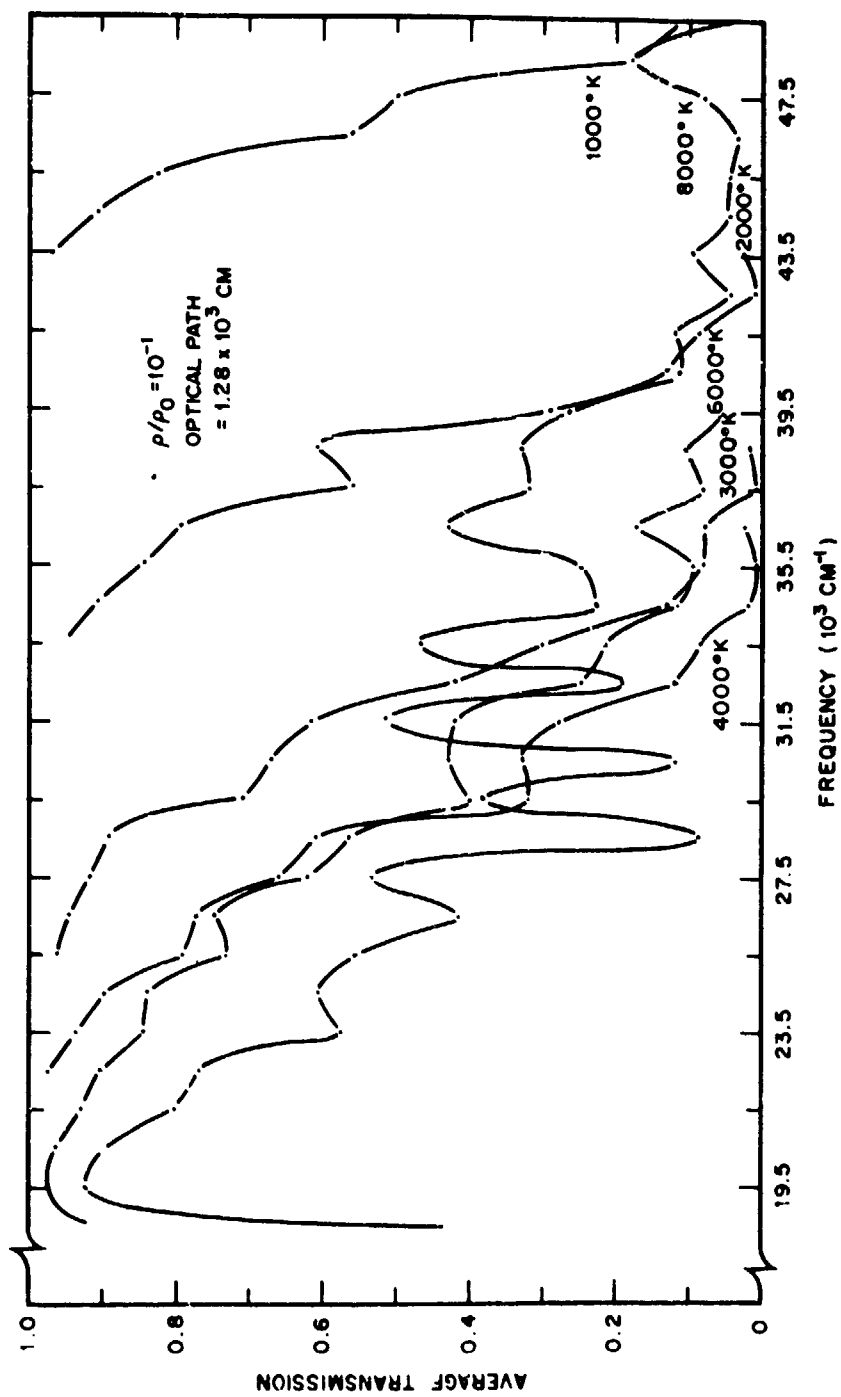
Fig. 77 Average transmission of optical radiation through a slab of heated air as a function of frequency for various temperatures. The optical path length is given in the figure.

115
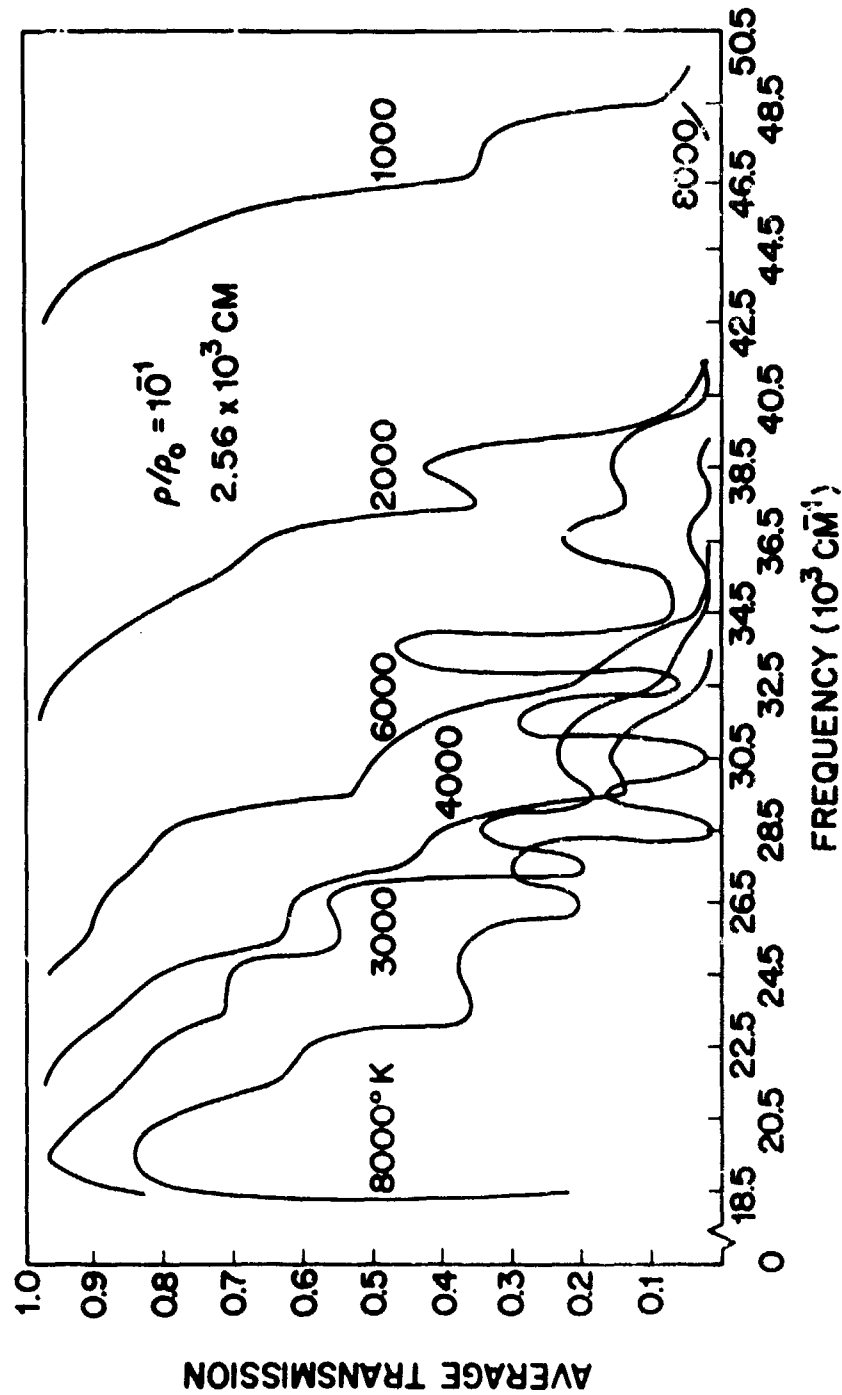
Fig. 78 Average transmission of optical radiation through a slab of
heated air as a function of frequency for various temperatures.
The optical path length is given in the figure.

116
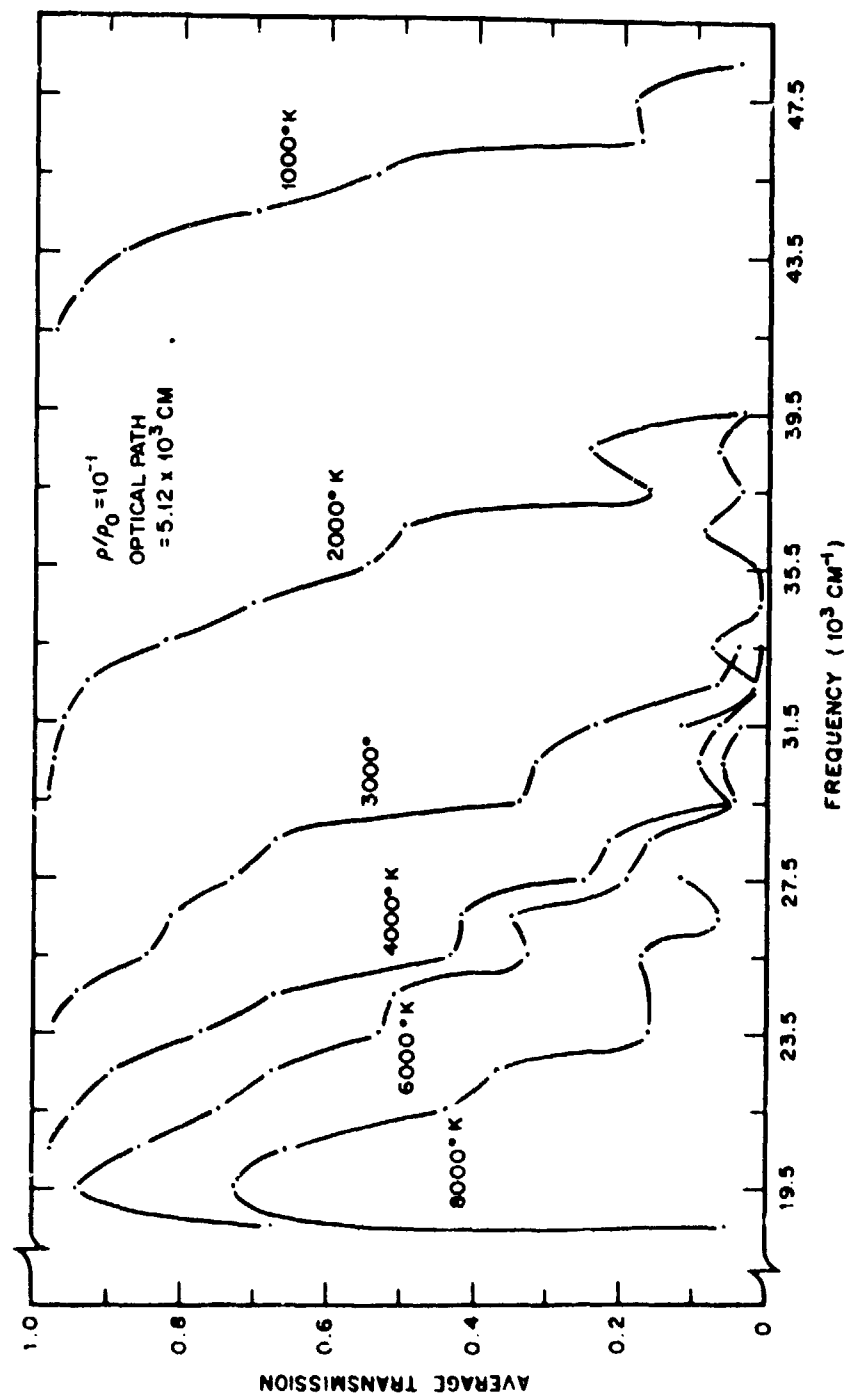
Fig. 79 Average transmission of optical radiation through a slab of heated air as a function of frequency for various temperatures. The optical path length is given in the figure.

The optical path length is given in the figure.

117
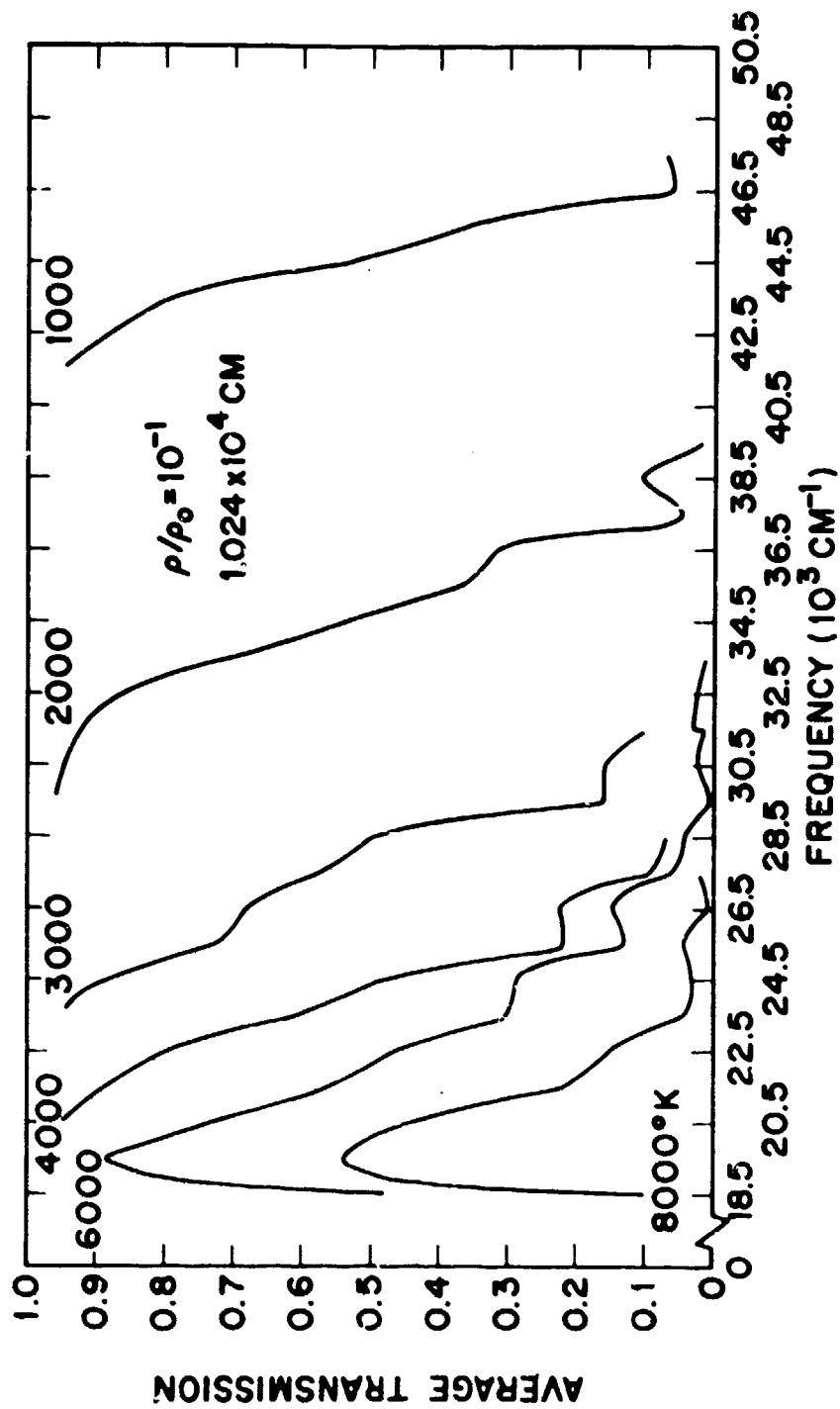
Fig. 80 Average transmission of optical radiation through a slab of heated air as a function of frequency for various temperatures. The optical path length is given in the figure.

118
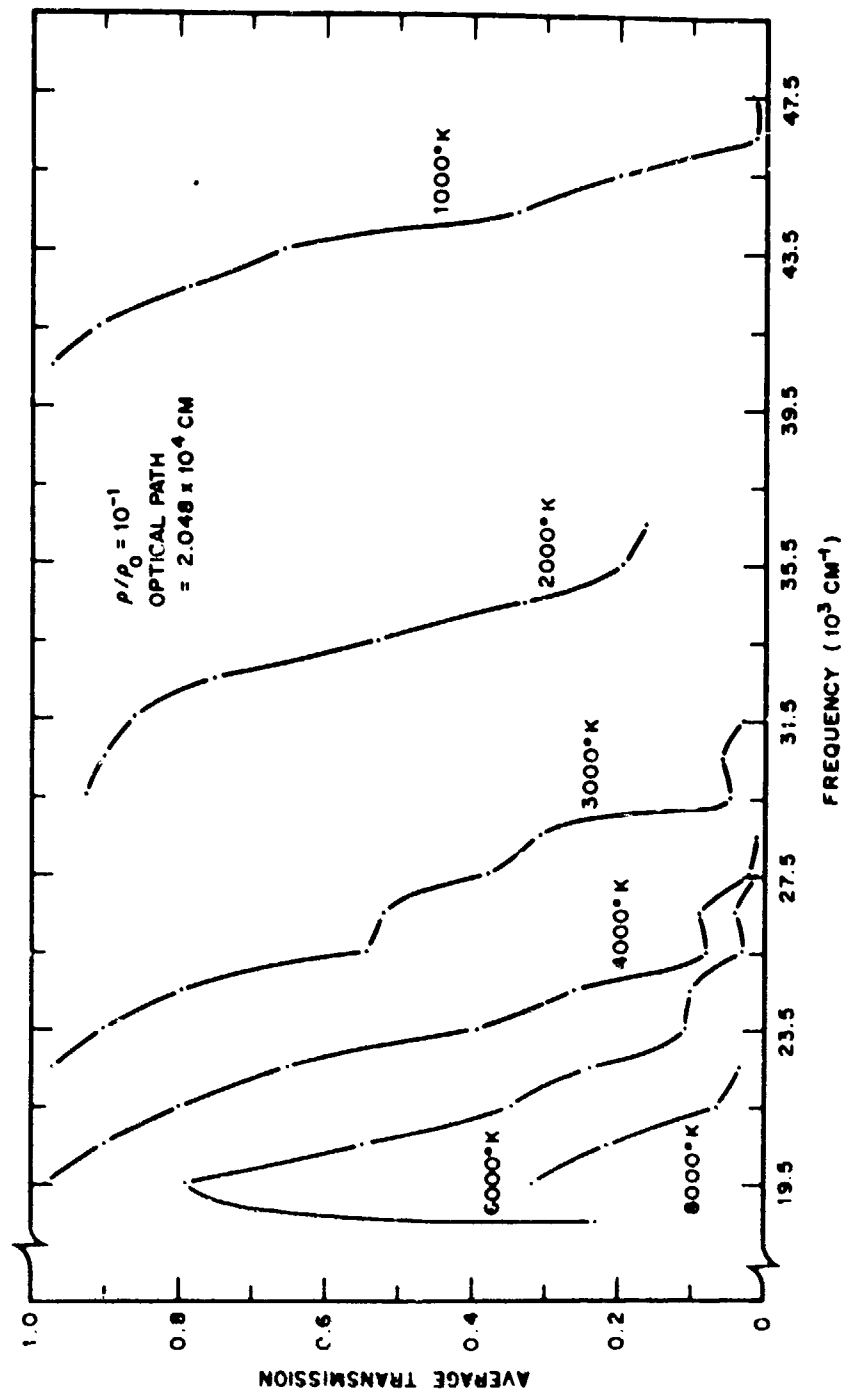
Fig. 81 Average transmission of optical radiation through a slab of heated air as a function of frequency for various temperatures. The optical path length is given in the figure.

119
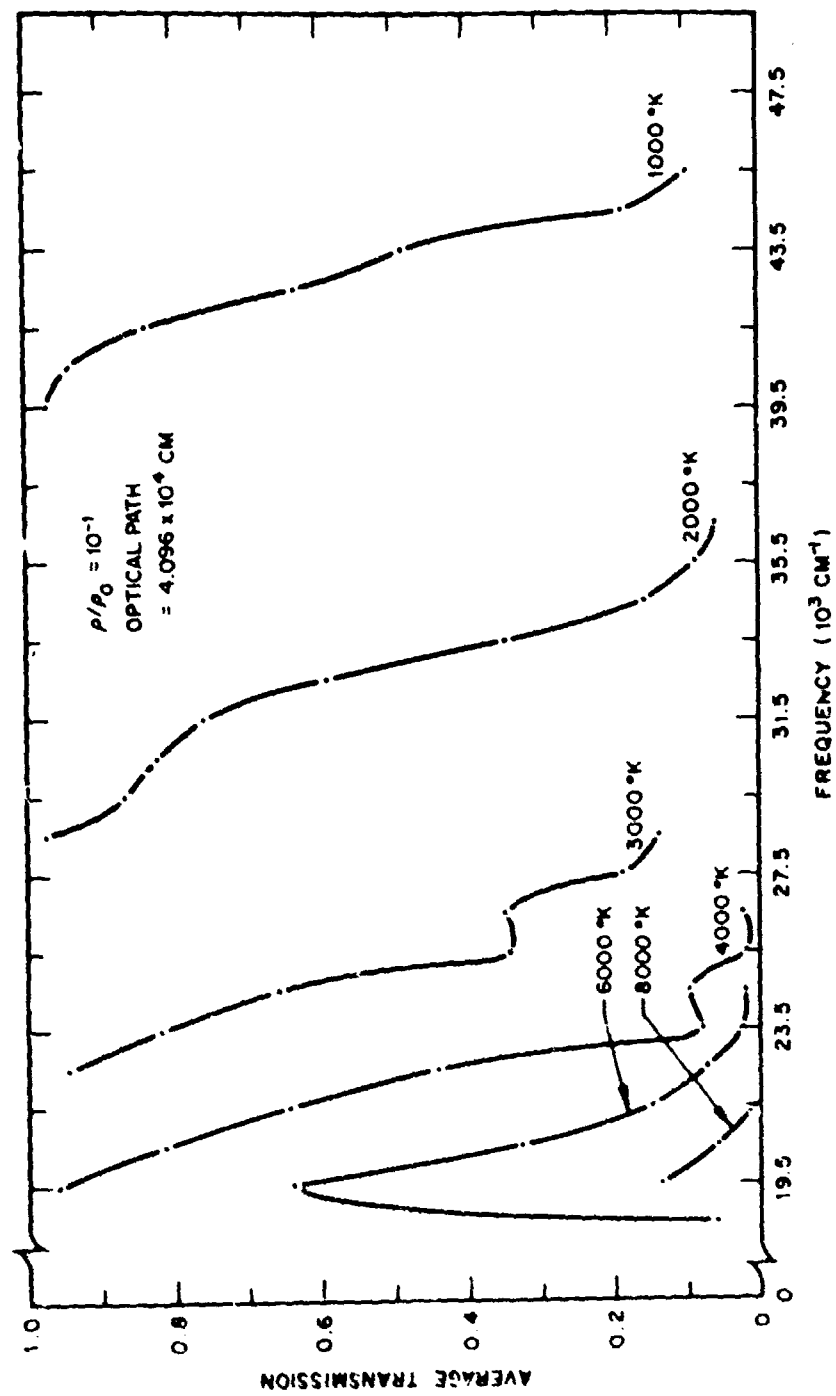
Fig. 82   Average transmission of optical radiation through a slab of heated air as a function of frequency for various temperatures. The optical path length is given in the figure.

120
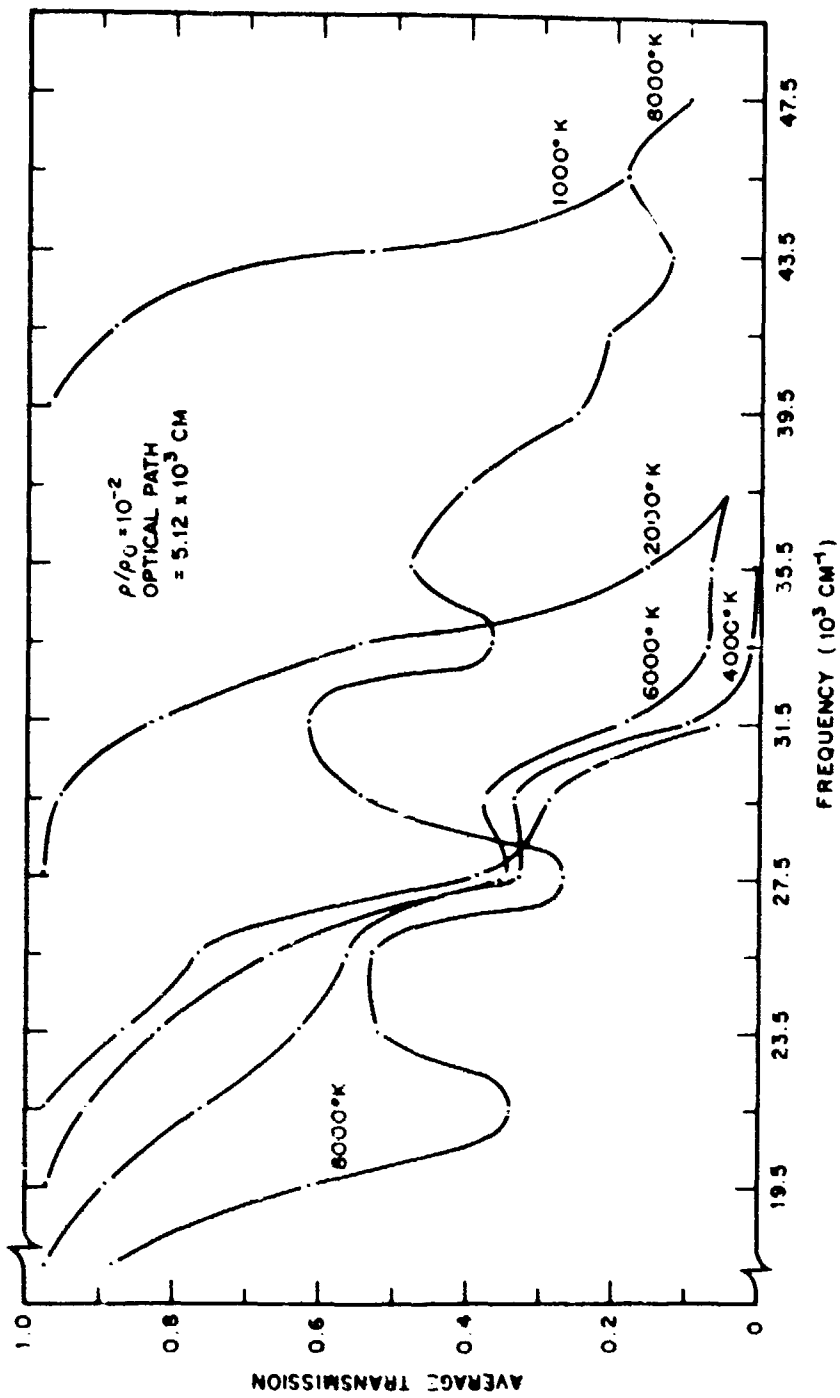
Fig. 83   Average transmission of optical radiation through a slab of heated air as a function of frequency for various temperatures. The optical path length is given in the figure.

121

Fig. 84 Average transmission of optical radiation through a slab of heated air as a function of frequency for various temperatures. The optical path length is given in the figure.

122
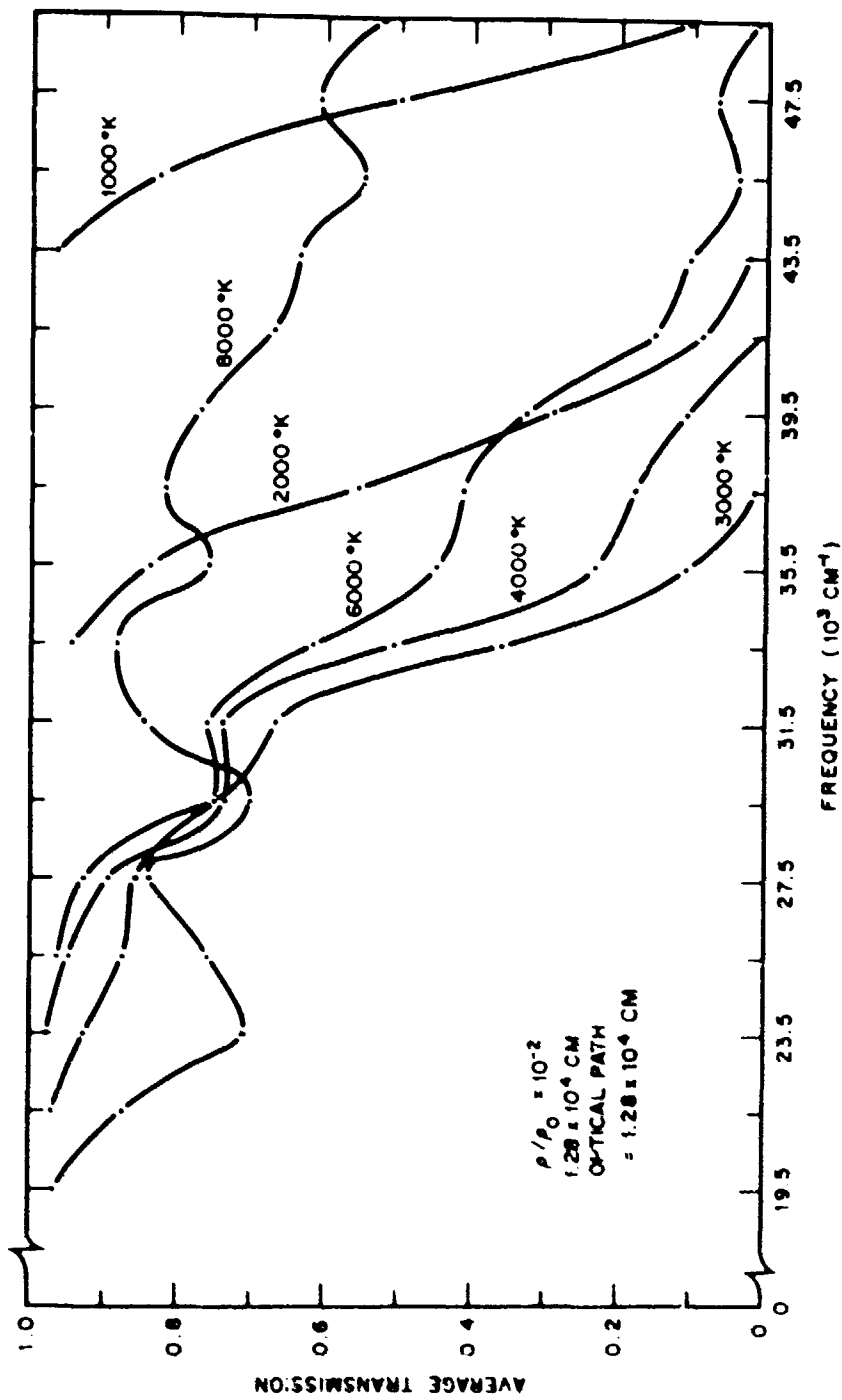
The optical path length is given in the figure.

Fig. 85 Average transmission of optical radiation through a slab of
heated air as a function of frequency for various temperatures.
The optical path length is given in the figure.

123
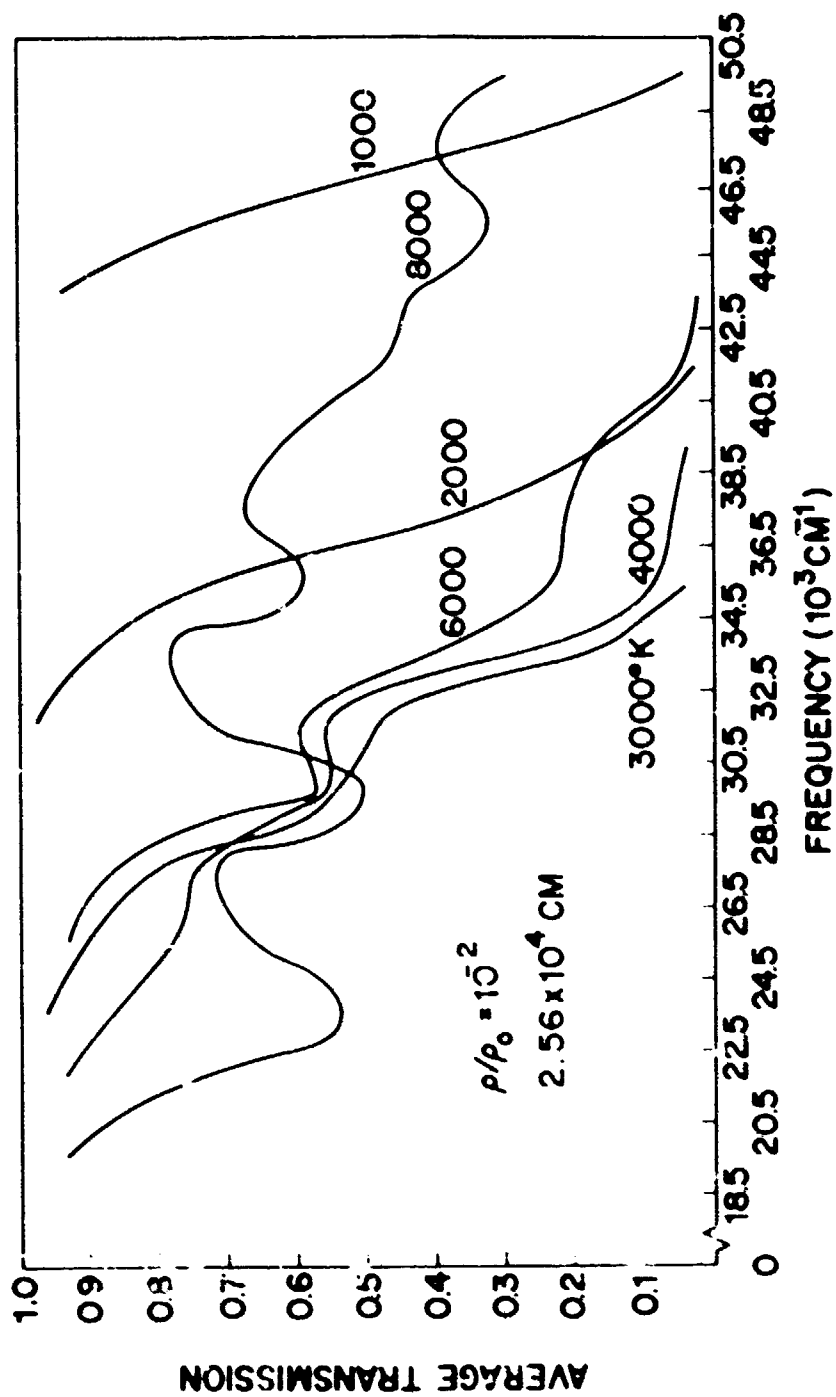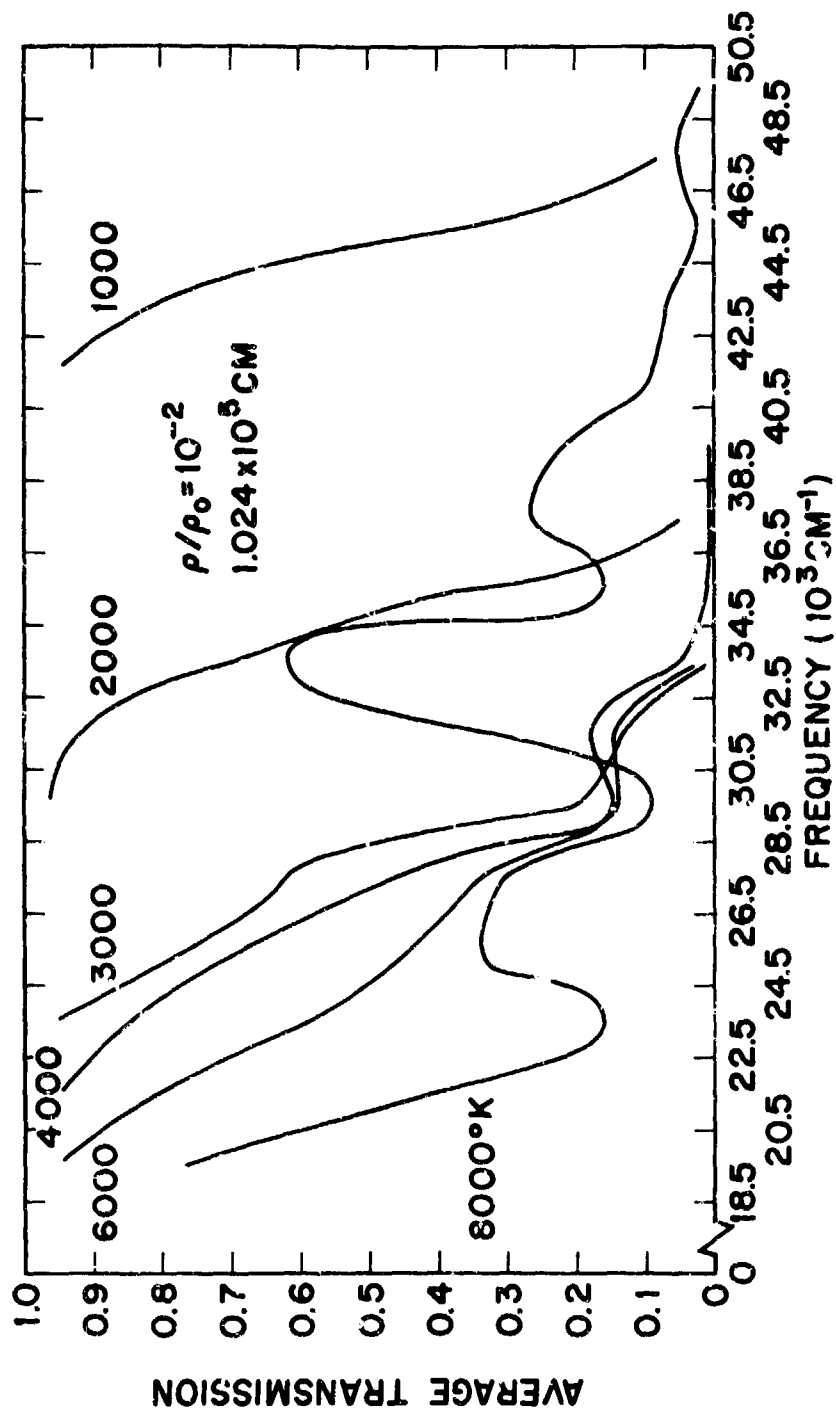
Fig. 86 Average transmission of optical radiation through a slab of heated air as a function of frequency for various temperatures. The optical path length is given in the figure.

124
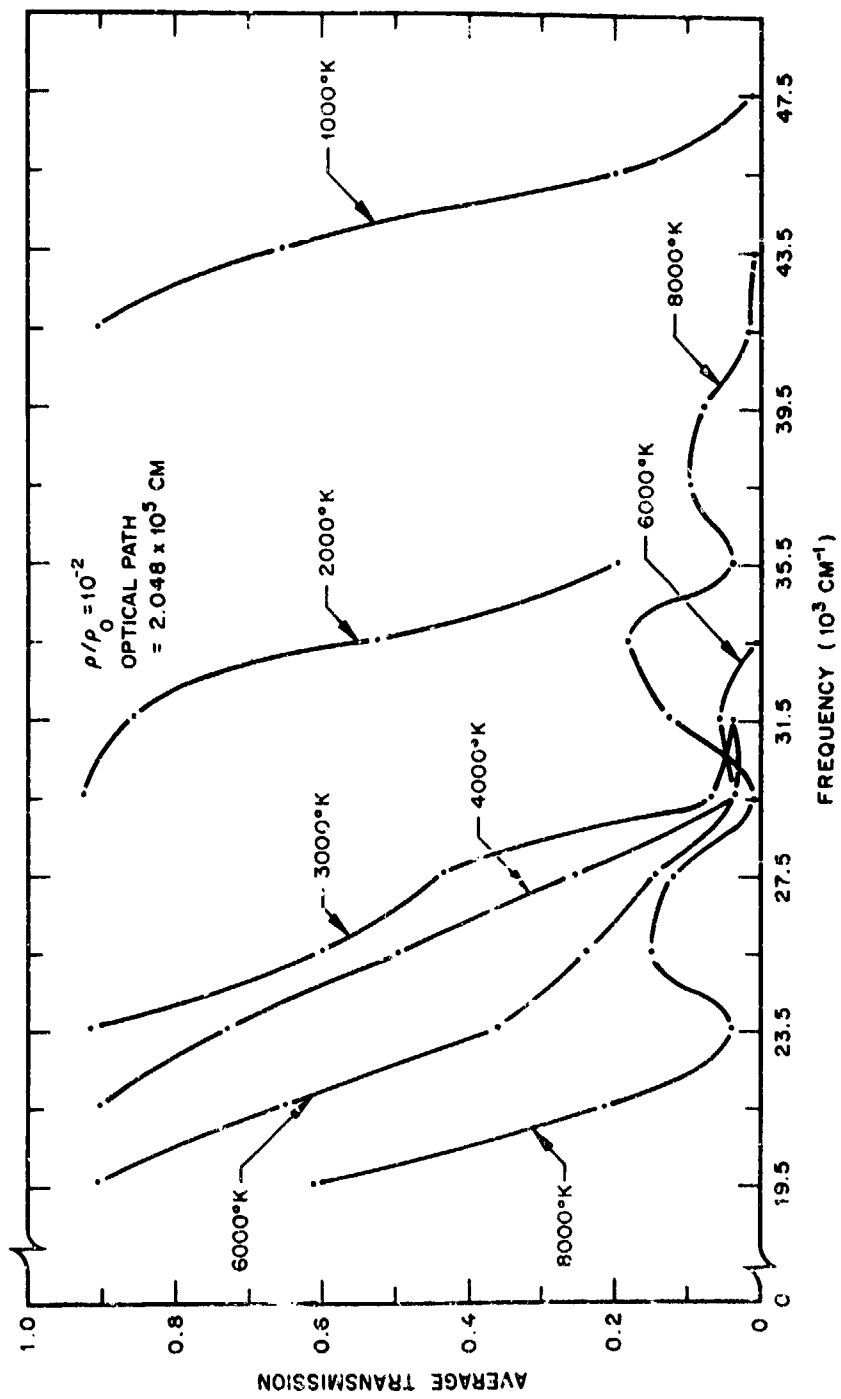
Fig. 87   Average transmission of optical radiation through a slab of
heated air as a function of frequency for various temperatures
The optical path length is given in the figure.

125
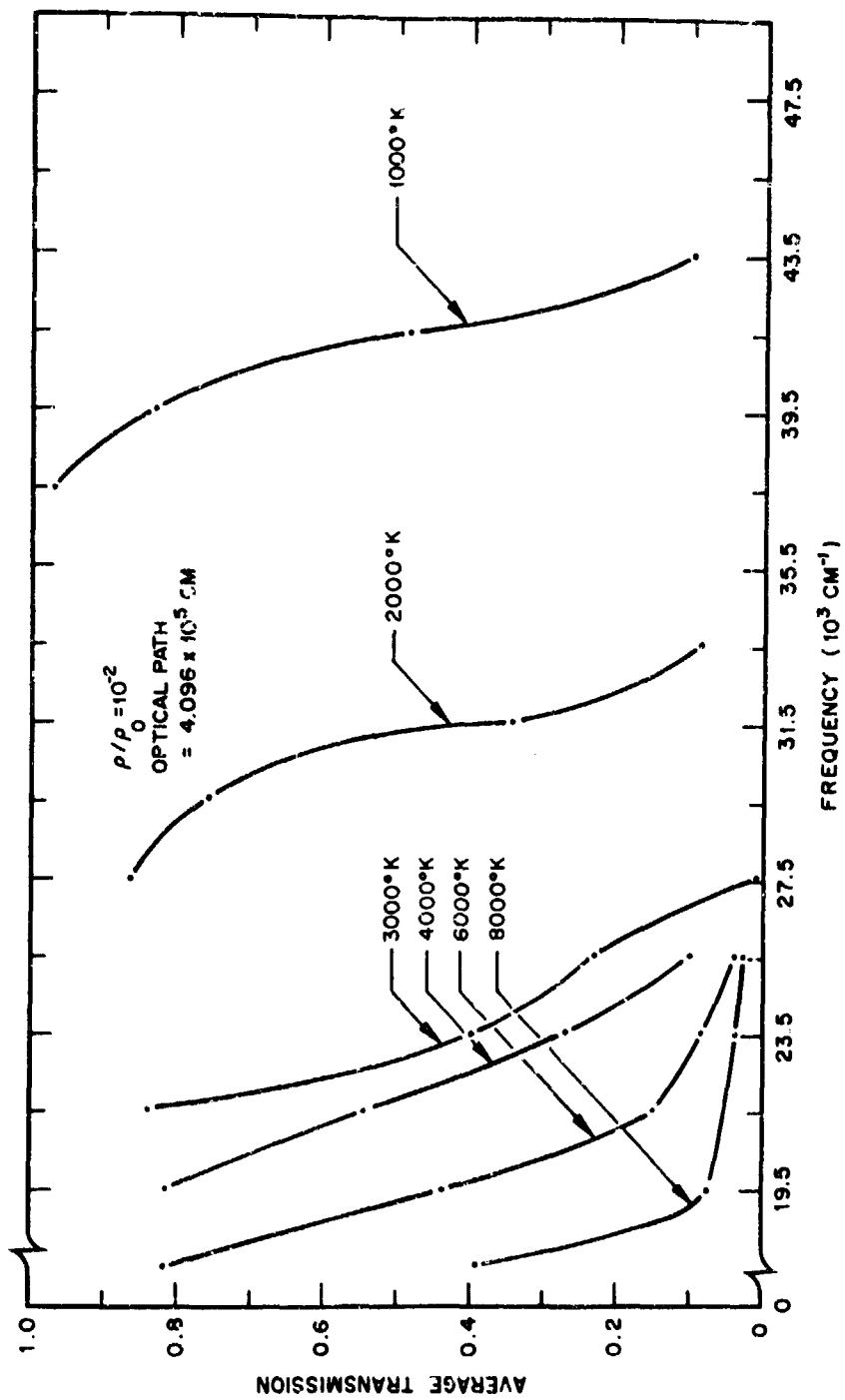
Fig. 88   Average transmission of optical radiation through a slab of heated air as a function of frequency for various temperatures. The optical path length is given in the figure.

126
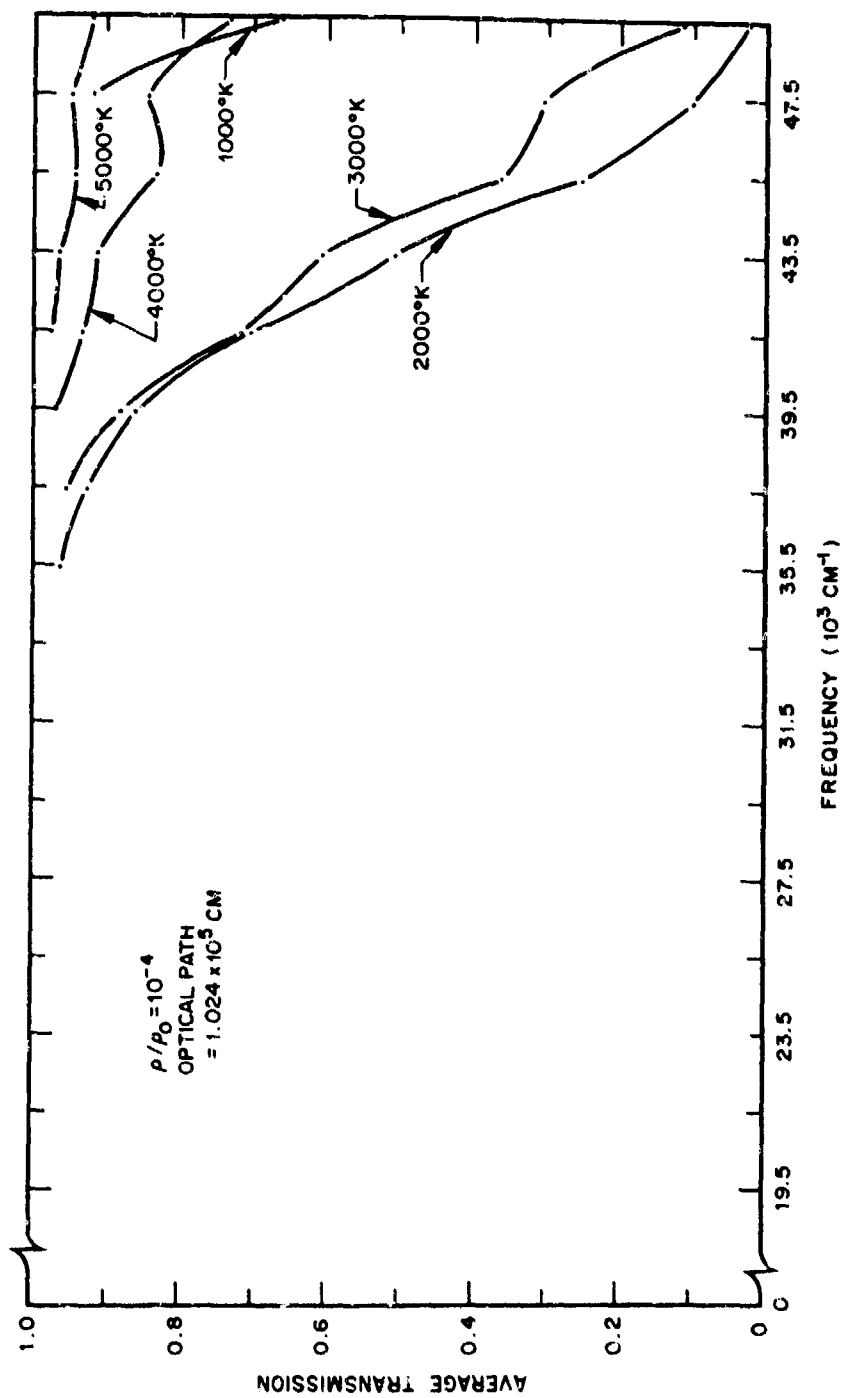
Fig. 89 Average transmission of optical radiation through a slab of
heated air as a function of frequency for various temperatures.
The optical path length is given in the figure.

The optical path length is given in the figure.

127

Fig. 90 Average transmission of optical radiation through a slab of
heated air as a function of frequency for various temperatures.
The optical path length is given in the figure.

128
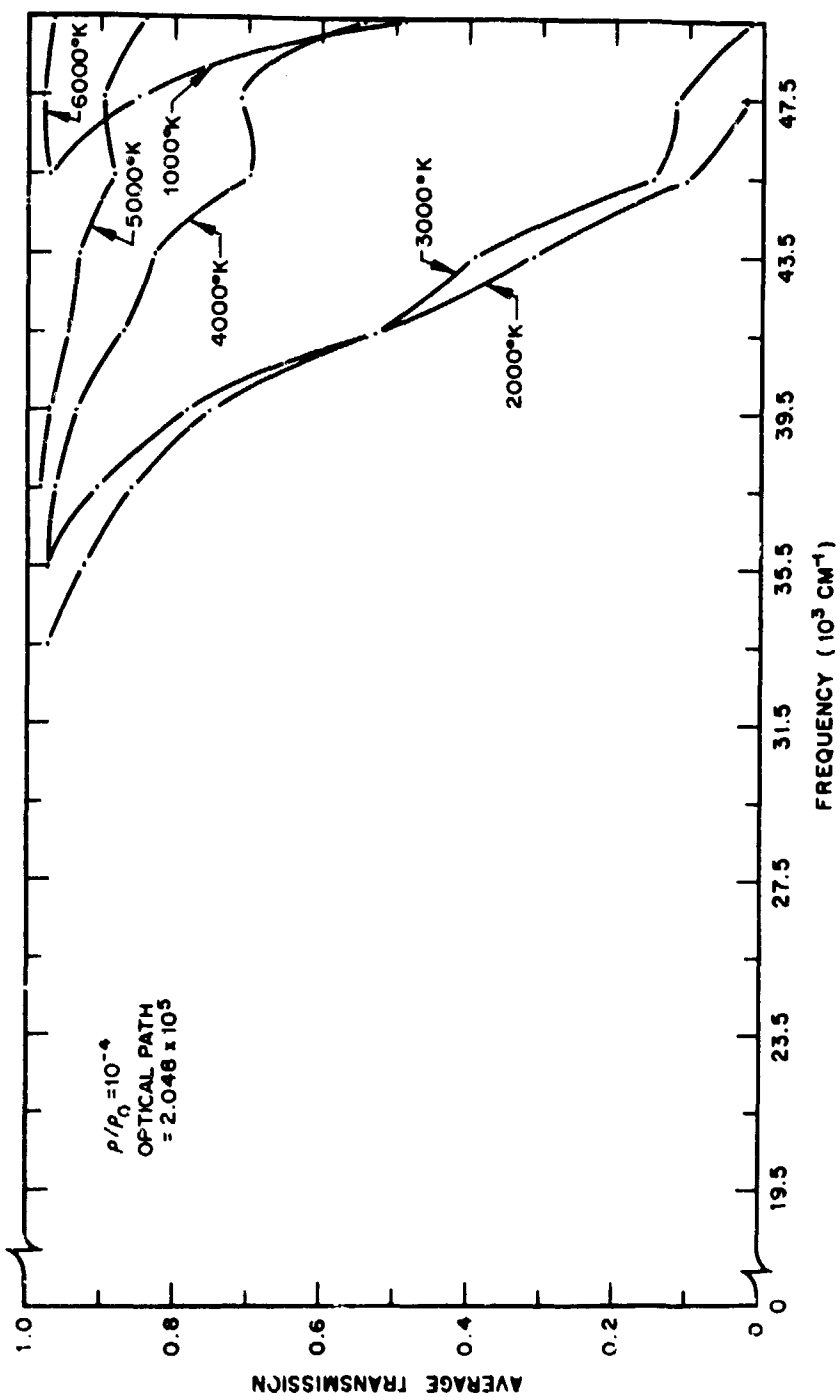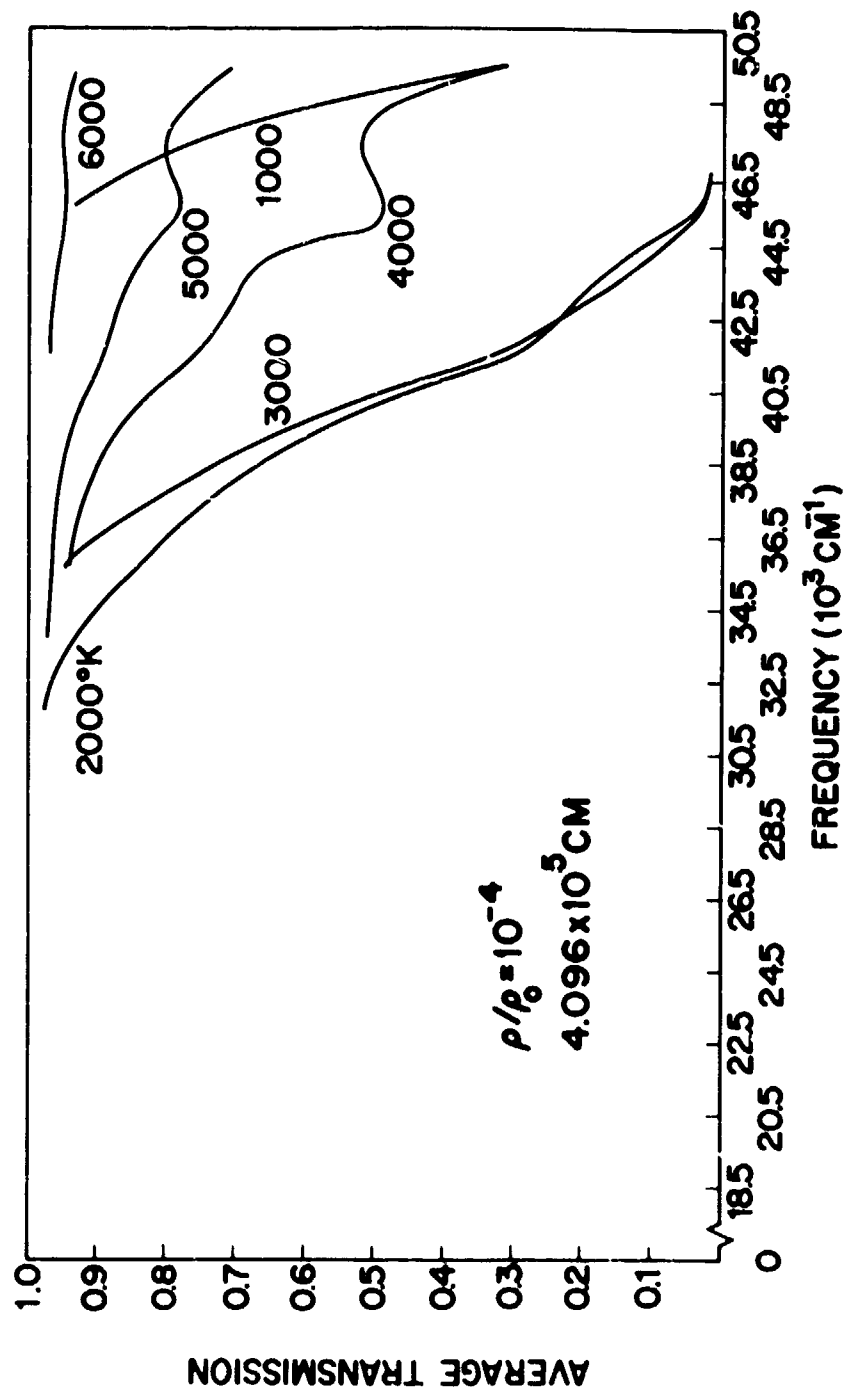
Fig. 91 Average transmission of optical radiation through a slab of
heated air as a function of frequency for various temperatures.
The optical path length is given in the figure.

REFERENCES

1. B. H. Armstrong, J. Sokoloff, R. W. Nicholls, D. H. Holland, and R. E. Meyerott, J. Quant. Spectrosc. Radiat. Transfer $\underline{1}$, 143 (1961).

2. R. E. Meyerott, J. Sokoloff, and R. W. Nicholls, Absorption Coefficients of Air (Air Force Cambridge Research Center, Bedford, Mass. 1960), Geophysics Research Paper No. 68.

3. G. Herzberg, Spectra of Diatomic Molecules (Van Nostrand, New York 1950).

4. M. Born and J. R. Oppenheimer, Ann. d. Phys. $\underline{84}$, 457 (1927).

5. R. W. Nicholls, Can. J. Phys. $\underline{38}$, 1705 (1960).

6. R. W. Nicholls, J. Res. N.B.S. $\underline{65A}$, 451 (1961).

7. R. W. Nicholls, J. Res. N.B.S. $\underline{66A}$, 227 (1962).

8. H. A. Bethe, The Specific Heat of Air up to 25,000°C (OSRD Report 369 1942).

9. S. R. Brinkley, Jr., J. G. Kirkwood, and J. M. Richardson, Tables of the Properties of Air Along the Hugoniot Curve and the Adiabatic Terminating in the Hugoniot. (OSRD Report 3550 1944).

10. P. Brix and G. Herzberg, Can. J. Phys. $\underline{32}$, 110 (1954).

11. R. Schlapp, Phys. Rev. $\underline{51}$, 342 (1937).

12. S. M. Naude, Proc. Roy. Soc. $\underline{136}$, 114 (1932).

13. A. Budo, Z. Physik 96, 219 (1935).

14. A. Budo, Z. Physik 98, 437 (1936).

15. A. Budo, Z. Physik 105, 579 (1937).

16. A. E. Douglas, Can. J. Phys. $\underline{30}$, 302 (1952).

17. E. Hill and J. H. Van Vleck, Phys. Rev. $\underline{32}$, 250 (1928).

18. R. H. Gillette and E. H. Eyster, Phys. Rev. 56, 1113 (1939).

19. R. F. Barrow and E. Miescher, Proc. Phys. Soc. A70, 219 (1957).

20. I. Deezsi, Acta Physica 9, 125 (1959).

21. L. T. Earls, Phys. Rev. 48, 423 (1935).

22. Y. Tanaka and A. S. Jursa, J. Opt. Soc. Am. 51, 1239 (1961).

23. F. R. Gilmore, Equilibrium Composition and Thermodynamic Properties of
    Air to 24,000°K, (Rand Corporation RM-1543, Santa Monica, California 1955).

24. C. E. Treanor and W. H. Wurster, J. Chem. Phys. 32, 758 (1960).

25. R. G. Bennett and F. W. Dalby, J. Chem. Phys. 31, 434 (1959).

26. J. C. Keck, J. C. Camm, B. Kivel, and T. Wentink, Amm. Phys. 7, 1 (1959).